Quantum transport through single-molecule devices: spin and vibration

Doctoral thesis
submitted to
the Department of Physics
at the Freie Universität Berlin

Florian Elste

April 2008

First Referee: Felix von Oppen
Second Referee: Ingo Peschel
Date of thesis defense: June 23, 2008

Quantum transport through single-molecule devices:
spin and vibration

Abstract

Over the past few years the emerging field of molecular electronics has stimulated the interest in understanding the physics of single-molecule transistors. Not only is this a result of promising technological applications, it has also been shown that the presence of specific internal molecular degrees of freedom leads to numerous novel quantum transport phenomena that go beyond the physics observed in larger nanostructural objects such as quantum dots or carbon nanotubes. In the present work we investigate the coupling of electronic degrees of freedom to (i) vibrations, (ii) spins, and (iii) chemical conformations in transport through molecular junctions.

Transport through magnetic molecules is discussed in relation to *molecular spintronics*, i.e. the idea of integrating the concepts of molecular electronics and spintronics. An essential requirement for spintronics devices is the ability to control and detect the spin. In this context, we find that magnetic anisotropy is crucial for slow spin relaxation. The spin moment transmitted from one lead of the molecular junction to the other depends strongly on the orientation of the molecular spin and can be much larger than the initial molecular spin itself. This effect of *giant spin amplification* allows one to effectively read out the spin information. Importantly, the leads need not be polarized. On the other hand, spin writing requires a molecular junction that consists of one ferromagnetic and one nonmagnetic lead. Interestingly, current-induced switching of the spin to a predetermined state only requires a finite bias voltage and is also possible in the absence of a magnetic field.

Furthermore, the proposed setup leads to interesting physics beyond the effect of spin writing, including the occurrence of large negative differential conductance (NDC) at high temperatures. This effect is the consequence of a new *spin blockade* mechanism. By this we mean the suppression of the single-electron tunneling rates for electrons of one spin species due to density-of-states effects.

The interplay of magnetic and vibrational degrees of freedom is investigated in transport through vibrating single-molecule transistors in the Kondo regime. We find that the dependence of the Kondo temperature on the gate voltage is much weaker than in conventional nanostructures in the regime of strong electron-phonon coupling. Moreover, the Coulomb blockade is strongly asymmetric about the charge degeneracy points (marking the transition from the non-Kondo to the Kondo valley), i.e. the peaks in the differential conductance are well pronounced on one side of the degeneracy points, whereas they almost vanish on the other side. Experimental evidence for these two unusual features has been obtained in recent transport experiments on organic complexes.

The main requirement for an electric circuit in nanoscale dimensions is a molecular device that can be switched between two distinct conductive states. Because of

intrinsic bistabilities many single-molecule junctions reveal current-induced switching behavior, e.g. involving cis and trans isomers of a molecule. We study this process for molecules which exhibit two (meta)stable conformations in the neutral state, but only a single stable conformation in the ionic state. While other recent works in this field consider switching processes which are stimulated by thermal activation or vibrational-assisted tunneling from one minimum of the double well to the other, we show that the switching may also be induced by the current involving two subsequent sequential tunneling processes. Here, our main focus of interest is the regime of strongly asymmetric couplings to the leads, corresponding to the experimental setup of a scanning tunneling microscope (STM) conductance measurement. We show that the transport dynamics can be described by a set of Fokker-Planck equations for the Wigner distribution function of the molecule. Our main result is that the average number of switching events per time becomes extremely small compared to the average electronic tunneling rate determined by the current. In other words, the time that the molecule is in one of the two conformations is long compared to the average time between subsequent tunneling events. Such remarkable behavior has been observed in recent STM experiments.

Contents

1 Introduction

1.1 Molecular electronics

The proposal to use single molecules for the fabrication of devices in electronic data processing goes back to a seminal work by Aviram and Ratner [1] in 1974, which may be regarded as the birth of the research field called molecular electronics. The idea was to construct a molecular rectifier by manipulating its electronic properties with functional donor and acceptor groups. However, since the state of the art was far away from the experimental realization of a single-molecule transistor, the vision of an electrical circuit based on molecular components remained an academic issue during the following decades.

Research in this area is mainly driven by the technological motivation to overcome the limits of semiconductor microelectronics. Since the invention of the transistor by Shockley, Bardeen, and Brattain in 1947 (Nobel prize 1956), the computer industry has been reporting a rapid progress in fabricating faster and faster chip devices. Improving their efficiency relies essentially on reducing the size of the chip features, since the velocity of the charge carriers is a property which is entirely controlled by the semiconductor material so that speed of data processing is essentially governed by the size of the components. The miniaturization trend in the history of computer hardware follows an empirical law stating that the number of transistors that can be placed on an integrated circuit is increasing exponentially, doubling approximately every two years. This observation was first made by G. E. Moore [2] in a 1965 paper and is illustrated in Fig. 1.1.

A particularly interesting aspect of molecular electronics, besides the prospect of further miniaturization, is the possibility of using chemical synthesis for the fabrication of device components. This approach called bottom-up would start from relatively simple molecules and be massively parallel, seeking to have single molecules arrange themselves into more complex structures by self-assembly. In contrast, the concept of top-down approaches consists of creating nanostructures by starting from larger devices and directly controlling the manufacture of smaller features while cutting materials into the desired shape, e.g. using electron beam lithography. The concept of bottom-up was already addressed by R. P. Feynman in his famous lecture at an American Physical Society meeting at Caltech in 1959, *There's Plenty of Room at the Bottom* [3]. In particular Feynman discussed the possibility of manipulating individual atoms on the nanoscale in relation to denser computer circuitry and microscopy that would go beyond the limitations of scanning electron microscopes those days. *Why cannot we write the entire 24 volumes of the Encyclopedia Britannica on the head of a pin?* [3] At that time Feynman's ideas were pure thought experiments,

since the necessary technologies had not been developed yet. However, 40 years later some of his ideas have been experimentally realized, e.g. by the development of the scanning tunneling microscopy and data storage devices such as the IBM Millipede [4], respectively.

Despite the reigning optimism about molecular electronics, industrial practicability standards and profitability requirements of molecular electronics have not been met yet. Since research in this area has just begun, it will only turn out in the future which specific concepts are also promising from an economic point of view. However, molecular electronics has also been receiving much attention independently of the above mentioned technological aspects. Aside from the possibility of enabling the next step in miniaturization towards smaller devices, molecular electronics has become of fundamental interest in that it poses numerous questions aiming at a deeper understanding of electronic transport on the molecular level. In this context, transport through single molecules has turned into a flourishing field at the interface between physics and chemistry. On the one hand, similarities to larger nanostructures have become evident in various experiments such as the observation of the Coulomb blockade and the Kondo effect [5–7]. On the other hand, it has been shown experimentally and theoretically that the presence of specific internal molecular degrees of freedom leads to novel quantum transport phenomena that go far beyond the physics observed in more conventional nanosized objects such as semiconductor quantum dots or carbon nanotubes [8–36]. An overview of the sizes of typical nanostructures and molecular devices is sketched in Fig. 1.2.

1.2 Molecular spintronics

An alternative strategy to go beyond conventional semiconductor-based microelectronics is known as spintronics. Complementary to molecular electronics, spintronics relies on using not only the charge of the electron but also its spin to store and process information, bringing the memory and logic functionality on the same chip with the electronic spin being the the ultimate logic bit [38]. In this respect spintronics has set a new paradigm.

The discovery of giant magnetoresistance (GMR) by P. Grünberg *et al.* [39] and A. Fert *et al.* [40], awarded the Nobel prize in 2007, is considered the birth of this field of research. The effect is observed in thin metal films of alternating ferromagnetic and nonmagnetic layers, manifesting itself as a significant decrease in electrical resistance due to the presence of a magnetic field. Giant magnetoresistance has been exploited commercially and has led to a number of patents in the computer industry. For instance, it has been used in modern hard disk drives and non-volatile semiconductor memory devices such as magnetoresistive random access memory (MRAM) chips. Furthermore, this emerging field of semiconductor-based spintronics is expected to have great potential to lead to a number of further technological applications in the future.

In semiconductors spin preserves coherence over extremely long times and dis-

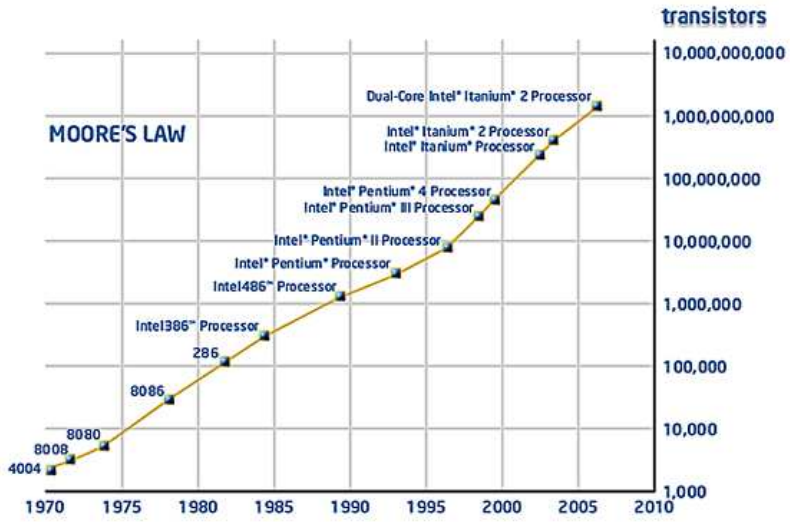

Figure 1.1: Moore's law. The number of transistors that can be placed on an integrated circuit is increasing exponentially, doubling approximately every two years. The figure is taken from Intel's webpage [37].

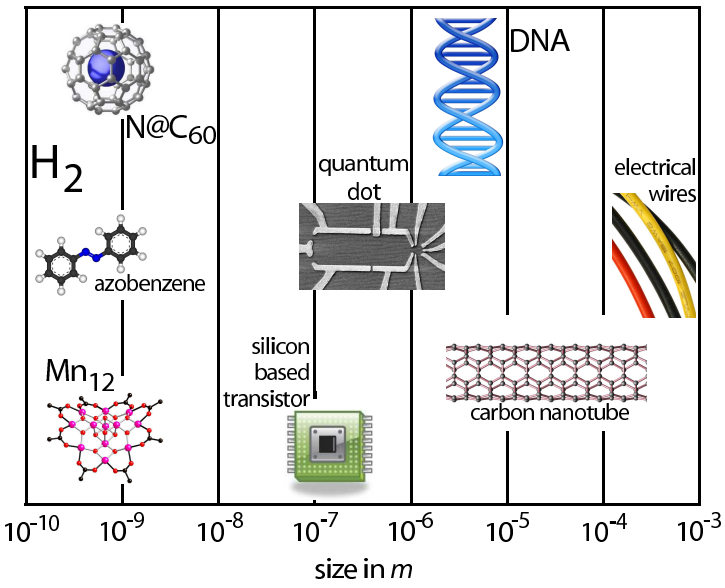

Figure 1.2: Illustration of length scales relevant for semiconductor-based electronics and molecular electronics. The figure of the quantum dot is taken from C. Schönenberger's group in Basel. The figure of the DNA molecule is taken from http://www.dnamnd.med.usyd.edu.au. The figures of the azobenzene molecule and Mn_{12} derivative are taken from the Wikipedia. The figure of the $N@C_{60}$ molecule is taken from W. Harneit's group in Berlin. The figure of the carbon nanotube is taken from http://people.cecs.ucf.edu/sseal/debs/debasis.htm.

tances and thus offers the prospect of being used for quantum logic [9; 11; 38; 41]. This idea is mainly based on the presence of spin-orbit interaction, which plays a ubiquitous role in semiconductor spintronics. However note that while spin-orbit interaction is an intrinsic property of the electronic structure that allows one to manipulate the spin by electric means only, as e.g. exploited in the spin Hall effect [42; 43], it is the main source of spin dephasing and responsible for spin decoherence at the same time.

Remarkably, only little efforts have been made on combining the promising concepts of molecular electronics and spintronics. The driving idea behind molecular spintronics consists of integrating these two strategies for the purpose of exploiting all their advantages. The spin presents an attractive degree of freedom to be used in logic devices, since the relevant energy scales are typically a few orders of magnitude smaller than those involved in manipulating the electron charge in a transistor. This can translate into devices exhibiting ultra-low power consumption and high speed [9; 11; 38; 41]. Moreover the molecular world provides all ingredients required for an electric network. Organic molecules have the advantage to be produced with low-temperature low-cost chemical methods instead of high-temperature solid-state techniques. Chemical synthesis allows the design of polymers with the desired electronic structure and conductivities ranging over several orders of magnitude. Furthermore, molecules can be anchored to metal substrates in various ways. The spin relaxation times of single-molecule transistors can be extremely long compared to the average electronic tunneling time which is governed by the current [9; 11; 38; 41].

The combination of molecular electronic and spintronics relies essentially on magnetic molecules, i.e. molecules with a local spin [44]. In this context, magnetic single-molecule transistors have been proposed as candidates for the experimental realization of molecular spintronics. Despite the fact that many molecules tend to be diamagnetic in the neutral state due to the presence of paired valence electrons in the molecular orbitals, there exists a large number of metal complexes which are paramagnetic. Some porphyrin complexes such as heme, which is based on a central iron ion, have a local spin $S = 2$. Manganese Mn_{12} complexes [45] and iron F_8 derivatives [46] even reveal a spin of length $S \simeq 10$. Endohedral fullerenes [47; 48] consisting of nitrogen doped or phosphorus doped C_{60} are paramagnetic due to the presence of three unpaired p electrons, resulting in a total spin $S = 3/2$. Furthermore, any molecule that is diamagnetic in the neutral state usually becomes paramagnetic when it is charged.

The prospect of using single-molecule magnets in the context of molecular spintronics is elucidated in Chapter 3, where our main focus is on concepts of spin reading and writing.

1.3 Experimental motivation

Over the past few years molecular electronics has fueled the interest in understanding the physics of single-molecule transistors. Experimental research in this field has been

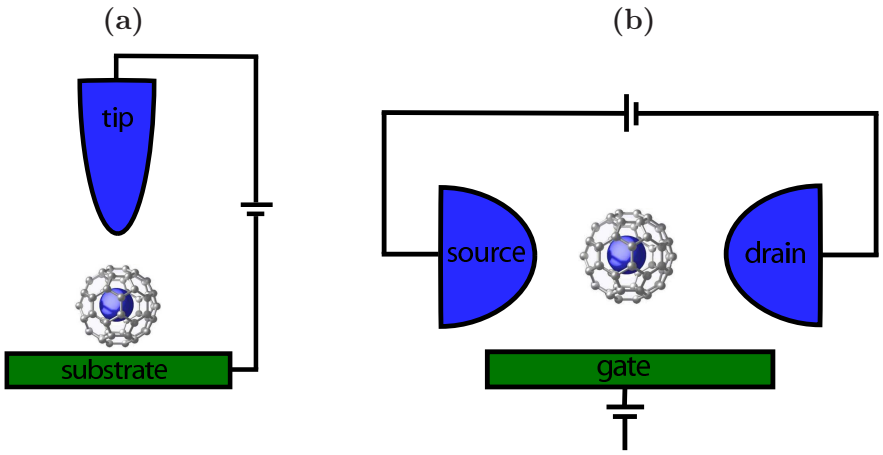

Figure 1.3: (a) Scanning tunneling microscope setup. Here the molecule is strongly coupled to the substrate and weakly coupled to the tip. (b) Setup of a three-terminal molecular junction. Here the molecule is symmetrically coupled to the source and drain electrode. The presence of an additional gate electrode allows one to shift the electrostatic potential of the molecule.

enabled and motivated by the development of new techniques which allow for the realization of single-molecule devices. In the following we survey the state of the art, even though the selection of listed works makes no claim to be complete.

Experimental works which propose to measure the conductivity of single molecules essentially fall into two classes. The first involves a scanning tunneling microscope (STM) setup [49]. Here the tip and the substrate layer serve as source and drain electrodes, respectively, cf. Fig. 1.3(a). The second is based on a molecular junction that is created by the use of the breakjunction technique [18] or electromigration [12]. Here the molecule is located in the gap of a metal wire that is adsorbed on a substrate surface, whereas the voltage drops off between the two edges of the gap, which serve as source and drain electrodes in this case, cf. Fig.1.3(b).

Both approaches have been employed by a number of groups and led to many interesting works. Scanning tunneling microscope experiments usually involve very asymmetric couplings to the leads. The molecule is relatively strongly coupled to the substrate, whereas it is much more weakly coupled to the tip electrode. As a consequence the spectrum of the molecule may be affected by presence of the substrate in an essential way. Its spectral function reveals additional broadenings of the peaks due to quantum fluctuations, which is expected to manifest itself as a broadening of the peaks in the differential conductance for temperatures small compared to the hybridization energy. On the other hand, molecular junctions usually imply weaker and more symmetric couplings to the leads. The molecular spectrum is hardly affected by the presence of the electrodes. Some of these experiments are performed with mechanically controllable break junctions [18]. In this approach, a

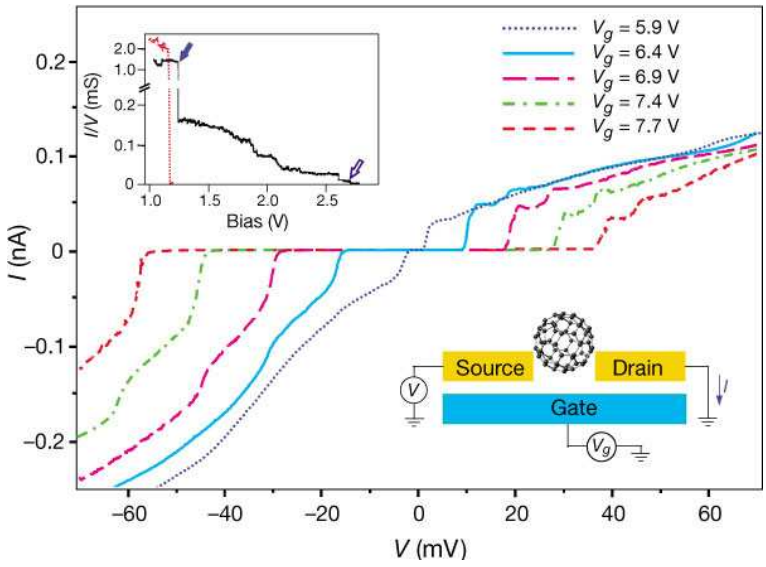

Figure 1.4: Experimental data for transport through single C_{60} by Park *et al.* [12]. The current-voltage characteristics show approximately equidistant steps due to the excitation of molecular phonons. The conductance gap in the vicinity of zero bias voltage represents the Coulomb blockade. The inset shows the current while opening the junction by electromigration.

metal wire is glued onto a flexible substrate by lithographical methods and fractured by bending the substrate, by which an adjustable tunneling gap can be established. The bending of the substrate is controlled by a piezo element. The breaking of the junction and the creation of the gap in the metal wire is indicated by a rapid reduction of the conductance by several orders of magnitude. Subsequently, organic molecules are being adsorbed onto the two electrodes of the break junction, which were broken in solution, resulting in formation of a self-assembled monolayer (SAM) on the electrodes. The piezo element allows for changing the molecule-lead coupling by adjusting the spacing between the electrodes, which is usually of the order of a nanometer. Alternatively the gap between the electrodes can be created by the process of electromigration [12]. Furthermore, molecular junctions also allow for an additional gate electrode, which is usually integrated in the experimental setup as a metal layer under the substrate. In the experiments by Park *et al.* [12] the entire structure was defined on a SiO_2 insulating layer on top of a doped silicon wafer. The presence of a gate electrode provides an additional control parameter that permits one to effectively shift the electrostatic energies of the molecule, turning the molecular junction into a transistor. Mainly for this reason, this technique has become very popular and received much attention in the context of molecular electronics.

Many experiments report transport phenomena which are similar to those effects observed in conventional nanostructures. The Coulomb blockade and the Kondo

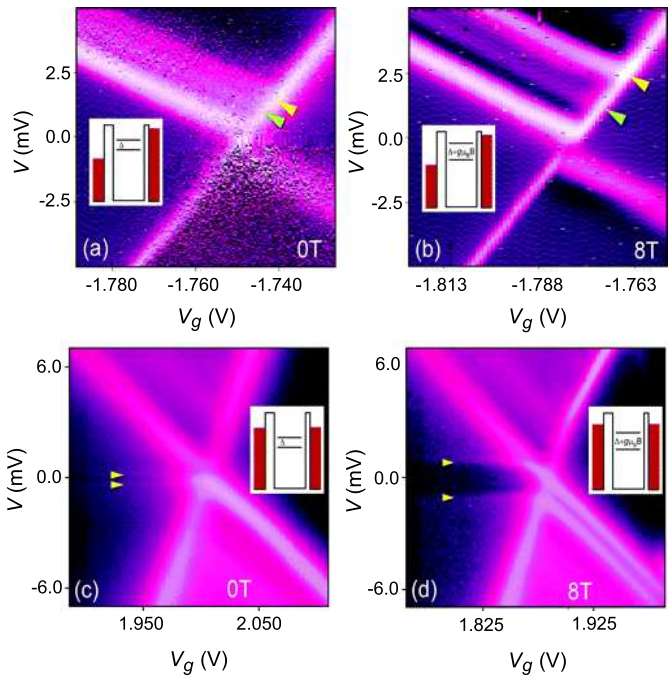

Figure 1.5: Experimental data for transport through single Mn_{12} by Jo *et al.* [23]. Two-dimensional plots of the differential conductance as a function bias V and gate voltage V_g show peaks due to magnetic excitations. The presence of a magnetic field (b),(d) leads to a shift of the peaks observed for vanishing magnetic field (a),(c).

effect [5–7] both arising due to large ionization energies and the small size of molecular structures are very prominent examples in this context.

However, understanding the physics in single-molecule transistors is not only motivated by promising technological applications, it has also been shown that the presence of specific internal molecular degrees of freedom leads to numerous novel quantum transport phenomena that go beyond the physics observed in larger nanostructures such as quantum dots. In this context, much attention has been paid to effects arising from the coupling of electronic degrees of freedom to (i) vibrations, (ii) spins, and (iii) different chemical conformations of the molecule.

Pioneering transport measurements on vibrating single-molecule transistors have been performed by Park *et al.* [12]. The conductance of a molecular junction consisting of a single C_{60} molecule connected to two gold electrodes has been investigated with respect to the coupling between the center-of-mass motion of the C_{60} molecule and single-electron hopping. This coupling leads to quantized oscillations of the C_{60} molecule against the gold surface and drives the molecule out of vibrational equilibrium at sufficiently large bias voltages. As a consequence, the motion of elec-

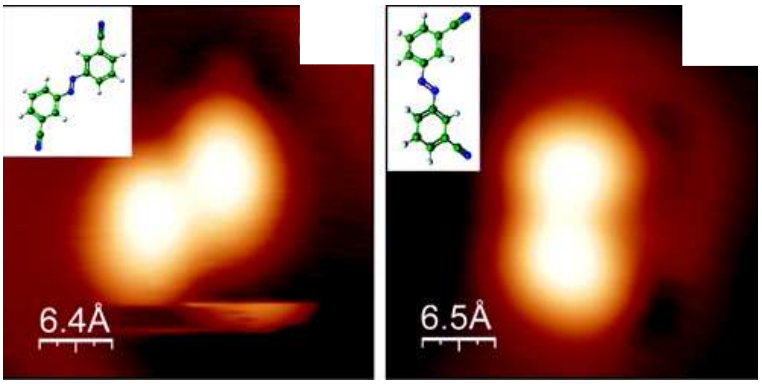

Figure 1.6: Scanning tunneling microscope images for azobenzene by Henningsen *et al.* [50]. Conformational switching is induced by the current through the molecule.

trons through the molecule is strongly modified by single-electron charging and the quantization of vibrational energy levels. A remarkable feature is the occurrence of equidistant vibrational sidebands in the differential conductance with an energy of approximately 5 meV, where each step in the tunneling current can be attributed to the excitation of a certain number of phonons, cf. Fig. 1.4. This excitation is reminiscent of the Franck-Condon processes encountered in electron-transfer and light-absorption processes in molecules, where the vibrational excitation accompanies the electronic motion [12]. This transport measurement has demonstrated that single-electron tunneling can be used to excite and probe the motion of a molecule, which behaves as a high-frequency nanomechanical oscillator.

The role of coupling between electronic and magnetic degrees of freedom in transport through single molecules has been considered in recent experiments on manganese Mn_{12} derivatives by Jo *et al.* [23] and Heersche *et al.* [22]. These experiments on devices incorporating magnetic molecules report signatures of magnetic states and their associated magnetic anisotropy. Among other phenomena, they focus on the fine structure of the Coulomb blockade peaks in the differential conductance dI/dV of single-molecule magnets, cf. Fig. 1.5. Here the occurrence of additional magnetic sidebands is due to magnetic excitations of the local spin. Each peak in the differential conductance corresponds to an inelastic sequential tunneling event, which changes the charge of the molecule by one and the spin by 1/2. Applying an external magnetic field that couples linearly to the magnetic moment of the molecule gives rise to an additional Zeeman splitting and allows one to distinguish these magnetic sidebands from vibrational sidebands and other observed structures. Furthermore, cotunneling processes, which give the dominant contribution to the tunneling current through the molecular junction in the Coulomb blockade regime, have been observed [23].

An essential requirement for electric circuits of nanoscale dimensions is a molec-

ular device that can be switched between two distinct conductive states. Because of intrinsic bistabilities many single-molecule junctions reveal switching behavior, e.g. involving cis and trans isomers of a molecule [50–60]. Among many other important works, a recent experiment on oligo-phenylenevinylene (OPV3) derivatives by Danilov *et al.* [51] has addressed the topic of current-induced conformational switching. The current-voltage characteristics show switching behavior between two distinct conformational states. Here the observed bistability leading to the switching behavior is associated with the breaking and reformation of a thiol bond in the contact zone between molecule and electrode. Remarkably, it takes approximately 10^{10} electrons tunneling through the molecular junction to induce a single switching event. In other words, the chemical conformation of the molecule persists over times extremely long compared to the average electronic tunneling time. Such low-quantum-yield switching has also been observed in various other experiments, for instance, in STM measurements on azobenzene derivatives [50].

In summary, a very large number of molecules ranging from the hydrogen molecule to DNA has been investigated experimentally in molecular junctions. Depending on the molecule-lead coupling, vibrational and magnetic excitations appear as steps or kinks in the current-voltage characteristics. The appearance of steps in the current (corresponding peaks in dI/dV) is characteristic of the weak coupling regime which is best realized in breakjunction-like experiments, whereas the kinks (corresponding steps in dI/dV) are usually observed in the strong coupling regime, realized in STM experiments. Specific aspects of experimental results will also be referred to in the following chapters, when we discuss in detail the roles of (i) electron-phonon interaction, (ii) magnetic anisotropy, and (iii) cis/trans-isomerism in single-molecule transistors.

Recently, research in the field of molecular electronics has also been inspired by the prevailing optimism about graphene-based electronics [61; 62]. Remarkably, at the time when silicon-based technology is approaching its natural limit, graphene seems to offer an exceptional choice among all other new candidate materials. While most approaches essentially rely on considering graphene as a new channel materials for field-effect transistors (FET), others are interested in studying its properties as a single electron transistor (SET) in the context of molecular electronics [61; 62]. Here the main advantage is that graphene nanostructures are stable down to a single benzene ring and that everything including conducting channels, quantum dots, barriers can be cut out from a graphene sheet in any size using conventional top-down methods such as electron-beam lithography and dry etching. Interestingly, for a minimum feature size of $\simeq 10\,\mathrm{nm}$, graphene reveals conductance gaps due to Coulomb blockade corresponding to energies of the order of eV, which should, in principle, allow SET circuitry operational at room temperature. Indeed, the main reason why SET architecture has failed to establish itself is the difficulties associated with the extension of its operation to room temperature due to poor stability of materials at the nanometer scale. Currently, graphene is considered a promising candidate to overcome these problems [61; 62].

1.4 Theoretical treatment

Theoretical works on quantum transport through molecules and other nanostructures fall into two classes. The first relies on a detailed modeling of the molecule and the contact region between the molecule and the leads by the use of density functional theory (DFT) [63; 64]. In a second step, electronic transport is described within a Landauer theory using the Kohn-Sham potentials of density functional theory [16; 65–67]. While this method is successful in obtaining the correct (experimentally observed) positions of energy resonances in the differential conductance, the main problem that it suffers from the fact that the conductivity of molecules is overestimated by one to two orders of magnitude. However, note that density functional theory, which was actually developed to obtain the ground state of an isolated atomic or molecular structure, is *per se* inappropriate for the description of nonequilibrium phenomena, since there exists no extension of the Hohenberg-Kohn theorems to scattering problems such a electronic transport, so far. The DFT approach should therefore be considered a first approximation rather than a realistic theoretical modeling of the transport problem. Furthermore, the inclusion of specific internal molecular degrees of freedom such as vibrations leads to conceptual problems.

Recently great efforts have been made to overcome these difficulties by approaches using time-dependent density functional theory (TDDFT), the main success of which has been its application to the calculation of excited states of many-particle systems. Time-dependent density functional theory relies on the Runge-Gross theorem [68], which is the time-dependent analogue of the Hohenberg-Kohn theorem [69] for DFT. Yet only time will tell if TDDFT is really suitable for an accurate description of single-molecule devices out of equilibrium [64; 70].

The second class of theoretical works on quantum transport through molecules relies on a parametric modeling of the relevant molecular levels. Many of these approaches start from a generic Anderson-like model and employ nonequilibrium (Keldysh) Green function methods [71; 72], density-matrix theory [73], and Wilson's renormalization group [74]. The molecular junction is usually described by a Hamiltonian of type

$$H = H_{\mathrm{mol}} + H_{\mathrm{leads}} + H_t, \tag{1.1}$$

where H_{mol} describes the molecule, H_{leads} describes the leads, and H_t describes the coupling between them. Usually H_{mol} and H_{leads} can be diagonalized exactly in the absence of the coupling, which allows for a perturbative expansion in H_t. This approach has been successful in describing most of the observed transport phenomena in quantum dots and is motivated by the fact that single-molecule junctions reveal similar effects. Its main advantage as compared to *ab initio* calculations is the possibility of including specific molecular degrees of freedom such as vibrations, spins, and chemical conformations. Furthermore, it also allows for a more realistic modeling of the leads, e.g. using a Luttinger-liquid model [75]. Electronic correlation effects, that are usually not included in DFT calculations, can readily be taken into account. Dissipative effects, which lead to the relaxation of vibrational modes or spin dynamics, can be described either phenomenologically in terms of additional

relaxations rates or more microscopically by adding the coupling to a bosonic bath or spin bath, respectively.

The present work belongs to the second group of approaches. Details on specific methods frequently used in quantum transport theory are contained in Chapter 2.

1.5 Overview

The present work is organized as follows. Chapter 2 contains an introduction to methods frequently used in quantum transport theory which serve as a basis for our main results discussed in the following chapters. We survey transport phenomena in mesoscopic systems and derive master equations from a density-matrix formalism. We compute the inelastic sequential tunneling rates for the transitions between the many-particle states of the system. The presence of vibrations and of the spin leads to the emergence of Franck-Condon matrix elements and Clebsch-Gordan coefficients in the rates, respectively. Subsequently, we calculate next-to-leading order tunneling processes. The transition rates for cotunneling are obtained within a T-matrix formalism. Furthermore, we consider the conductance of Anderson-type models in general and discuss the Meir-Wingreen-formula. We consider transport within the Keldysh formalism showing schematically how the classical equations of motion can be obtained from that approach. Finally, we discuss Kondo transport and renormalization group techniques.

In Chapter 3 we consider transport through single-molecule magnets. Our motivation derives from the idea of *molecular spintronics* [11; 41; 76] which consists of integrating the promising concepts of molecular electronics and spintronics. We propose that the coupling between electronic and magnetic degrees of freedom leads to interesting many-body effects that go beyond the well-understood occurrence of emission sidebands in the differential conductance due to inelastic electronic tunneling. In this respect, the most essential requirement for spintronics devices is the ability to effectively control and detect the spin. We show that magnetic *anisotropy* is crucial for slow spin relaxation in magnetic molecules, which can be exploited in the context of current-induced spin reading and writing. One of our main findings is that the current can be highly polarized for time periods which are exponentially long as a function of the molecular excitation energies, if the molecule in the junction is prepared in a magnetic initial state. The net spin moment transmitted from one lead to the other depends strongly on the initial orientation of the molecular spin and can be much larger than the initial molecular spin itself. This *spin amplification effect* effectively allows one to *read out* the spin information. Importantly, the leads need not be polarized. However, spin writing requires a molecular junction that consists of one ferromagnetic and one nonmagnetic lead. Interestingly, current-induced switching of the spin to a predetermined state only requires the presence of an electric field in form of a bias voltage, but no magnetic field, and is thus a comparatively fast process.

The proposed setup leads to interesting physics beyond the effect of spin writing,

including the occurrence of large negative differential conductance (NDC) at high temperatures. This effect is distinct from the NDC found at low temperatures in the fine structure of the differential conductance peaks due to inelastic processes. Instead it is related to a new *spin blockade* mechanism. By this we mean the suppression of the single-electron tunneling rates for electrons of one spin species due to density-of-states effects. We also find that the *charge* transmitted through a molecule prepared in a particular spin state depends strongly on the initial state in certain parameter regimes. This effect is related to the giant spin amplification mentioned above but appears in the charge channel and is thus more robust against relaxation processes.

A very prominent spin-related transport phenomenon known as the Kondo effect is considered in Chapter 4. Here we are particularly interested in the interplay of magnetic and vibrational degrees of freedom in transport through vibrating single-molecule transistor. We find that the coupling between electronic and vibrational degrees of freedom results in an unusual behavior of the differential conductance, which is distinct from the physics observed in larger nanostructures. First the dependence of the Kondo temperature on the gate voltage is much weaker than in quantum dots. Second the Coulomb blockade is strongly asymmetric about the charge degeneracy points (marking the transition from the non-Kondo to the Kondo valley), i.e. the peaks in the differential conductance are well pronounced on one side of the degeneracy points, whereas they almost vanish on the other side. Experimental evidence for these two unusual features has been obtained in recent transport experiments on organic complexes [19; 77; 78]. The Kondo temperature, which is determined by the exchange coupling constant, is computed employing a Schrieffer-Wolff transformation of the Anderson-Holstein Hamiltonian and a *poor man's scaling* approach. The sequential tunneling regime is described using rate equations.

The topic of current-induced conformational switching is addressed in Chapter 5. Motivated by recent experiments on azobenzene derivatives, we study this process for molecules which exhibit two (meta)stable conformations in the neutral state, but only a single stable conformation in the ionic state. We derive and analyze appropriate Fokker-Planck equations, obtained from a density-matrix formalism starting from a generic model, and present comprehensive analytical and numerical results for the switching dynamics. In particular, we are interested in the quantum yield which is the probability for a single electron tunneling through the system to switch the molecule. We first derive a set of quasi-classical Boltzmann equations which describe the tunneling dynamics in the absence of dissipation. Subsequently, the Boltzmann equation is extended to account for dissipation, resulting in a set of Fokker-Planck equations. This allows us to derive a formal solution for the quantum yield, which is based on this Fokker-Planck equation. Finally, the formal solution is analyzed in detail, both analytically and numerically.

We show that conformational switching may also be induced by the current involving two subsequent sequential tunneling processes. Here, our main focus is the regime of strongly asymmetric couplings to the leads, corresponding to the experimental setup of a scanning tunneling microscope conductance measurement. We treat the current flow within the sequential tunneling approximation, which is justi-

fied in setups with passivated substrates. Our central finding is that there exists a rather sharp crossover between two qualitatively different switching mechanisms as a function of temperature. For low temperatures, the switching process is induced by tunneling electrons when the vibrational coordinate is close to the minimum of the cis state. We call this process current-induced switching. Beyond a critical temperature, switching is strongly dominated by tunneling processes which occur close to the maximum of the barrier between the cis and the trans states. We refer to this process as thermally activated. Remarkably, this happens long before the temperature becomes of the order of the barrier height. Experimentally, the two switching mechanisms are readily distinguished by their different temperature dependences. While the current-induced switching exhibits only weak temperature sensitivity, thermal activation processes follow Arrhenius behavior. Moreover, our results predict that the quantum yield depends exponentially on the tunneling rate to the substrate which makes it highly sensitive to the level of passivation of the substrate.

2 Quantum Transport Theory

In the present chapter we survey transport phenomena in mesoscopic systems and discuss formalisms frequently used in quantum transport theory, which provide the basis for the research presented in the remaining chapters of this thesis. We derive master equations describing the electronic tunneling through a tunnel junction and a Golden-Rule expression for the inelastic sequential transition rates. Employing a T-matrix formalism this approach is readily generalized to include higher-order processes such as cotunneling. For mesoscopic tunnel junctions that can be modeled by an Anderson-type Hamiltonian, the conductance is directly related to the spectral function of the single impurity, as shown by Meir and Wingreen [79]. Furthermore, we show how the classical equations of motion can be obtained from the Keldysh formalism. In the end, we discuss Kondo transport and renormalization group techniques.

2.1 Transport phenomena in mesoscopic systems

Mesoscopic systems reveal a number of nonequilibrium phenomena which differ distinctly from the transport properties of macroscopic electric devices. Most strikingly, quantum dots, carbon nanotubes and single molecules usually do not show ohmic response over wide ranges of bias voltage. In such systems, the feature size is smaller than the electron mean free path [80]. Understanding transport through nanostructures goes beyond the laws of classical electrodynamics and requires a quantum mechanical description, taking into account both the discreteness of the electronic charge and electronic interferences.

Many mesoscopic systems show a significant suppression of the conductance at low bias voltages. This behavior known as the Coulomb blockade is characteristic of tunnel junctions, where the system (e.g. a molecule or a quantum dot) is separated from the leads by large potential barriers. In equilibrium electronic tunneling through the junction is *blocked* entirely. Only if the energy of the charge carriers in the leads is increased by applying a bias voltage V can the barrier be overcome to allow for the flow a large current. The critical bias threshold for the onset of tunneling processes is determined by the charging energy of the quantum dot or the molecule, respectively, and is revealed as a step in the current I and a corresponding peak in the differential conductance dI/dV. Increasing the bias voltage further may excite higher charge states and open up additional transport channels, resulting in further peaks in dI/dV. In many experiments the electrostatic energies can be shifted by applying a gate voltage.

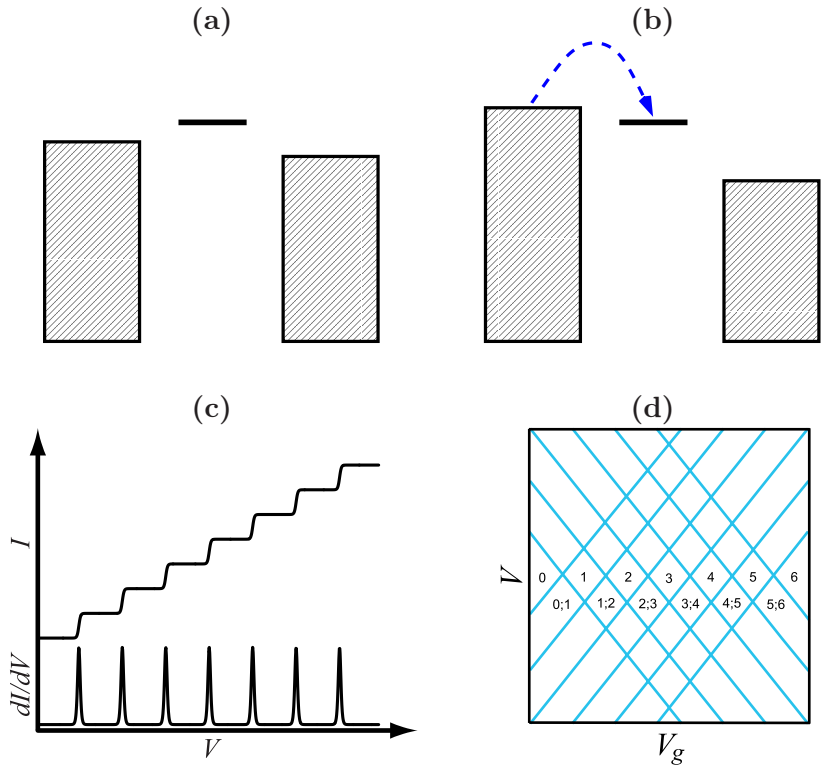

Figure 2.1: Energy scheme of a quantum dot (a) in the Coulomb blockade and (b) in the sequential tunneling regime. In (a) the lead electrons do not have enough energy to tunnel onto the dot. In contrast, in (b) electrons can tunnel from the left lead onto the dot and, subsequently, from the dot into the right lead, resulting in a large current. (c) Current I and differential conductance dI/dV as a function of bias V. (d) Differential conductance dI/dV as a function of bias V and gate voltage V_g. The characteristic pattern revealed in the density plot is known as *Coulomb diamonds*. The numbers denote the accessible charge states.

Plotting the differential conductance dI/dV as a function of bias voltage V and gate voltage V_g leads to a characteristic two-dimensional pattern named *Coulomb diamonds*, cf. Fig. 2.1. Each peak separating two plateaus with different conductance can be attributed to a certain charging energy of the system. The energetically accessible charge states are different for each plateau. Also note that the equilibrium (zero bias) occupancy changes as a function of gate voltage.

In the regime of weak system-lead coupling transport is usually described by rate equations for the occupation probabilities of the many-body states. To lowest-order in the tunneling amplitude, the rates are given by an expression equivalent to Fermi's Golden Rule describing sequential tunneling processes. However, if these processes are suppressed due to blockade mechanisms, such as the Coulomb blockade or the Franck-Condon blockade [29], transport is dominated by next-to-leading order pro-

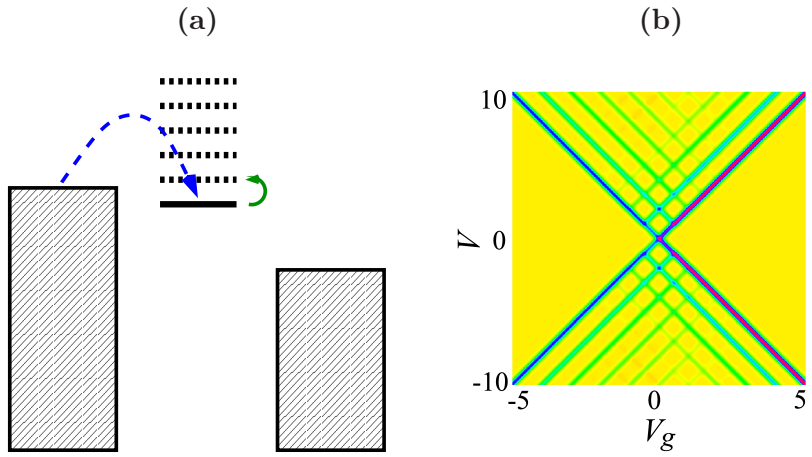

Figure 2.2: (a) Energy scheme and (b) differential conductance dI/dV as a function of bias V and gate voltage V_g, obtained for a vibrating single-molecule transistor. Each excitation of phonons corresponds an inelastic tunneling process revealed as a peak in dI/dV. Figure (b) is taken from Ref. [29]. Voltages are given in multiples of the vibrational ground state energy.

cesses called cotunneling, describing the coherent transfer of an electron from one terminal of the junction to another. Sequential tunneling and cotunneling rates can be derived using a density-matrix approach or T-matrix formalism, as shown in the following section.

In contrast to transport through quantum dots, electronic tunneling through single-molecule junctions is strongly affected by inelastic scattering processes resulting from the presence of internal molecular degrees of freedom. Consider, for instance, a vibrating molecule between two electrodes. In case of strong enough coupling between the electronic and vibrational degrees of freedom, electrons can excite a phonon on the molecule while passing through the junction, if their energy is sufficiently high. Likewise, electronic tunneling may also involve the excitation or de-excitation of several phonons. For a harmonic potential surface of the vibrational mode, the equidistant excitation spectrum of the molecule leads to equidistant peaks in the differential conductance, where each peak represents the excitation of a certain number of phonons, cf. Fig. 2.2. If vibrational relaxation is slow compared to the average tunneling time, the current may effectively drive the molecule out thermal equilibrium, cf. e.g. Refs. [14; 29].

Other causes of inelastic scattering observed in transport through single-molecule transistors are, for instance, magnetic excitations of a local spin and switching between different chemical conformations.

A very prominent spin-related transport phenomenon in mesoscopic systems known as the Kondo effect is the coherent exchange between the spin of a single impurity and the Fermi sea of conduction electrons. The Kondo effect is well known

from the study of the resistivity of metals due to scattering off magnetic impurities. There the scattering causes an increase in the resistivity with decreasing temperature. The anomalous behavior, first explained by Kondo in 1964 [81], turns out to be an intriguing many-body effect [82; 83]. Interestingly, the quantum dot with an odd number of additional electrons behaves in a similar way as the spin one-half magnetic impurity. The occurrence of the Kondo resonance has been observed for numerous nanostructures. Strikingly, here it manifests itself as an enhancement of the zero bias *conductance* at low temperatures.

A theoretical description of the Kondo effect is possible in terms of the Anderson model and renormalization group techniques. We will come back to more details in the last section of the present chapter.

2.2 Master equation

In this section we derive master equations describing the quantum transport in the regime of weak coupling to a reservoir. The molecular junction is modeled by an Anderson-like Hamiltonian of the form $H = H_{\rm mol} + H_{\rm leads} + H_t$, with $H_{\rm leads} = \sum_{\alpha\mathbf{k}} \epsilon_{\mathbf{k}} a^\dagger_{\alpha\mathbf{k}} a_{\alpha\mathbf{k}}$ and $H_t = \sum_{\alpha\mathbf{k}\sigma} t_\alpha\, a^\dagger_{\alpha\mathbf{k}\sigma} d_\sigma + \text{h.c.}$, where $a^\dagger_{\alpha\mathbf{k}\sigma}$ creates an electron with momentum $\mathbf{k}$, spin σ and $\epsilon_{\mathbf{k}}$ in lead α, while $d^\dagger_\sigma$ creates an electron with spin σ on the molecule. Specific molecular degrees of freedom are described by the $H_{\rm mol}$. The main requirement for the use of rate equations is the presence of temperatures large compared to the current-induced level broadening of the molecular states.

The starting point of the derivation is the von Neumann equation describing the time evolution of the density matrix ρ of the system,

$$\frac{\partial \rho(t)}{\partial t} = -\frac{i}{\hbar}\left[H_t(t), \rho(t)\right]. \tag{2.1}$$

Integrating from time zero to time t gives

$$\rho(t) = \rho(0) - i\int_0^t dt' \left[H_t(t'), \rho(t')\right], \tag{2.2}$$

and

$$\frac{\partial \rho(t)}{\partial t} = -\frac{i}{\hbar}\left[H_t(t), \rho(0)\right] - \frac{1}{\hbar^2}\int_0^t dt' \left[H_t(t), \left[H_t(t'), \rho(t')\right]\right], \tag{2.3}$$

respectively. Here operators O with an explicit time argument are in the interaction picture,

$$O(t) = e^{i(H_{\rm mol}+H_{\rm leads})t/\hbar}\, O\, e^{-i(H_{\rm mol}+H_{\rm leads})t/\hbar}. \tag{2.4}$$

The dynamics of the molecule is described by the reduced density matrix which is obtained by tracing out the degrees of freedom of the leads,

$$\rho_{\rm mol}(t) = \mathrm{Tr}_{\rm leads}\, \rho(t). \tag{2.5}$$

Solving Eq. (2.3) for ρ relies on two approximations [73; 84]. The large-reservoir approximation allows us to write the density matrix as a direct product,

$$\rho(t) \simeq \rho_{\mathrm{mol}}(t) \otimes \rho_{\mathrm{leads}}, \tag{2.6}$$

of the density matrices $\rho_{\mathrm{mol}}(t)$ and ρ_{leads} describing the degrees of freedom of the molecule and the leads. In addition, we neglect effects of the molecule on the leads, which are assumed to remain in separate thermal equilibria despite the applied bias voltage and which are described by Fermi distribution functions,

$$f_\alpha(\epsilon) = \frac{1}{e^{\frac{\epsilon-\mu_\alpha}{T}}+1}, \tag{2.7}$$

at chemical potentials μ_α. The Markov approximation permits us to replace

$$\rho_{\mathrm{mol}}(t') \simeq \rho_{\mathrm{mol}}(t) \tag{2.8}$$

in Eq. (2.3) and to replace the lower limit of integration by minus infinity, which means that memory effects of the molecular dynamics are ignored. In other words the change of ρ_{mol} at time t should only depend on ρ_{mol} at time t itself on a coarse-grained time average. These substitutions lead us to

$$\frac{\partial \rho_{\mathrm{mol}}(t)}{\partial t} = -\int_0^t dt' \mathrm{Tr}_{\mathrm{leads}} \left[H_t(t), \left[H_t(t'), \rho_{\mathrm{mol}}(t) \otimes \rho_{\mathrm{leads}}\right]\right]. \tag{2.9}$$

The time correlation functions in Eq. (2.9) are supposed to decay fast for times $t-t'$ long compared to the electronic relaxation time of the leads. Therefore, we may introduce $t'' = t - t'$ as a new variable and let the upper limit of integration go to infinity,

$$\frac{\partial \rho_{\mathrm{mol}}(t)}{\partial t} = -\int_0^\infty dt'' \mathrm{Tr}_{\mathrm{leads}} \left[H_t, \left[H_t(-t''), \rho_{\mathrm{mol}} \otimes \rho_{\mathrm{leads}}\right]\right]. \tag{2.10}$$

Going back to the Schrödinger picture yields

$$\frac{\partial \rho_{\mathrm{mol}}}{\partial t} = -i\left[H_{\mathrm{mol}}, \rho_{\mathrm{d}}\right] - \int_0^\infty dt'' \mathrm{Tr}_{\mathrm{leads}} \left[H_t, \left[H_t(-t''), \rho_{\mathrm{mol}} \otimes \rho_{\mathrm{leads}}\right]\right], \tag{2.11}$$

where the first term describes the unperturbed time evolution. Opening the double commutator gives four terms, $\partial\rho_{\mathrm{mol}}/\partial t \equiv -i\left[H_{\mathrm{d}}, \rho_{\mathrm{d}}(t)\right] + A + B + C + D$, which read [85; 86]

$$A = -\mathrm{Tr}_{\mathrm{leads}} \int_0^\infty dt''\ H_t e^{-i(H_{\mathrm{mol}}+H_{\mathrm{leads}})t''} H_t e^{i(H_{\mathrm{mol}}+H_{\mathrm{leads}})t''} \rho_{\mathrm{mol}}(t) \otimes \rho_{\mathrm{leads}}, \tag{2.12}$$

$$B = \mathrm{Tr}_{\mathrm{leads}} \int_0^\infty dt''\ H_t \rho_{\mathrm{mol}}(t) \otimes \rho_{\mathrm{leads}} e^{-i(H_{\mathrm{mol}}+H_{\mathrm{leads}})t''} H_t e^{i(H_{\mathrm{mol}}+H_{\mathrm{leads}})t''}, \tag{2.13}$$

$$C = \mathrm{Tr}_{\mathrm{leads}} \int_0^\infty dt''\ e^{-i(H_{\mathrm{mol}}+H_{\mathrm{leads}})t''} H_t e^{i(H_{\mathrm{mol}}+H_{\mathrm{leads}})t''} \rho_{\mathrm{mol}}(t) \otimes \rho_{\mathrm{leads}} H_t, \tag{2.14}$$

$$D = -\mathrm{Tr}_{\mathrm{leads}} \int_0^\infty dt''\ \rho_{\mathrm{mol}}(t) \otimes \rho_{\mathrm{leads}} e^{-i(H_{\mathrm{mol}}+H_{\mathrm{leads}})t''} H_t e^{i(H_{\mathrm{mol}}+H_{\mathrm{leads}})t''} H_t. \tag{2.15}$$

Inserting the tunneling Hamiltonian H_t and tracing over the degrees of freedom of the leads,

$$\mathrm{Tr}_{\mathrm{leads}}\left(\rho_{\mathrm{leads}} a^{\dagger}_{\alpha_1\mathbf{k}_1\sigma_1} a_{\alpha_2\mathbf{k}_2\sigma_2}\right) = \delta_{\alpha_1\alpha_2}\delta_{\mathbf{k}_1\mathbf{k}_2}\delta_{\sigma_1\sigma_2} f_\alpha(\epsilon_{\mathbf{k}}), \tag{2.16}$$

$$\mathrm{Tr}_{\mathrm{leads}}\left(\rho_{\mathrm{leads}} a_{\alpha_1\mathbf{k}_1\sigma_1} a^{\dagger}_{\alpha_2\mathbf{k}_2\sigma_2}\right) = \delta_{\alpha_1\alpha_2}\delta_{\mathbf{k}_1\mathbf{k}_2}\delta_{\sigma_1\sigma_2}\left[1 - f_\alpha(\epsilon_{\mathbf{k}})\right], \tag{2.17}$$

we obtain

$$\begin{aligned} A &= -\int_0^\infty dt'' \Big\{ \sum_{\alpha\mathbf{k}\sigma} |t_\alpha|^2 f(\epsilon_{\mathbf{k}} - \mu_\alpha) e^{i\epsilon_{\mathbf{k}} t''} d_\sigma e^{-iH_{\mathrm{mol}} t''} d^{\dagger}_\sigma e^{iH_{\mathrm{mol}} t''} \rho_{\mathrm{mol}} \\ &\quad + |t_\alpha|^2 \left[1 - f(\epsilon_{\mathbf{k}} - \mu_\alpha)\right] e^{-i\epsilon_{\mathbf{k}} t''} d^{\dagger}_\sigma e^{-iH_{\mathrm{mol}} t''} d_\sigma e^{iH_{\mathrm{mol}} t''} \rho_{\mathrm{mol}} \Big\}, \end{aligned} \tag{2.18}$$

$$\begin{aligned} B &= \int_0^\infty dt'' \Big\{ \sum_{\alpha\mathbf{k}\sigma} |t_\alpha|^2 \left[1 - f(\epsilon_{\mathbf{k}} - \mu_\alpha)\right] e^{i\epsilon_{\mathbf{k}} t''} d_\sigma \rho_{\mathrm{mol}} e^{-iH_{\mathrm{mol}} t''} d^{\dagger}_\sigma e^{iH_{\mathrm{mol}} t''} \\ &\quad + |t_\alpha|^2 f(\epsilon_{\mathbf{k}} - \mu_\alpha) e^{-i\epsilon_{\mathbf{k}} t''} d^{\dagger}_\sigma \rho_{\mathrm{mol}} e^{-iH_{\mathrm{mol}} t''} d_\sigma e^{iH_{\mathrm{mol}} t''} \Big\}, \end{aligned} \tag{2.19}$$

$$\begin{aligned} C &= \int_0^\infty dt'' \Big\{ \sum_{\alpha\mathbf{k}\sigma} |t_\alpha|^2 \left[1 - f(\epsilon_{\mathbf{k}} - \mu_\alpha)\right] e^{-i\epsilon_{\mathbf{k}} t''} e^{-iH_{\mathrm{mol}} t''} d_\sigma e^{iH_{\mathrm{mol}} t''} \rho_{\mathrm{mol}} d^{\dagger}_\sigma \\ &\quad + |t_\alpha|^2 f(\epsilon_{\mathbf{k}} - \mu_\alpha) e^{i\epsilon_{\mathbf{k}} t''} e^{-iH_{\mathrm{mol}} t''} d^{\dagger}_\sigma e^{iH_{\mathrm{mol}} t''} \rho_{\mathrm{mol}} d_\sigma \Big\}, \end{aligned} \tag{2.20}$$

$$\begin{aligned} D &= -\int_0^\infty dt'' \Big\{ \sum_{\alpha\mathbf{k}\sigma} |t_\alpha|^2 f(\epsilon_{\mathbf{k}} - \mu_\alpha) e^{-i\epsilon_{\mathbf{k}} t''} \rho_{\mathrm{mol}} e^{-iH_{\mathrm{mol}} t''} d_\sigma e^{iH_{\mathrm{mol}} t''} d^{\dagger}_\sigma \\ &\quad + |t_\alpha|^2 \left[1 - f(\epsilon_{\mathbf{k}} - \mu_\alpha)\right] e^{i\epsilon_{\mathbf{k}} t''} \rho_{\mathrm{mol}} e^{-iH_{\mathrm{mol}} t''} d^{\dagger}_\sigma e^{iH_{\mathrm{mol}} t''} d_\sigma \Big\}. \end{aligned} \tag{2.21}$$

For the bias voltage drop,

$$eV = \mu_L - \mu_R \tag{2.22}$$

we always consider the case of symmetric capacitive couplings if not stated otherwise,

$$\mu_L = -\mu_R = \frac{eV}{2}. \tag{2.23}$$

Deriving an equation of motion for the occupation probabilities,

$$P^n \equiv \langle n| \rho_{\mathrm{mol}} |n\rangle, \tag{2.24}$$

of the molecular many-body states n requires the evaluation of matrix elements $\langle n|\partial\rho_{\mathrm{mol}}/\partial t|n\rangle$. The summation over momenta can be rewritten as an integral over energy, where we assume the density of state ν_α of each lead α to be constant. The time integral over exponentials then yields delta functions expressing the energy conservation during the tunneling processes. Finally we arrive at a set of coupled rate equations,

$$\frac{\partial P^n}{\partial t} = \sum_{m\neq n} P^m R_{m\to n} - P^n \sum_{m\neq n} R_{n\to m}. \tag{2.25}$$

with tunneling rates

$$R_{n\to m} = \frac{2\pi}{\hbar}\sum_{\alpha\sigma}|t_\alpha|^2\nu_\alpha\Big(f_\alpha(-\epsilon_n^{\rm d}+\epsilon_m^{\rm d})|C_{nm}^\sigma|^2 + \big[1-f_\alpha(\epsilon_n^{\rm d}-\epsilon_m^{\rm d})\big]\,|C_{mn}^\sigma|^2\Big), \quad (2.26)$$

for the transition from molecular many-body state n to state m. Here we have assumed rapid dephasing for the vanishing of off-diagonal matrix elements of the density matrix [87]. Equation (2.26), which is equivalent to Fermi's Golden Rule, gives the lowest-order contribution to the total tunneling rate within the perturbative expansion in H_t.

Equation (2.25) describing the dynamics of all molecular degrees of freedom expresses the conservation of probability. The change of the occupation probability of any state n, $\partial P^n/\partial t$, is governed by the net flow of probabilities into this molecular state, $\sum_{m\neq n} P^m R_{m\to n}$, and out of this molecular state, $P^n\sum_{m\neq n} R_{n\to m}$. The interesting physics arising from the presence of specific molecular degrees of freedom is essentially contained in the overlap matrix elements

$$C_{mn}^\sigma \equiv \langle m|d_\sigma|n\rangle, \quad (2.27)$$
$$C_{mn}^{\sigma\dagger} \equiv \langle m|d_\sigma^\dagger|n\rangle. \quad (2.28)$$

This matrix determines the relative weights and selection rules for the current-induced transitions between two molecular eigenstates. For instance C_{mn}^σ ($C_{mn}^{\sigma\dagger}$) can only be non-vanishing if the occupancy of state n is larger (smaller) than the occupancy of state m. We come back to the role of selection rules for magnetic and vibrational quantum numbers at a later time.

2.3 T-matrix and generalized Fermi's Golden Rule

The Golden-Rule expression for the transition rates derived in the previous section can be readily generalized to include higher-order tunneling processes. Here the initial state $|i\rangle$ and the final state $|f\rangle$ are coupled by multiple scatterings described by the perturbation H_t. The following discussion is based on Ref. [83].

In the interaction picture, the time evolution of any state $|\psi\rangle$ due to the perturbation H_t is given by the Schrödinger equation

$$i\hbar\frac{\partial}{\partial t}|\psi(t)\rangle = H_t(t)|\psi(t)\rangle. \quad (2.29)$$

This means that the wave functions $|\psi\rangle$ at time t_0 and $|\psi\rangle$ at time t are related to one another by a unitary operator,

$$|\psi(t)\rangle = U(t,t_0)|\psi(t_0)\rangle. \quad (2.30)$$

The iterative solution for the time evolution operator U is given by

$$U(t,t_0) = 1 + \frac{1}{i\hbar}\int_{t_0}^t dt_1\, H_t(t_1) + \frac{1}{(i\hbar)^2}\int_{t_0}^t dt_1\, H_t(t_1)\int_{t_0}^{t_1} dt_2\, H_t(t_2) + \cdots. \quad (2.31)$$

In the Schrödiner picture the corresponding time evolution operator is $e^{-iH_0t/\hbar}U(t,t_0)e^{iH_0t_0/\hbar}$, where $H_0 = H - H_t$ is the unperturbed Hamiltonian, and the time dependence of the initial state is given by

$$|i(t)\rangle = e^{-iH_0t/\hbar}U(t,t_0)e^{iH_0t_0/\hbar}|i\rangle. \tag{2.32}$$

The probability of finding the system in state $|f\rangle$ with energy E_f at time t on the condition that it had been initially prepared in state $|i\rangle$ with energy E_i, before the perturbation was switched on, is given by the overlap $P_{if}(t) = |\langle f|i(t)\rangle|^2$. The time derivative $dP_{if}(t)/dt$ is therefore the change in probability per unit time, which we interpret as the transition rate Γ_{if} between initial and final state. Evaluating all time integrals one obtains

$$\Gamma_{if} = \frac{2\pi}{\hbar}\,|\langle f|T|i\rangle|^2\;\delta(E_f - E_i), \tag{2.33}$$

where the T-matrix is self-consistently given by

$$T = H_t + H_t\,\frac{1}{E_i - H_0 + i\eta}\,T. \tag{2.34}$$

This expression is a generalization of Fermi's Golden Rule. To second order in the H_t one recovers the sequential tunneling rates derived in the previous section. Next-to-leading-order processes are proportional to the fourth power of the tunneling matrix elements t_α. If the lowest-order processes are suppressed due to blockade mechanisms, e.g. due to the Coulomb blockade or the Franck-Condon blockade, *cotunneling* processes naturally yield the dominant contribution to the electronic transport. A cotunneling process describes the coherent transfer of an electron from one terminal of the nanostructure to another. Importantly, the intermediate state may have an energy that is much larger than the energy of the initial state. Thus cotunneling is referred to as a virtual process.

To fourth order in the tunneling Hamiltonian, the transition rate for transferring an electron from lead α to lead α' while changing the molecular state from n to n' yields

$$\Gamma^{nn'}_{\alpha\alpha'} = \frac{2\pi}{\hbar}\left|\langle f|\langle n'|H_t\frac{1}{E_i - H_0}H_t|n\rangle|i\rangle\right|^2\delta(E_f - E_i). \tag{2.35}$$

In this notation the initial state $|n\rangle|i\rangle$ and final state $|n'\rangle|f\rangle = |n'\rangle a^\dagger_{\alpha'\mathbf{k}'\sigma'}a_{\alpha\mathbf{k}\sigma}|i\rangle$ have energies E_i and E_f, respectively, where $|i\rangle$ refers to the equilibrium state of the left and the right Fermi sea and $|n\rangle$ to the molecular state n. For simplicity, we restrict ourselves to the case of infinite U, i.e. double occupation of the molecule is energetically forbidden. Then the total cotunneling rates describing virtual transitions

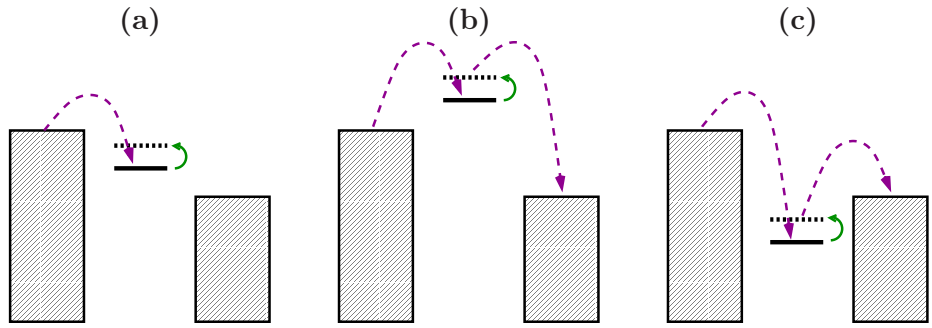

Figure 2.3: Inelastic sequential tunneling and cotunneling schematically exemplified. Sequential tunneling processes (a) usually give the dominant contribution to the current through a junction outside the Coulomb blockade. Their amplitude is linear in the transfer matrix element t_α. However, in the Coulomb blockade cotunneling processes play a crucial role, when the energy transport channels are either far above (b) or below (c) the Fermi energies of the leads. Their amplitude is quadratic in t_α.

between two empty ($\Gamma^{nn',00}_{\alpha\alpha'}$) and two singly occupied molecular states ($\Gamma^{nn',11}_{\alpha\alpha'}$) read

$$\begin{aligned}
\Gamma^{nn',00}_{\alpha\alpha'} &= \frac{2\pi}{\hbar}|t_\alpha|^2|t_{\alpha'}|^2 \sum_{\mathbf{k}\mathbf{k}'\sigma\sigma'} \delta(E_f - E_i) \\
&\quad \times \left| \sum_{\alpha''\mathbf{k}''\sigma''} \sum_{\alpha'''\mathbf{k}'''\sigma'''} \langle i|\langle n'|a^\dagger_{\alpha\mathbf{k}\sigma} a_{\alpha'\mathbf{k}'\sigma'} a^\dagger_{\alpha'''\mathbf{k}'''\sigma'''} d_{\sigma'''} \frac{1}{E_i - H_0} d^\dagger_{\sigma''} a_{\alpha''\mathbf{k}''\sigma''}|n\rangle|i\rangle \right|^2 \\
&= \frac{2\pi}{\hbar}|t_\alpha|^2|t_{\alpha'}|^2 \sum_{\sigma\sigma'} \nu_\alpha(\sigma)\nu_{\alpha'}(\sigma') \int d\epsilon \left| \sum_{n''} \frac{C^{\sigma'}_{n'n''} C^{\sigma *}_{nn''}}{\epsilon + \epsilon_n - \epsilon_{n''}} \right|^2 \\
&\quad \times f_\alpha(\epsilon)\,[1 - f_{\alpha'}(\epsilon + \epsilon_n - \epsilon_{n'})], \qquad (2.36) \\
\Gamma^{nn',11}_{\alpha\alpha'} &= \frac{2\pi}{\hbar}|t_\alpha|^2|t_{\alpha'}|^2 \sum_{\mathbf{k}\mathbf{k}'\sigma\sigma'} \delta(E_f - E_i) \\
&\quad \times \left| \sum_{\alpha''\mathbf{k}''\sigma''} \sum_{\alpha'''\mathbf{k}'''\sigma'''} \langle i|\langle n'|a^\dagger_{\alpha\mathbf{k}\sigma} a_{\alpha'\mathbf{k}'\sigma'} d^\dagger_{\sigma'''} a_{\alpha'''\mathbf{k}'''\sigma'''} \frac{1}{E_i - H_0} a^\dagger_{\alpha''\mathbf{k}''\sigma''} d_{\sigma''}|n\rangle|i\rangle \right|^2 \\
&= \frac{2\pi}{\hbar}|t_\alpha|^2|t_{\alpha'}|^2 \sum_{\sigma\sigma'} \nu_\alpha(\sigma)\nu_{\alpha'}(\sigma') \int d\epsilon \left| \sum_{n''} \frac{C^{\sigma'}_{n''n} C^{\sigma *}_{n''n'}}{-\epsilon + \epsilon_{n'} - \epsilon_{n''}} \right|^2 \\
&\quad \times f_\alpha(\epsilon)\,[1 - f_{\alpha'}(\epsilon + \epsilon_n - \epsilon_{n'})]. \qquad (2.37)
\end{aligned}$$

Since the above expressions diverge due to second-order poles from the energy denominators, the cotunneling rates cannot be evaluated directly. Therefore, we apply a regularization scheme that follows Refs. [29; 88–90] and is motivated by the observation that Eqs. (2.36) and (2.37) do not take into account the fact that the intermediate state obtains a finite width due to the tunneling. We come back to this

point in Chapter 3 in the context of cotunneling through monolayers of magnetic molecules.

2.4 Conductance for Anderson-type models

Many nanostructured junctions are described by the Anderson model,

$$H = \epsilon_d \sum_\sigma n_\sigma + U\, n_\uparrow n_\downarrow + \sum_{\alpha\mathbf{k}\sigma} \left(t_\alpha d_\sigma^\dagger a_{\alpha\mathbf{k}\sigma} + t_\alpha^* a_{\alpha\mathbf{k}\sigma}^\dagger d_\sigma \right) + \sum_{\alpha\mathbf{k}\sigma} \epsilon_{\mathbf{k}}\, a_{\alpha\mathbf{k}\sigma}^\dagger a_{\alpha\mathbf{k}\sigma}. \quad (2.38)$$

Here $d_\sigma^\dagger$ ($a_{\mathbf{k}\sigma}^\dagger$) creates an electron with energy ϵ_d (with energy $\epsilon_{\mathbf{k}}$ and momentum $\mathbf{k}$) and spin σ on the dot (in the reservoir), U is the local Coulomb repulsion of the electrons and $n_\sigma = d_\sigma^\dagger d_\sigma$.

In the linear response limit the conductance G, defined as the proportionality coefficient between the current I through the sample and the voltage V applied to it,

$$I = G\,V \quad (2.39)$$

is given by the Kubo formula

$$G = -\frac{e^2}{h}\Gamma \lim_{\omega\to 0} \mathrm{Im}\left[\frac{1}{\omega} C^R(\omega)\right] \quad (2.40)$$

where $C^R(\omega)$ is the retarded current-current correlator

$$C^R(t-t') = -\Theta(t-t')\langle [I_\alpha(t), I_\alpha(t')]\rangle \quad (2.41)$$

in the energy domain and I_α is the usual current operator. Calculating the expectation value of the commutator gives

$$G = \frac{e^2}{h} \int d\omega \frac{\Gamma_L \Gamma_R}{\Gamma_L + \Gamma_R} A(\omega) \left(-\frac{\partial f(\omega)}{\partial \omega} \right). \quad (2.42)$$

This equation is remarkable in the sense that it directly relates the spectral function $A(\omega)$ of a mesoscopic system to its conductance. In the regime of strong coupling to the leads the level broadening can become large compared to the thermal energy. Thus computing the spectral function in the presence of tunneling couplings allows one to study the conductance of a mesoscopic system to any order in the hybridization H_t.

Equation (2.42) can also be generalized to finite bias voltages. This was done by Meir and Wingreen [79] who showed that the intuitive result

$$I = \frac{e^2}{h} \int d\omega \frac{\Gamma_L \Gamma_R}{\Gamma_L + \Gamma_R} A(\omega) \Big[f(\omega - \mu_L) - f(\omega - \mu_R) \Big] \quad (2.43)$$

gives the current at any bias voltage $V = (\mu_L - \mu_R)/e$, where μ_L and μ_R are the chemical potentials of the left and right reservoirs, respectively.

2.5 Keldysh Formalism

Complementary to the density-matrix approach introduced in the previous sections, rate equations describing the quantum transport through mesoscopic systems can be obtained from the Keldysh formalism in some particular cases [91]. Here the main idea consists in deriving an equation of motion for the Keldysh Green function and interpreting this as a distribution function of the system. Our goal is to discuss this concept by deriving the rate equations and computing the tunneling current for the resonant-level model,

$$H = H_0 + H_t, \tag{2.44}$$

with

$$H_0 = \epsilon_d \, d^\dagger d + \sum_{\alpha \mathbf{k}} \epsilon_{\mathbf{k}} \, a^\dagger_{\alpha \mathbf{k}} a_{\alpha \mathbf{k}} \tag{2.45}$$

and

$$H_t = \sum_{\alpha \mathbf{k}} \left[t_\alpha \, a^\dagger_{\alpha \mathbf{k}} d + t^*_\alpha \, d^\dagger a_{\alpha \mathbf{k}} \right]. \tag{2.46}$$

The starting point is Dyson's equation

$$G = G_0 + G_0 \, \Sigma \, G \tag{2.47}$$

for the matrix Green function

$$G \equiv \begin{pmatrix} G^R & G^K \\ 0 & G^A \end{pmatrix} \tag{2.48}$$

and matrix self energy

$$\Sigma \equiv \begin{pmatrix} \Sigma^R & \Sigma^K \\ 0 & \Sigma^A \end{pmatrix}, \tag{2.49}$$

where G^R (Σ^R), G^A (Σ^A) and G^K (Σ^K) denote the retarded Green function (retarded self energy), advanced Green function (advanced self energy), and Keldysh Green function (Keldysh self energy), respectively. The propagator G_0 denotes the free matrix Green function. Here G is related to the contour-ordered Green function in Keldysh space by Larkin-Ovchinnikov transformation [72]. Using that the free Green function solves the Schrödinger equation, we can rewrite Eq. (2.47) as

$$\left(i\hbar \frac{\partial}{\partial t} - H_0 - \Sigma \right) G = 1, \qquad G \left(i\hbar \frac{\partial}{\partial t} - H_0 - \Sigma \right) = 1, \tag{2.50}$$

where the square brackets denote the commutator, while the curly brackets denote the anticommutator. Taking the sum and the difference gives

$$\left[i\hbar \frac{\partial}{\partial t} - H_0 - \Sigma, G \right] = 0 \qquad \left\{ i\hbar \frac{\partial}{\partial t} - H_0 - \Sigma, G \right\} = 2. \tag{2.51}$$

The Keldysh component of the commutator yields

$$\left[i\hbar \frac{\partial}{\partial t} - H_0 - \Sigma, G^K \right] = \Sigma^R G^K + \Sigma^K G^A - G^R \Sigma^K + G^K \Sigma^A. \tag{2.52}$$

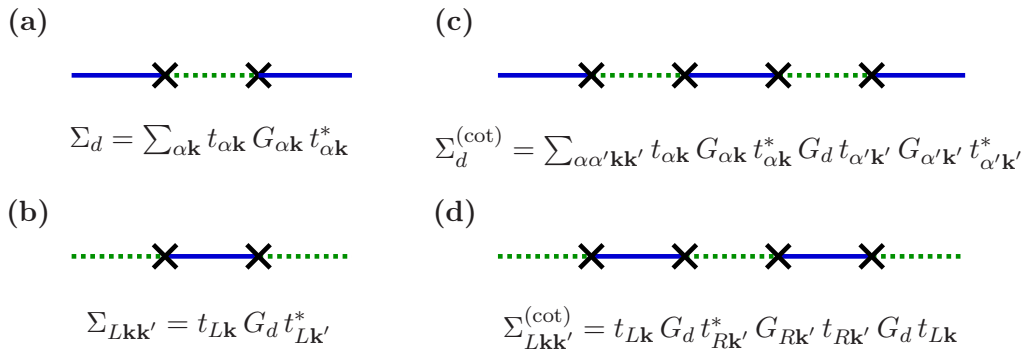

Figure 2.4: Self energy contributions of leading [(a),(c)] and next-to-leading order [(b),(d)] in the molecule-lead coupling. The solid lines denote the propagator electronic G_d of the single impurity, whereas the dashed lines denote the electronic propagator $G_{\alpha\mathbf{k}}$ of lead α.

So far, all Green functions G and self energies Σ depend on two times t_1 and t_2. For a semiclassical description it is useful to introduce sum coordinates, $T = (t_1+t_2)/2$, and difference coordinates, $t = t_1 - t_2$ and Fourier transform to the difference coordinates,

$$G(T,\omega) = \frac{1}{\hbar}\int dt\, e^{i\omega t} G(T + t/2, T - t/2). \tag{2.53}$$

Passing to the Wigner representation gives

$$\frac{\partial G^K}{\partial T} = -\frac{i}{\hbar}\left[\left(\Sigma^R - \Sigma^A\right) G^K - \left(G^A - G^R\right)\Sigma^K\right] \tag{2.54}$$

in the semiclassical limit $\hbar \to 0$. To lowest order the self energies of the single-impurity and the leads shown in Fig. 2.4 are given by

$$\Sigma_d^{R,A} = \mp i\pi \sum_{\mathbf{k}} \delta(\epsilon_{\mathbf{k}} - \omega)\Big(|t_{L\mathbf{k}}|^2 + |t_{R\mathbf{k}}|^2\Big), \qquad \Sigma_d^K = \sum_{\mathbf{k}} |t_{L\mathbf{k}}|^2 G^K_{L\mathbf{k}} + \sum_{\mathbf{k}} |t_{R\mathbf{k}}|^2 G^K_{R\mathbf{k}}, \tag{2.55}$$

and

$$\Sigma^{R,A}_{L\mathbf{k}\mathbf{k}'} = \mp i\pi\, \delta(\omega - \epsilon_d)\, t_{L\mathbf{k}} t^*_{L\mathbf{k}'}, \qquad \Sigma^K_{L\mathbf{k}\mathbf{k}'} = t_{L\mathbf{k}} t^*_{L\mathbf{k}'} G^K_d\,. \tag{2.56}$$

Using that the spectral function is sharply peaked at the charging energy ϵ_d compared to Σ_d^K,

$$\left(G^R - G^A\right) \simeq -2\pi i\, \delta(\omega - \epsilon_d), \tag{2.57}$$

we obtain

$$\frac{\partial G^K_d}{\partial T} = \frac{1}{\hbar}\Big(\Gamma_L + \Gamma_R\Big) G^K_d + \frac{2\pi}{\hbar}\,\delta(\omega - \epsilon_d) \sum_{\mathbf{k}} \Big(|t_{L\mathbf{k}}|^2 G^K_{L\mathbf{k}} + |t_{R\mathbf{k}}|^2 G^K_{R\mathbf{k}}\Big), \tag{2.58}$$

where $\Gamma_\alpha \equiv 2\pi \sum_{\mathbf{k}} \delta(\epsilon_{\mathbf{k}} - \omega)\, |t_{\alpha\mathbf{k}}|^2$. Integrating this equation over ω and using that the Keldysh function of the leads is also strongly peaked, $G^K_{\alpha\mathbf{k}} \simeq \delta(\omega - \epsilon_{\mathbf{k}}) \int d\omega G^K_{\alpha\mathbf{k}}$,

gives

$$\frac{\partial g_d^K}{\partial T} = \frac{2\pi}{\hbar} \sum_{\alpha \mathbf{k}} \delta(\epsilon_d - \epsilon_{\mathbf{k}}) \left(g_{\alpha \mathbf{k}}^K - g_d^K \right), \tag{2.59}$$

where $g^K \equiv \int d\omega G^K$. Interpreting g_d^K as the distribution function, i.e. as the occupation probability, of the single impurity, $g_d^K = P^1$, and $g_{\alpha \mathbf{k}}^K$ as the distribution function of lead α, $g_{\alpha \mathbf{k}}^K = f_{\alpha \mathbf{k}}$, we recover the rate equation describing the dynamics of the resonant-level model,

$$\frac{\partial P^1}{\partial T} = \frac{2\pi}{\hbar} \sum_{\alpha \mathbf{k}} |t_{\alpha \mathbf{k}}|^2 \, \delta(\epsilon_d - \epsilon_{\mathbf{k}}) \left(f_{\alpha \mathbf{k}} P^0 - [1 - f_{\alpha \mathbf{k}}] \, P^1 \right). \tag{2.60}$$

The current through lead α is then given by

$$I_\alpha = e \, \frac{2\pi}{\hbar} \sum_{\mathbf{k}} |t_{\alpha \mathbf{k}}|^2 \, \delta(\epsilon_d - \epsilon_{\mathbf{k}}) \, \left(f_{\alpha \mathbf{k}} P^0 - [1 - f_{\alpha \mathbf{k}}] \, P^1 \right). \tag{2.61}$$

Similarly, one can compute higher-order corrections to the transition rates. For instance, the cotunneling matrix self energies of the leads, shown in Fig. 2.4, read

$$\Sigma_{L \mathbf{k} \mathbf{k}'}^{(\mathrm{cot})} = |t_{L \mathbf{k}}|^2 \sum_{\mathbf{k}'} |t_{R \mathbf{k}'}|^2 \begin{pmatrix} G_d^R G_{R\mathbf{k}}^R G_d^R & G_d^R G_{R\mathbf{k}}^R G_d^K + G_d^R G_{R\mathbf{k}}^K G_d^A + G_d^K G_{R\mathbf{k}}^A G_d^A \\ 0 & G_d^A G_{R\mathbf{k}}^A G_d^A \end{pmatrix}. \tag{2.62}$$

In the limit $\epsilon_d \gg 0$, where $G_d^{R,A} = 1/(\omega - \epsilon_d \pm i\eta) \simeq 1/\epsilon_d$, we obtain

$$\begin{aligned} \Sigma_{L \mathbf{k}}^{(\mathrm{cot})} &\simeq \frac{|t_{L\mathbf{k}}|^2}{\epsilon_d} \sum_{\mathbf{k}'} \frac{|t_{R\mathbf{k}'}|^2}{\epsilon_d} \begin{pmatrix} G_{R\mathbf{k}}^R & G_{R\mathbf{k}}^K \\ 0 & G_{R\mathbf{k}}^A \end{pmatrix} \\ &= \frac{|t_{L\mathbf{k}}|^2}{\epsilon_d} \sum_{\mathbf{k}'} \frac{|t_{R\mathbf{k}'}|^2}{\epsilon_d} \begin{pmatrix} -i\pi \, \delta(\omega - \epsilon_{\mathbf{k}'}) & G_{R\mathbf{k}}^K \\ 0 & i\pi \, \delta(\omega - \epsilon_{\mathbf{k}'}) \end{pmatrix}, \end{aligned} \tag{2.63}$$

which gives

$$\frac{\partial g_{L\mathbf{k}}^K}{\partial T} = \frac{2\pi}{\hbar} \sum_{\mathbf{k}\mathbf{k}'} \frac{|t_{L\mathbf{k}}|^2 |t_{R\mathbf{k}'}|^2}{\epsilon_d^2} \delta(\epsilon_{L\mathbf{k}'} - \epsilon_{R\mathbf{k}'}) \left[g_{R\mathbf{k}'}^K - g_{L\mathbf{k}}^K \right]. \tag{2.64}$$

Interpreting again $g_{\alpha \mathbf{k}'}^K$ as the distribution function of the leads, we recover the cotunneling transition rates proportional to $1/\epsilon_d^2$ for the regime, where the resonant level is far away from the Fermi energies of the leads.

The above derivation can be readily generalized to obtain Boltzmann equations for the case of an additional external field or disorder potentials. However, including the presence of local interactions for the single impurity usually turns out to be non-trivial.

2.6 Kondo transport and renormalization group

A quantitative description of the build-up of Kondo correlations in quantum dots is possible in terms of the single-impurity Anderson model, Eq. (2.38) [5; 6]. A Schrieffer-Wolff transformation [92] relates the Anderson model to the Kondo model,

$$H_K = -\sum_{\alpha\alpha'\mathbf{k}\mathbf{k}'} J_{\alpha\alpha'}\, \mathbf{s}_{\alpha\alpha'\mathbf{k}\mathbf{k}'} \cdot \mathbf{S}, \tag{2.65}$$

describing the coherent exchange between the spin of a localized state, $\mathbf{S} \equiv \sum_{\sigma\sigma'} d^\dagger_\sigma(\boldsymbol{\sigma}_{\sigma\sigma'}/2)d_{\sigma'}$, and the spins of the Fermi sea of delocalized electrons, $\mathbf{s}_{\alpha\alpha'\mathbf{k}\mathbf{k}'} \equiv \sum_{\sigma\sigma'} a^\dagger_{\alpha\mathbf{k}\sigma}(\boldsymbol{\sigma}_{\sigma\sigma'}/2)a_{\alpha'\mathbf{k}'\sigma'}$. Here $\boldsymbol{\sigma} = (\sigma^x, \sigma^y, \sigma^z)$ denotes the vector of the Pauli matrices. Equation (2.65) is obtained from Eq. (2.38) using a canonical transformation of the form

$$\tilde{H} \simeq e^S H e^{-S}, \tag{2.66}$$

where the generator

$$S = \sum_{\alpha\mathbf{k}\sigma}\left[\frac{t_\alpha}{\epsilon_\mathbf{k} - \epsilon_d - U} n_{\bar{\sigma}} a^\dagger_{\alpha\mathbf{k}\sigma} d_\sigma + \frac{t_\alpha}{\epsilon_\mathbf{k} - \epsilon_d}(1 - n_{\bar{\sigma}}) a^\dagger_{\alpha\mathbf{k}\sigma} d_\sigma\right] - \text{h.c.} \tag{2.67}$$

is chosen such that the Hamiltonian $\tilde{H}$ has no terms first order in the tunneling amplitude t_α. Carrying out the transformation requires to expand the exponentials in Eq. (2.66),

$$\tilde{H} = H_0 - \frac{1}{2}[S,[S,H_0]] - \frac{1}{3}[S,[S,[S,H_0]]] - \frac{1}{8}[S,[S,[S,[S,H_0]]]] + \ldots. \tag{2.68}$$

Here H_0 includes all terms of the Anderson model except for tunneling Hamiltonian. Evaluation of all relevant commutators yields the following expression for the exchange coupling,

$$J_{\alpha\alpha'\mathbf{k}\mathbf{k}'} = t^*_\alpha t_{\alpha'}\left(\frac{1}{\epsilon_k - \epsilon_d} + \frac{1}{\epsilon'_k - \epsilon_d} + \frac{1}{U + \epsilon_d - \epsilon_k} + \frac{1}{U + \epsilon_d - \epsilon'_k}\right). \tag{2.69}$$

Importantly, the exchange is purely antiferromagnetic,

$$J_{\alpha\alpha'} \simeq 2t^*_\alpha t_{\alpha'} \frac{U}{\epsilon_d(\epsilon_d + U)} < 0, \tag{2.70}$$

assuming that only states close to the Fermi energy, $k, k' \simeq k_F$, have to be taken into account.

The anomalous scattering behavior arises by performing a perturbation theory calculation to third order in the exchange coupling, revealing the divergence that is the precursor of the Kondo resonance [83]. In the same spirit as our approach to cotunneling, we consider the amplitude for the tunneling of an electron from the left lead L to the right lead R, i.e. the final state of the electron system is $|f^e_{k\sigma\mathbf{k}'\sigma'}\rangle \equiv a^\dagger_{R\mathbf{k}\sigma} a_{Lk'\sigma'}|i^e\rangle$, where $|i^e\rangle$ denotes the initial state of lead electrons. In

addition, the spin of the dot may change, i.e. we must sum over all possible initial states $|\sigma_i\rangle$ and final states $|\sigma_f\rangle$ of the dot spin.

The rate for transferring electrons from left to right can be written as

$$\Gamma_{RL} = \frac{2\pi}{\hbar} \sum_{i\mathbf{k}\mathbf{k}'\sigma\sigma'\sigma_i\sigma_f} p_i \left| t^{i(1)}_{R\mathbf{k}\sigma L\mathbf{k}'\sigma',\sigma_i\sigma_f} + t^{i(2)}_{R\mathbf{k}\sigma L\mathbf{k}'\sigma',\sigma_i\sigma_f} + \cdots \right|^2 \delta(\xi_{\mathbf{k}} - \xi_{\mathbf{k}'}), \quad (2.71)$$

where p_i denotes the distribution function of possible initial states i. To first order in H_K the amplitude for the electron transfer from left to right is

$$t^{i(1)}_{R\mathbf{k}\sigma L\mathbf{k}'\sigma',\sigma_i\sigma_f} = \langle f^e_{\mathbf{k}\sigma\mathbf{k}'\sigma'}| \, \langle\sigma_f|H_K|\sigma_i\rangle|i^e\rangle = \frac{J_{RL}}{2} \sum_{j=x,y,z} \langle\sigma_f|S^j|\sigma_i\rangle \sigma^j_{\sigma\sigma'} n^i_{L\mathbf{k}'\sigma'}(1 - n^i_{R\mathbf{k}\sigma}), \quad (2.72)$$

where $n^i_{\alpha\mathbf{k}\sigma}$ is the occupation of the single-particle state $\mathbf{k}\sigma$ in lead α in the initial state. Evaluating all spin sums yields

$$\Gamma^{(2)}_{RL} \simeq \frac{2\pi}{\hbar}\nu_0^2 \frac{3J^2_{RL}}{4} \int d\xi n(\xi - \mu_L)[1 - n(\xi - \mu_R)] \quad (2.73)$$

for the second order contribution to the tunnel rate. Here ν_0 is the density of states, which we assume to be constant.

The next-to-leading contribution to the tunneling rate is given by

$$\Gamma^{(3)}_{RL} \simeq \frac{4\pi}{\hbar} \sum_{i\mathbf{k}\mathbf{k}'\sigma\sigma'\sigma_i\sigma_f} p_i \, \mathrm{Re}\left\{ \left[t^{i(1)}_{R\mathbf{k}\sigma L\mathbf{k}'\sigma',\sigma_i\sigma_f} \right]^* t^{i(2)}_{R\mathbf{k}\sigma L\mathbf{k}'\sigma',\sigma_i\sigma_f} \right\} \delta(\xi_{\mathbf{k}} - \xi_{\mathbf{k}'}) \quad (2.74)$$

Expansion of the T-matrix gives

$$t^{i(2)}_{Rk\sigma Lk'\sigma',\sigma_i\sigma_f} = \langle f^e_{\mathbf{k}\sigma\mathbf{k}'\sigma'}|\langle\sigma_f|H_K \frac{1}{E_i - H_{\mathrm{leads}} + i\eta} H_K|\sigma_i\rangle|i^e\rangle. \quad (2.75)$$

This second-order term must involve one term with J_{RL} and one term with J_{RR} or J_{LL} in order for $t^{i(2)}_{Rk\sigma Lk'\sigma'}$ to be non-zero. After straightforward calculations one arrives at the following expression for the third-order tunneling rate

$$\Gamma^{(3)}_{RL} \simeq \frac{6\pi}{8}(J_{RL}\nu_0)^2 \int d\xi \, n(\xi - \mu_L) \, [1 - n(\xi - \mu_R)] \left(\sum_\beta J_{\beta\beta}\nu_0 \int_{-D}^{D} d\xi_1 \frac{n(\xi_1 - \mu_\beta)}{\xi_1 - \xi} \right). \quad (2.76)$$

Here D denotes the band width. A similar expression can be derived for scattering from right to left, and after subtracting the two, one obtains

$$I = \frac{e}{2\pi} \int d\xi \, [n(\xi - \mu_L) - n(\xi - \mu_R)] \, T(\xi) \quad (2.77)$$

for the Kondo current, where

$$T(\xi) \simeq \frac{3}{4}(2\pi J_{RL}\nu_0)^2 \left(1 + \sum_\beta \frac{J_{\beta\beta}\nu_0}{2} \int_{-D}^{D} d\xi_1 \frac{n(\xi_1 - \mu_\beta)}{\xi_1 - \xi} \right). \quad (2.78)$$

This expression for the transmission coefficient shows that there occurs a peak in the conductance at low temperatures, since for $T \ll D$ both μ_β and ξ are relatively small, so that the conductance diverges logarithmically at low temperatures [83],

$$\int_{-D}^{D} d\xi_1 \frac{n(\xi_1 - \mu_\beta)}{\xi_1 - \xi} \simeq \int_{-D}^{D} d\xi_1 \frac{n(\xi_1)}{\xi_1} \simeq \int_{-D}^{-T} d\xi_1 \frac{1}{\xi_1} = \ln(T/D). \tag{2.79}$$

We can give a simple estimate of the temperature at which the Kondo resonance starts to dominate transport by noticing when the last term in the parenthesis in Eq. (2.78) is comparable to the first. This defines the so-called Kondo temperature,

$$T_K = D \exp\left(-\frac{1}{\nu_0 \sum_\beta J_{\beta\beta}}\right). \tag{2.80}$$

The form of the Kondo temperature shows that it is non-perturbative in the exchange coupling. Thus we do not expect to gain more insight by continuing the perturbative expansion.

An estimate of the Kondo temperature can also be obtained using Wilson's renormalization group [74]. Employing *poor man's scaling* [82; 93] yields equations for the renormalization flow which relate the Kondo temperature to the antiferromagnetic exchange. To carry out the scaling one divides the conduction band into states, $0 < |\epsilon_{\mathbf{k}}| < D - |\delta D|$, which are retained, and states within $|\delta D|$ of the band edge which are to be eliminated. One finds that the lowest-order correction to the Hamiltonian is proportional to squares of the exchange coupling.

The elimination of virtual scattering to the band edges in the lowest order results in a Hamiltonian of the same form but with renormalized couplings $J(D)$ which effectively depend on the band width D,

$$J(D) = J + \delta J(D). \tag{2.81}$$

The scaling equations assume the form

$$\frac{dJ_{LL}}{d\ln D} = \nu_0(J_{LL}^2 + J_{LR}^2), \tag{2.82}$$

$$\frac{dJ_{RR}}{d\ln D} = \nu_0(J_{RR}^2 + J_{LR}^2), \tag{2.83}$$

$$\frac{dJ_{LR}}{d\ln D} = \nu_0 J_{LR}(J_{LL} + J_{RR}). \tag{2.84}$$

For the case of symmetric couplings to the leads, $J_{LL} = J_{RR} = J_{LR} = J$, they reduce to

$$\frac{dJ}{d\ln D} = 2\nu_0 J^2. \tag{2.85}$$

The solution of Eq. (2.85) reads

$$J(D) \simeq \frac{J}{1 - 2\nu_0 J \ln D/T}. \tag{2.86}$$

This defines the Kondo temperature as the energy scale as of the logarithmic divergence as

$$T_K \sim e^{-1/2\nu_0 J}. \tag{2.87}$$

It is this renormalization of the exchange coupling,

$$J(T) \simeq J \, \frac{1}{\ln T/T_K}, \tag{2.88}$$

which is the origin of the logarithmic behavior of the conductance at low temperature. It can be shown that the conductance of the Kondo resonance approaches the limit $2e^2/h$ at zero temperature. The crossover between the *underdeveloped* Kondo regime discussed above, $T > T_K$, and the strong coupling Kondo regime, $T < T_K$, has been discussed extensively in the literature and is reviewed, for instance, in Ref. [94].

In the presence of a finite bias voltage, many physical quantities such as the conductance are not determined by low-energy excitations, since all states with energies of order of the applied voltage contribute to exchange scattering processes. But as long as the cutoff is large compared to the voltage, $D \gg V$, one usually expects the *poor man's scaling* approach to hold. However, it should be remarked that there exists no general theory of renormalization out of equilibrium, so far.

3 Transport through magnetic molecules—spin reading and writing

3.1 Experimental motivation

Investigating spin-dependent electronic transport through magnetic molecules is motivated by the idea of *molecular spintronics* to integrate the promising concepts of molecular electronics and spintronics [8; 10; 11; 15; 24; 38; 41; 95]. A particularly interesting aspect of molecular electronics, besides the prospect of further miniaturization, is the possibility of using chemical synthesis for the fabrication of device components, whereas spintronics is discussed in relation to magnetic memory and quantum computation. However, employing magnetic molecules as memory devices in a nanoscale electric circuit requires a deeper understanding of their transport properties.

Recent experimental research on single-molecule magnets has focused on the fine structure of the Coulomb blockade peaks in the differential conductance. Seminal experiments by Jo *et al.* [23] have reported the occurrence of magnetic sidebands in transport through Mn_{12} derivatives in a molecular junction, cf. Fig. 3.1(a). These are due to magnetic excitations of the local anisotropic spin of length $S \simeq 9$. Each peak in the differential conductance can be attributed to an inelastic sequential tunneling event, which changes the molecular spin by 1/2. Applying an external magnetic field that couples linearly to the magnetic moment of the molecule gives rise to an additional Zeeman splitting, which allows for distinguishing magnetic from vibrational sidebands. Furthermore, cotunneling processes, which give the dominant contribution to the tunneling current through the molecular junction in the Coulomb blockade regime, have been observed [23].

Further measurements on Mn_{12} by Heersche *et al.* [22] have revealed the occurrence of novel spin-blockade mechanisms. A striking observation is the occurrence of complete current suppression outside the Coulomb blockade regime due to the presence of magnetic blocking states, cf. Fig. 3.1(b). Magnetic excitations on the energy scale of the anisotropy barrier of the molecule are responsible for negative differential conductance features. Transport calculations, taking into account the high-spin ground state and excited states of the molecule, are in agreement with a current blockade mechanism involving non-degenerate spin multiplets.

Experiments on cobalt Co^{2+} complexes in a molecular junction by Liang *et al.* [19] have shown that the coupling between the local molecular spin and the spins of the lead electrons may also give rise to the build-up of Kondo correlation, cf. Fig. 3.1(c).

The tunneling spectra of individual magnetic endohedral fullerenes $N@C_{60}$ have

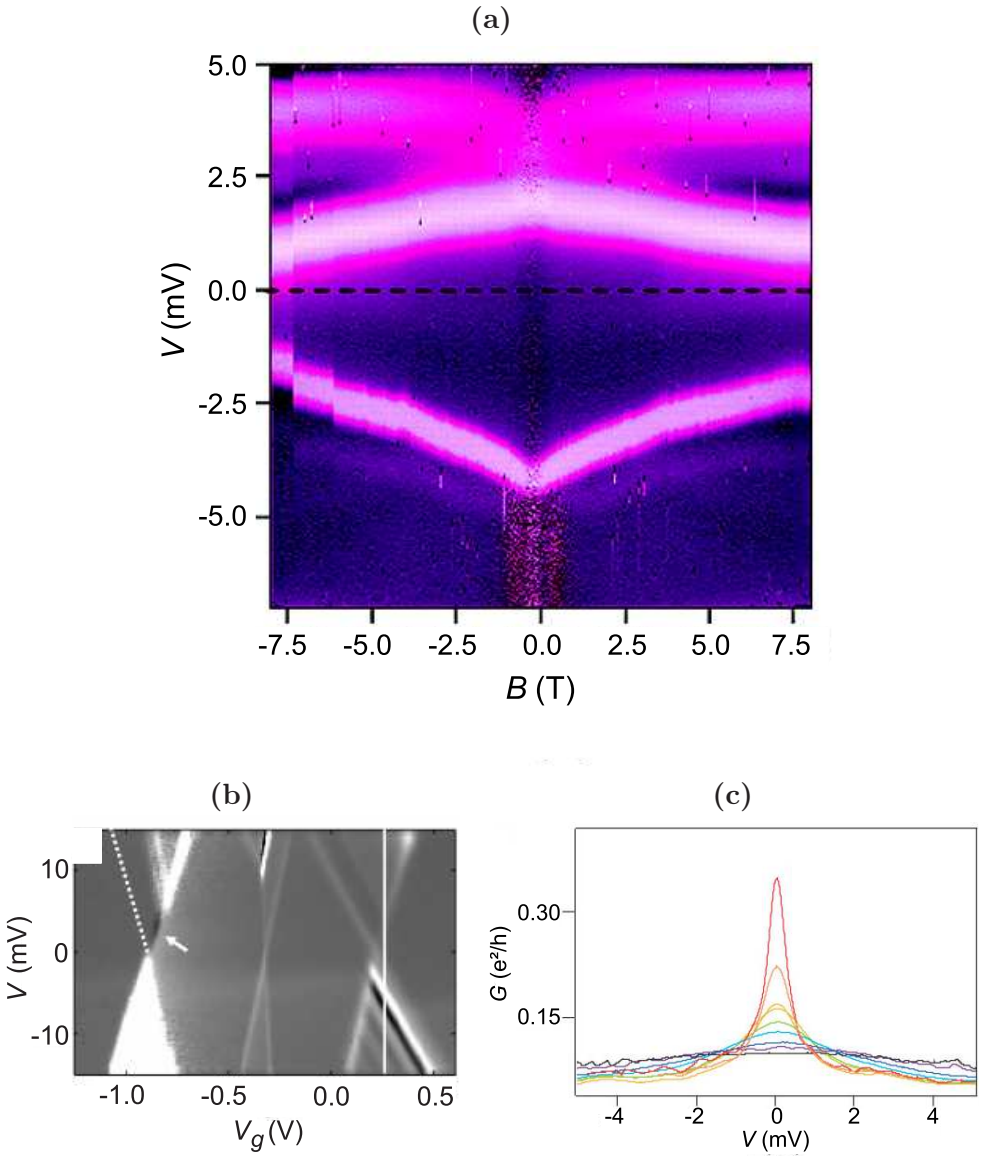

Figure 3.1: (a) Color plot of the differential conductance dI/dV of Mn_{12} as a function of bias voltage V and magnetic field B at fixed gate voltage V_g, taken from Ref. [23]. (b) Differential conductance of Mn_{12} as a function of gate voltage V_g and bias voltage V_b, taken from Ref. [22]. A region of complete current suppression (left degeneracy point, arrow) and low-energy excitations with negative differential conductance (right degeneracy point) are observed. The dashed line near the left degeneracy point indicates the suppressed diamond edge [22]. (c) Plot of the conductance G versus bias voltage V at various temperatures, obtained from a single-V_2 transistor, taken from Ref. [19]. The temperatures of the measurements (in K) are $T = 0.3$, 1.0, 2.0, 3.1, 4.2, 6.3, 9.0, 14 and 20, in order of decreasing peak height.

been studied in recent experiments by Grose *et al.* [35]. Here the authors report spin excitations revealed in the differential conductance, which are the consequence of the exchange coupling between the nitrogen spin and the electron(s) on the C_{60} cage. While the nitrogen atom retains its three p electrons and has a constant spin 3/2, the spin of the C_{60} molecule changes due to the electronic tunneling. The fact that the entire molecule remains magnetic is verified by observing a low-spin to high-spin transition as a function of magnetic field and by the existence of nonequilibrium tunneling originating from low-energy excited states [35].

Furthermore, spin-dependent transport through nonmagnetic molecular nanostructures has been studied extensively over the past few years [96–100]. Pioneering experiments by Tsukagoshi *et al.* [96] have reported the injection of spin-polarized electrons from ferromagnetic contacts into multi-walled carbon nanotubes, finding direct evidence for coherent transport of electron spins and hysteretic magnetoresistance. Very weak spin-orbit coupling suggests extremely long spin relaxation times and the possibility of coherent spin propagation over large distances, which presents an encouraging result for the development of practical nanotube spintronic devices. These findings have stimulated a growing activity in this area, including experiments on spin transport through polymers [97; 98] and molecular junctions [99], and optical pump/probe experiments through molecular bridges [100].

The purpose of the following sections is to elucidate some of these experimental findings theoretically and to discuss the role of single-molecule magnets in relation to molecular spintronics. Our main focus is on spin reading and writing.

3.2 Model

We consider a single magnetic molecule connected to two metallic leads which serve as source and drain electrodes. The molecular junction is described by a Hamiltonian of the form

$$H = H_{\mathrm{mol}} + H_{\mathrm{leads}} + H_t, \tag{3.1}$$

where H_{mol} represents the molecular degrees of freedom, H_{leads} represents the leads, and H_t the tunneling of electrons between the molecule and the leads.

The molecule is assumed to consist of only a single non-degenerate orbital which is involved in the electronic transport. Electrons interact with one another via local Coulomb repulsion, i.e. doubly occupying the molecule costs additional charging energy. Furthermore, the orbital spin $\mathbf{s}$ is coupled to a local impurity spin $\mathbf{S}$, which remains constant despite the current-induced nonequilibrium. This means that the molecule is paramagnetic even in the neutral state, when $\mathbf{s}$ vanishes and the total spin is given by $\mathbf{S}$. In some molecules the local spin is isotropic, e.g. in endohedral fullerenes [48; 85; 86]. Here rotational symmetry in spin space can only be broken due to the presence of an external magnetic field. However, many molecules such as Mn_{12} or heme possess a magnetic anisotropy [22; 23]. The simplest Hamiltonian describing the electronic and spin degrees of freedom of an anisotropic magnetic

molecule reads

$$H_{\mathrm{mol}} = (\epsilon_d - eV_g)\, n + \frac{U}{2}\, n(n-1) - J\, \mathbf{s}\cdot\mathbf{S} - K_2\, (S^z)^2 - B(s^z + S^z). \tag{3.2}$$

Here, $n \equiv d_\uparrow^\dagger d_\uparrow + d_\downarrow^\dagger d_\downarrow$ denotes the number operator counting the electrons on the molecule, where $d_\sigma^\dagger$ (d_σ) creates (annihilates) an electron with spin σ and single-electron energy ϵ_d, which can be shifted by applying a gate voltage V_g. The parameter U denotes the Coulomb repulsion of the electrons in the orbital. If not stated otherwise, we consider the limit $U \to \infty$, i.e. double occupation of the molecule is energetically forbidden, since our main effects do not depend on the presence of finite charging energies. The electronic spin operator $\mathbf{s}$ is given by

$$\mathbf{s} \equiv \sum_{\sigma\sigma'} d_\sigma^\dagger \frac{\boldsymbol{\sigma}_{\sigma\sigma'}}{2} d_{\sigma'}, \tag{3.3}$$

where $\boldsymbol{\sigma} \equiv (\sigma_x, \sigma_y, \sigma_z)$ denotes the vector of Pauli matrices. The parameter J denotes the exchange interaction between an electron in the orbital and the local spin of length S. We define the operator for the total spin as

$$\mathbf{S}_{\mathrm{tot}} \equiv \mathbf{s} + \mathbf{S}. \tag{3.4}$$

We restrict ourselves to the case of *easy-axis* magnetic anisotropy, $K_2 > 0$, i.e. we consider an anisotropy-induced *energy barrier*. For simplicity we assume the g-factors of the two spins to be identical and only take into account an external magnetic field B which is applied along the anisotropy axis, pointing into, say, z direction. Transport through magnetic molecules with non-collinear anisotropy axis and magnetic field has been studied in Ref. [87]. Arbitrary angles between the easy axis and the field lead to the violation of certain spin selection rules, resulting in a much richer fine structure in the differential conductance.

The passage of a charge current is due to a finite bias voltage V between the two metallic electrodes L (left) and R (right), which are modeled as non-interacting Fermi gases,

$$H_{\mathrm{leads}} = \sum_{\alpha\mathbf{k}\sigma} \epsilon_{\alpha\mathbf{k}\sigma}\, a_{\alpha\mathbf{k}\sigma}^\dagger a_{\alpha\mathbf{k}\sigma}. \tag{3.5}$$

Here $a_{\alpha\mathbf{k}\sigma}^\dagger$ ($a_{\alpha\mathbf{k}\sigma}$) creates (annihilates) an electron with energy $\epsilon_{\alpha\mathbf{k}\sigma}$, momentum $\mathbf{k}$, and spin σ in lead $\alpha = L, R$.

The hybridization of the molecular orbital with the leads is described by a tunneling Hamiltonian,

$$H_t = \sum_{\alpha\mathbf{k}\sigma} \left[t_\alpha\, a_{\alpha\mathbf{k}\sigma}^\dagger d_\sigma + t_\alpha^*\, d_\sigma^\dagger a_{\alpha\mathbf{k}\sigma} \right], \tag{3.6}$$

where we consider the case of symmetric contacts, $t_L \simeq t_R$ in the following, e.g. realized in many breakjunction experiments [12].

The molecule-lead coupling is assumed to be sufficiently weak, such that the tunneling may be treated perturbatively. The unperturbed Hamiltonian is readily diagonalized. Since the charge n of the molecule is a good quantum number, the solutions

for the eigenstates fall into charge sectors with $n = 0, 1, 2$ electrons. For $n = 0$ and $n = 2$ the local spin decouples from the electronic system, since the z-component of the total spin, $s^z + S^z = S^z$, commutes with $H_{\rm mol}$. For both cases, one obtains $2S+1$ eigenstates enumerated by the magnetic quantum number m of the z component of the total spin $s^z + S^z = S^z$. Their eigenenergies $\epsilon(n, m)$ are

$$\epsilon(0, m) = -K_2 m^2 - Bm, \tag{3.7}$$

$$\epsilon(2, m) = 2(\epsilon - eV_{\rm g}) + U - K_2 m^2 - Bm. \tag{3.8}$$

In contrast, in the $n = 1$ sector the total spin $\mathbf{S}_{\rm tot} \cdot \mathbf{S}_{\rm tot}$ does not commute with $H_{\rm mol}$ for nonvanishing K_2. However, its z component $S^z_{\rm tot} = s^z + S^z$ does. Thus the eigenvalue m of $S^z_{\rm tot}$ is still a good quantum number. The subspace in the $n = 1$ sector has dimension $2(2S + 1)$. A suitable basis is formed by product states,

$$\{|\downarrow\rangle, |\uparrow\rangle\} \otimes \{|-S\rangle, \ldots, |S\rangle\}, \tag{3.9}$$

where $|\downarrow\rangle$ and $|\uparrow\rangle$ denote the two eigenstates of $\mathbf{s}$, while $|m\rangle$ denotes the $2S + 1$ eigenstates of the local spin $\mathbf{S}$. The states with extremal magnetic quantum numbers $m = -S - 1/2$ and $S + 1/2$ are

$$|1, -S - 1/2\rangle = |\downarrow\rangle|-S\rangle, \qquad |1, S + 1/2\rangle = |\uparrow\rangle|S\rangle. \tag{3.10}$$

Their energies are

$$\epsilon(1, -S - 1/2) = \epsilon_d - eV_{\rm g} + B(S + 1/2) - \frac{JS}{2} - K_2 S^2, \tag{3.11}$$

$$\epsilon(1, S + 1/2) = \epsilon_d - eV_{\rm g} - B(S + 1/2) - \frac{JS}{2} - K_2 S^2. \tag{3.12}$$

All other values for magnetic quantum numbers, $-S-1/2 < m < S+1/2$, appear as eigenvalues of two product states, namely $|\downarrow\rangle|m+1/2\rangle$ and $|\uparrow\rangle|m-1/2\rangle$. Therefore, the remaining eigenstates of $H_{\rm mol}$ must be linear combinations of two product states with the same m. Inserting the ansatz

$$|\psi\rangle = \alpha|\downarrow\rangle|m + 1/2\rangle + \beta|\uparrow\rangle|m - 1/2\rangle \tag{3.13}$$

and noting that

$$\mathbf{s} \cdot \mathbf{S} = s^z S^z + \frac{s^+ S^- + s^- S^+}{2}, \tag{3.14}$$

we find that the Hamiltonian in the two-dimensional subspace spanned by the two product states reads

$$\begin{aligned} H_{\rm mol} &= \left[\epsilon_d - eV_{\rm g} - Bm + \frac{J}{4} - K_2\left(m^2 + \frac{1}{4}\right)\right]\begin{pmatrix} 1 & 0 \\ 0 & 1 \end{pmatrix} \\ &+ \begin{pmatrix} J\frac{m}{2} - K_2 m & -\frac{J}{2}\sqrt{S(S+1) - m^2 + 1/4} \\ -\frac{J}{2}\sqrt{S(S+1) - m^2 + 1/4} & -J\frac{m}{2} + K_2 m \end{pmatrix}. \end{aligned} \tag{3.15}$$

The resulting eigenenergies are

$$\epsilon^{\pm}(1,m) = \epsilon_d - eV_\mathrm{g} - Bm + \frac{J}{4} - K_2\left(m^2 + \frac{1}{4}\right) \pm \Delta E(m), \tag{3.16}$$

with

$$\Delta E \equiv \sqrt{K_2(K_2 - J)m^2 + \left[\frac{J}{4}(2S+1)\right]^2}, \tag{3.17}$$

for the normalized eigenstates

$$\begin{aligned} |1,m\rangle^{\pm} = {} & \frac{(2K_2 - J)m \mp 2\Delta E}{2\sqrt{\Delta E}\sqrt{2\Delta E \mp (2K_2 - J)m}} |\downarrow\rangle|m + 1/2\rangle \\ & + \frac{J\sqrt{S(S+1) - m^2 + 1/4}}{2\sqrt{\Delta E}\sqrt{2\Delta E \mp (2K_2 - J)m}} |\uparrow\rangle|m - 1/2\rangle, \end{aligned} \tag{3.18}$$

for $-S + 1/2 \leq m \leq S - 1/2$. The states with $m = -S - 1/2$ and $m = S + 1/2$ mentioned above can be reobtained from Eq. (3.18), since the prefactor of one of the two product states vanishes in these cases. One obtains $|1, -S{-}1/2\rangle = |1, -S{-}1/2\rangle^{\pm}$ and $|1, S + 1/2\rangle = |1, S + 1/2\rangle^{\pm}$, which completes the enumeration of eigenstates of H_mol.

The Hamiltonian in Eq. (3.2) is the simplest one with an anisotropy-induced energy barrier, which exhibits the essential physics of reading, storing, and writing molecular-spin information, as will be discussed in the present chapter. We want to remark that the model does not take into account magnetic quantum tunneling through the anisotropy barrier in the absence of electronic tunneling. The reason is that this effect, which has been studied in Ref. [22], is typically very weak in the sense that it involves only processes of higher order in the tunneling amplitude.

Transport is described within the rate equation approach discussed in Chapter 2. The main assumption is that the molecule-lead coupling is sufficiently weak, so that the hybridization with the leads can be treated as a small perturbation. The underlying physics is that thermal energies dominate over lead-induced energy broadenings of the molecular levels. This approach is thus referred to as the high-temperature limit of electronic transport [14]. The derivation of rate equations relies on two crucial approximations. Due to the large-reservoir approximation, the leads are hardly affected by the coupling to the molecule such that they remain in separate thermal equilibria despite the applied bias voltage and can be described by Fermi distribution functions $f_\alpha(\epsilon) = 1/[e^{(\epsilon-\mu_\alpha)/T} + 1]$ at chemical potentials μ_α. Formally speaking, the density matrix of the full system can be approximated by the direct product of the density matrices of the molecule and the leads, cf. Eq. (2.6). Due to the Markov approximation memory effects of the molecular dynamics can be neglected. The rate equations for the occupations P^n of many-particle states n read

$$\frac{dP^n}{dt} = \sum_{m \neq n} P^m R_{m\to n} - P^n \sum_{m \neq n} R_{n\to m}, \tag{3.19}$$

where the rates for a transition from state n with energy ϵ_n to state m with energy ϵ_m are given by an expression equivalent to Fermi's Golden Rule,

$$R_{n\to m} = \sum_{\alpha\sigma} \Gamma_{\alpha\sigma} f(\epsilon_m - \epsilon_n - \mu_\alpha) \left(|C^\sigma_{nm}|^2 + |C^\sigma_{mn}|^2 \right). \tag{3.20}$$

Here

$$\Gamma_{\alpha\sigma} = \frac{2\pi}{\hbar} |t_\alpha|^2 \nu_{\alpha\sigma} \tag{3.21}$$

is the typical rate for the tunneling of electrons with spin σ between the molecule and lead α, i.e. the average electronic tunneling time is given by

$$\tau_0 = \left(\sum_{\alpha\sigma} \Gamma_{\alpha\sigma} \right)^{-1}. \tag{3.22}$$

The overlap matrix elements $C^\sigma_{mn} \equiv \langle m|d_\sigma|n\rangle$ ($C^{\sigma\dagger}_{mn} \equiv \langle m|d_{\sigma\dagger}|n\rangle$) are sums of Clebsch-Gordan coefficients and can be computed numerically. Note that, by definition, C^σ_{mn} ($C^{\sigma\dagger}_{mn}$) can only be finite if the electron number of state n is larger (smaller) by 1 than the electron number of state m.

One of the central quantities we are interested in is the tunneling current between the two electrodes. Its operator is given by the commutator

$$I^\alpha = i \left[H, e \sum_{\mathbf{k}\sigma} a^\dagger_{\alpha\mathbf{k}\sigma} a_{\alpha\mathbf{k}\sigma} \right] = -i\, e \sum_{\mathbf{k}\sigma} \left[t_\alpha\, d^\dagger_\sigma a_{\alpha\mathbf{k}\sigma} - t^*_\alpha\, a^\dagger_{\alpha\mathbf{k}\sigma} d_\sigma \right]. \tag{3.23}$$

Following the same steps as in the derivation of the transition rates, second-order perturbation theory yields the following expression for the sequential tunneling current,

$$I^\alpha = e \sum_{ml\sigma} \Gamma_{\alpha\sigma} \Big(f(\epsilon_l - \epsilon_m - \mu_\alpha) |C^\sigma_{ml}|^2 - [1 - f(\epsilon_m - \epsilon_l - \mu_\alpha)]\, |C^\sigma_{lm}|^2 \Big) P^m. \tag{3.24}$$

The spin-resolved current is defined in an obvious way,

$$I^{\sigma\alpha} = e \sum_{ml} \Gamma_{\alpha\sigma} \Big(f(\epsilon_l - \epsilon_m - \mu_\alpha) |C^\sigma_{ml}|^2 - [1 - f(\epsilon_m - \epsilon_l - \mu_\alpha)]\, |C^\sigma_{lm}|^2 \Big) P^m, \tag{3.25}$$

which allows one to write the *spin current* as

$$I^\alpha_s \equiv \frac{I^{\uparrow\alpha} - I^{\downarrow\alpha}}{2e}. \tag{3.26}$$

Here the factor 1/2 accounts for the electron spin.

3.3 Spin amplification, reading, and writing in transport through anisotropic magnetic molecules

3.3.1 Fine structure of the Coulomb blockade

The anisotropy-induced energy barrier of the single-molecule magnet partially lifts the degeneracy of the molecular levels. In the differential conductance dI/dV this manifests itself as a splitting of the Coulomb blockade peaks. The resulting fine structure of the peaks in two-dimensional plots of dI/dV as a function of bias voltage V and gate voltage V_g is shown in Fig. 3.2. For comparison, vanishing anisotropy is considered in Fig. 3.2(a), whereas an anisotropy barrier of $K_2 = 0.04\,\mathrm{eV}$ is considered in Fig. 3.2(b). Each peak can be attributed to an inelastic sequential tunneling process, for which the occupancy changes by unity, $\Delta n = 1$, while the magnetic quantum number changes by $\Delta m = 1/2$. The fine structure of the Coulomb peaks in the differential conductance reveals several interesting features which are specific of the presence magnetic degrees of freedom and which are absent, for instance, in vibrating single-molecule transistors.

Most strikingly, the number of fine structure peaks in dI/dV is different for the two opposite sides of the degeneracy point. In addition, the distance between two subsequent peaks varies a lot. In contrast, the presence of vibrational degrees of freedom usually gives rise to equidistant peaks on both sides of the degeneracy point. In the following we will briefly explain the physics behind these characteristic fine structure patterns.

For the chosen parameters, the peaks on the left side of the crossing point correspond to transitions from empty to singly occupied states. In equilibrium, i.e. at zero bias voltage, the molecule is in the ground state with $n = 0$, $|m| = 2$. The first peak involves the transitions with $|m| = 2 \to 5/2$. Transitions with $|m| = 1 \to 3/2$, $|m| = 0 \to 1/2$, and $|m| = 1 \to 1/2$ are already possible at lower bias voltages, but they are not excited since the corresponding initial states with $|m| = 1$ and $|m| = 0$ are not occupied in Coulomb blockade regime. The second peak in dI/dV corresponds to transitions $|m| = 2 \to 3/2$. The next peaks can be attributed to transitions with $|m| = 1 \to 3/2$, $|m| = 0 \to 1/2$, $|m| = 1 \to 1/2$, $|m| = 2 \to 3/2$.

The peaks on the right side correspond to transitions from singly occupied to empty states. In equilibrium the molecule is in the ground state with $n = 1$ and $|m| = 5/2$. The first peak corresponds to transitions with $|m| = 5/2 \to 2$. The transitions with $|m| = 3/2 \to 2$, $|m| = 1/2 \to 1$, $|m| = 3/2 \to 2$, $|m| = 1/2 \to 0$, $|m| = 3/2 \to 1$ and $|m| = 1/2 \to 1$ are energetically possible already at lower bias voltages but cannot be excited, since the corresponding initial states have not been occupied yet. The next two peaks belong to transitions with $|m| = 1/2 \to 0$, $|m| = 3/2 \to 1$. Note that several transitions appear twice because there are two states with magnetic quantum numbers $\pm 3/2$ and $\pm 1/2$, respectively. For a local spin of length $S = 2$, there exist nine energetically different transitions obeying the selection rules, as illustrated from Figs. 3.2(c),(d).

Interestingly, one of the peaks in Fig. 3.2(b) exhibits negative differential conduc-

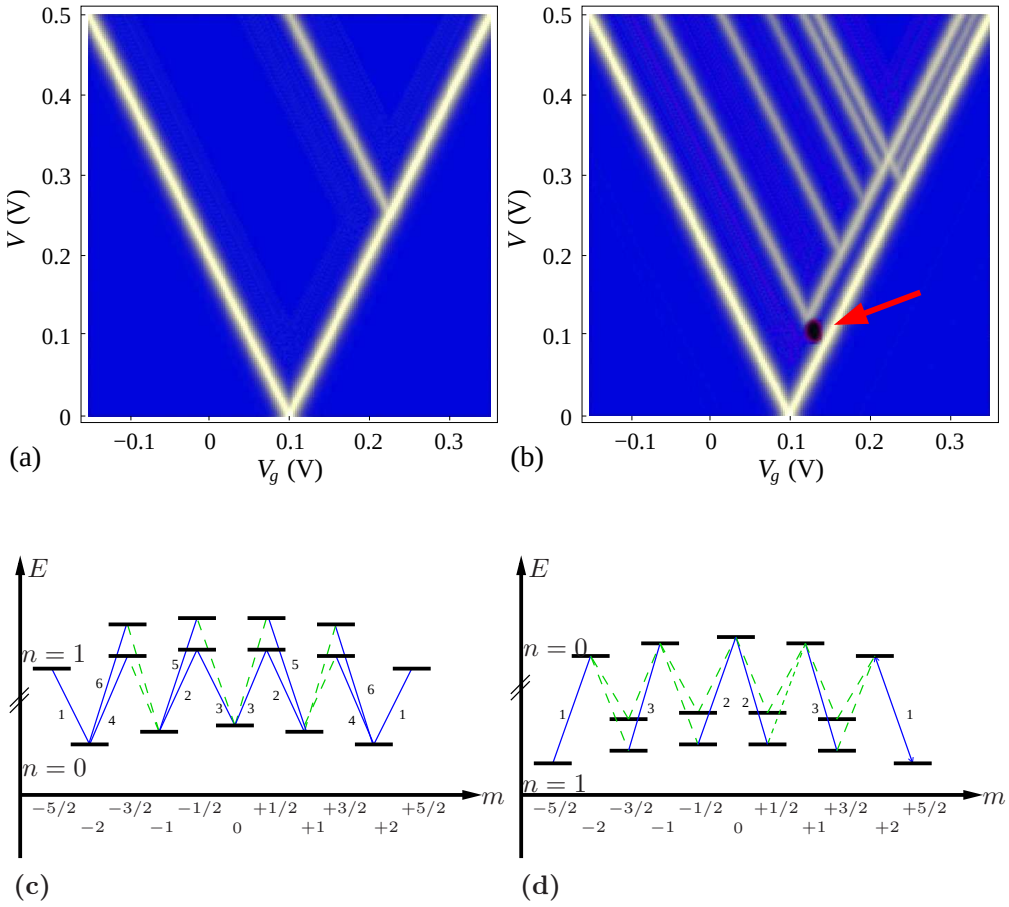

Figure 3.2: (a),(b) Differential conductance dI/dV as a function of gate voltage V_g and bias voltage V. Yellow (bright) colors denote positive values of the differential conductance, dark red colors denote negative values. In (a) results for an isotropic molecular spin are shown. Here we assume $T = 2\,\mathrm{meV}$ for the thermal energy, $\epsilon = 0.2\,\mathrm{eV}$ for the molecular single-particle energy, $J = 0.1\,\mathrm{eV}$ for the exchange coupling, and vanishing magnetic field $B = 0$. Coulomb blockade is found to the left and right of the V-shaped region, whereas within this region a nonzero steady-state current is flowing. The satellite line results from the exchange splitting of energy levels for $n = 1$. In (b) an anisotropy of $K_2 = 0.04\,\mathrm{eV}$ is assumed, leading to a complex splitting of the dI/dV peaks. We find one peak with NDC (arrow). (c),(d) Energy level scheme and allowed transitions between many-particle states with zero electrons ($n = 0$) and one electron ($n = 1$). (c) The $n = 0$ multiplet is energetically lower than the $n = 1$ multiplet. For the chosen parameters, the sequence of peaks in dI/dV can be attributed to the following transitions from empty to singly occupied states, starting at low bias voltage, $|m| = 2 \to 5/2$, $|m| = 2 \to 3/2$, $|m| = 1 \to 3/2$, $|m| = 0 \to 1/2$, $|m| = 1 \to 1/2$, $|m| = 2 \to 3/2$. (d) Reverse case. For the chosen parameters, the sequence of peaks in dI/dV can be attributed to the following transitions from empty to singly occupied states, starting at low bias voltage, $|m| = 5/2 \to 2$, $|m| = 1/2 \to 0$, $|m| = 3/2 \to 1$. Solid arrows mark transitions that occur as peaks in the differential conductance, whereas dashed arrows mark transitions that do not appear in dI/dV, since the corresponding levels are still unoccupied when these transitions become energetically possible.

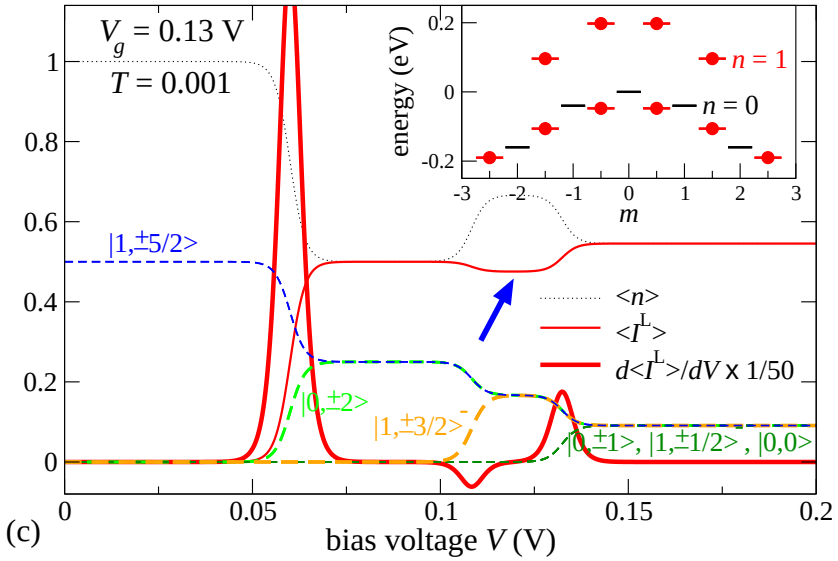

Figure 3.3: Occupation and steady-state current in units of e/τ_0, dI/dV in units of e/τ_0 per volt, and probabilities of various states (dashed) for a cut through the NDC region in Fig. 3.2(b) at the lower thermal energy $T = 1\,\mathrm{meV}$. The arrow indicates the plateau with reduced current. Inset: Molecular energy levels of states with $n = 0$ (black bars) and $n = 1$ (red/gray bars with circles) and magnetic quantum numbers m.

tance. To elucidate this effect we plot in Fig. 3.3 the current, differential conductance, and relevant occupation probabilities at constant gate voltage at a lower temperature.

At low bias voltage only the degenerate ground states $|1, 5/2\rangle$ and $|1, -5/2\rangle$ are occupied and no current is flowing. For increasing bias first the transitions to $|0, \pm 2\rangle$ become possible, cf. the energy-level scheme in the inset in Fig. 3.3. The current then increases to a plateau. On this plateau the four states have equal probability and one obtains

$$I^L = \frac{e}{2} R^L_{|1,\pm 5/2\rangle \to |0,\pm 2\rangle}. \tag{3.27}$$

Next, the transitions from $|0, \pm 2\rangle$ to $|1, \pm 3/2\rangle^-$ become active and the system reaches a new plateau, denoted by an arrow in Fig. 3.3, with

$$I^L = \frac{e}{3} \left(R_{|1,\pm 5/2\rangle \to |0,\pm 2\rangle} + R_{|1,\pm 3/2\rangle^- \to |0,\pm 2\rangle} \right). \tag{3.28}$$

Since for these particular parameters $R_{|1,\pm 3/2\rangle^- \to |0,\pm 2\rangle} / R_{|1,\pm 5/2\rangle \to |0,\pm 2\rangle} < 1/2$ due to the coefficients in Eq. (3.18), the current is *smaller* than on the first plateau, leading to negative differential conductance in the crossover region. The transitions between plateaus are rounded due to the thermal broadening at nonzero temperatures. This mechanism is different from the one found for Mn_{12} complexes [22]—in our case there is no blocking state in which the molecule becomes trapped due to suppressed

outgoing transition rates. On the contrary, the probabilities P^n are equal for all accessible states n.

3.3.2 Spin amplification effect

We now turn to the relaxation of the molecular spin. Consider, for instance, a molecule that is prepared in state $|0,2\rangle$. Assume that at time $t = 0$ a finite bias voltage is switched on, which forces the occupation probabilities of the molecular states to approach a nonequilibrium distribution. In the absence of an external magnetic field, the steady state is a mixed state with equal probabilities for states with magnetic quantum numbers $+m$ and $-m$. One may thus ask the question how fast the average molecular spin decays. Figure 3.4(a) shows the time dependence of the average occupation,

$$n(t) \equiv \sum_i n_i P^i(t), \tag{3.29}$$

and the spin polarization,

$$m(t) \equiv \sum_i m_i P^i(t). \tag{3.30}$$

The time evolution of various occupation probabilities is obtained by solving the non-stationary rate equation, Eq. (3.19), which can be rewritten in matrix form,

$$\dot{\mathbf{P}} = A\,\mathbf{P}, \tag{3.31}$$

where $\mathbf{P} \equiv (P^1, P^2, \dots)$ denotes the vector of all occupation probabilities and A is a matrix with components $A_{nm} = R_{m\to n} - \delta_{nm} \sum_{m'} R_{n\to m'}$. The solution of Eq. (3.31) takes the form

$$\mathbf{P}(t) = e^{At}\,\mathbf{P}(0), \tag{3.32}$$

where the matrix exponential can be calculated numerically. The time evolution (3.32) shows that the conditional probability of finding the molecule in state n at a time t, if it was prepared in state m at time zero, is given by $\mathcal{P}(n|m;t) = (e^{At})_{nm}$, which allows us to calculate the temporal behavior of various observables.

As can be seen from Fig. 3.4(a), the average occupation approaches the constant value $1/2$ on the time scale τ_0, the typical time for a single tunneling event. As soon as the bias voltage is large enough to overcome the Coulomb blockade and allows for the passage of electrons, the molecule spends half of the time in the empty state and half of its time in the charged state.

However, the spin polarization shows a quite different behavior with *two* distinct time scales. Initially, $m(t)$ approaches a quasi-steady state on the time scale τ_0, which in this case has *higher* polarization, since the state $|1,5/2\rangle$ has significant weight. Then, $m(t)$ decays to zero more slowly. This decay is slow because the molecule must pass through several intermediate states to reach a state with opposite spin polarization, essentially performing a one-dimensional random walk, as indicated in the level scheme in Fig. 3.4(b). Figure 3.4(a) shows that the spin relaxation initially becomes slightly faster for increasing K_2. This is due to the change of matrix elements

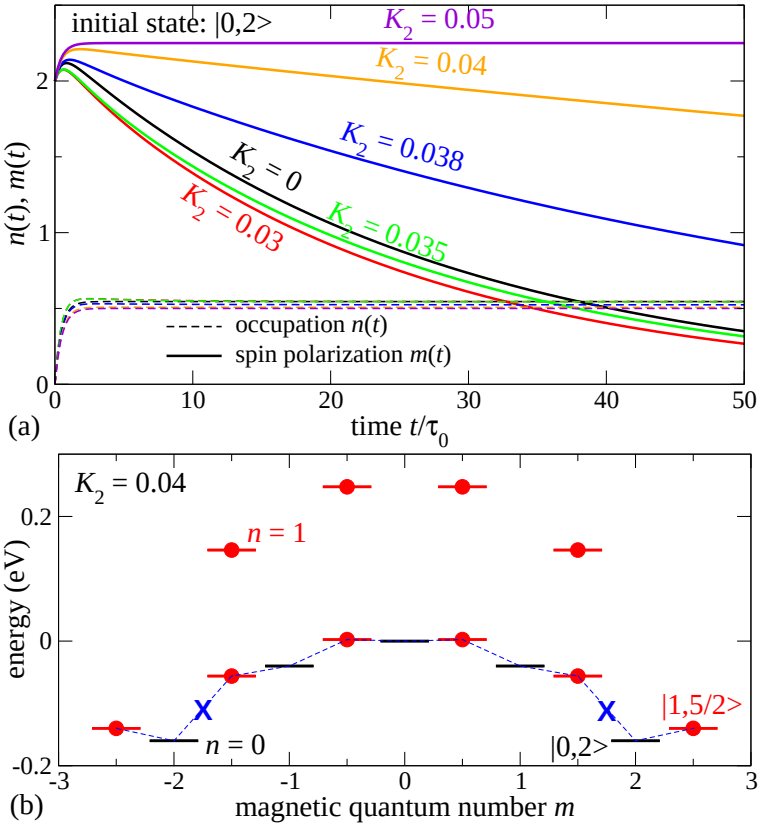

Figure 3.4: (a) Time evolution of the occupation probability $n(t)$ and average spin polarization $m(t)$ for bias voltage $V = 0.2\,\mathrm{V}$, and $T = 2\,\mathrm{meV}$, $S = 2$, $\epsilon_d = 0.12\,\mathrm{eV}$, $U = 1\,\mathrm{eV}$, $J = 0.1\,\mathrm{eV}$, and $B = 0$ for various anisotropies K_2. The gate voltage V_g is absorbed into ϵ_d. The molecule is prepared in state $|0, 2\rangle$ at time $t = 0$. (b) Molecular energy levels for states with occupancy $n = 0$ (black bars) and $n = 1$ (red/gray bars with circles) for the parameters from (a) and $K_2 = 0.04\,\mathrm{eV}$. Active transitions are denoted by dashed lines. The crosses denote the transitions that next become thermally suppressed for larger K_2 or smaller bias V.

C^{σ}_{ij} with K_2. For anisotropies $K_2 \gtrsim 0.04\,\mathrm{eV}$ the decay becomes very slow, since two of the transitions needed to reverse the spin, denoted by the crosses in Fig. 3.4(b), become higher in energy than $eV/2$ and are thus forbidden for $T \to 0$ and thermally activated for $T > 0$.

Importantly, in the regime of thermally activated (slow) spin relaxation a sizeable steady-state current is flowing, since transitions between the states $|0, \pm 2\rangle$ and $|1, \pm 5/2\rangle$ are still possible, see Fig. 3.4(b). This should lead to a significant spin polarization of the current,

$$p^{\alpha} = \frac{I^{\alpha}_{\uparrow} - I^{\alpha}_{\downarrow}}{I^{\alpha}_{\uparrow} + I^{\alpha}_{\downarrow}}, \tag{3.33}$$

since the transitions involving the states $|0, \pm 2\rangle$ and $|1, \pm 5/2\rangle$ only allow for the

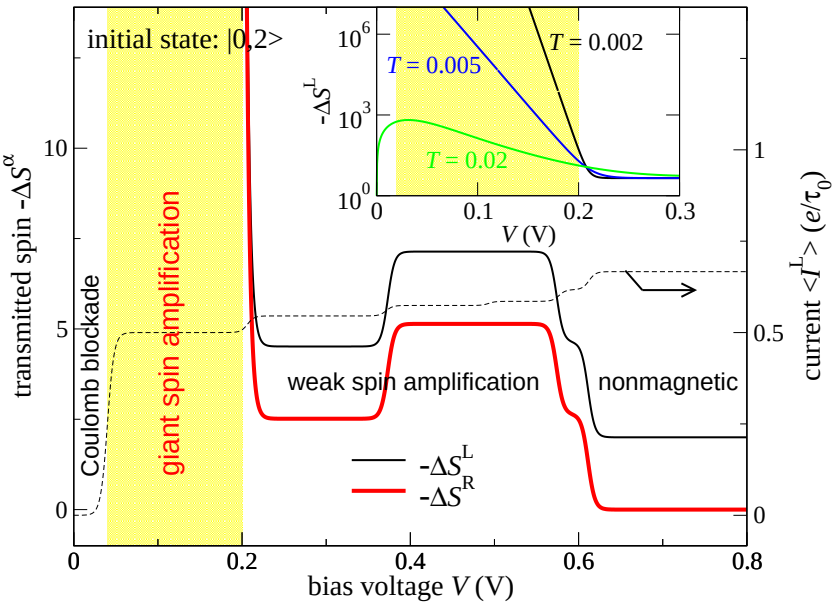

Figure 3.5: Total transmitted spin through the left and right leads for a magnetic molecule prepared in the $n = 0$ maximum spin state $|0, 2\rangle$, as functions of bias voltage. The parameters are the same as in Fig. 3.4 with $K_2 = 0.04\,\mathrm{eV}$. The steady-state current is also shown. The inset shows the spin transmitted through the left lead on a logarithmic scale as a function of bias voltage for three different temperatures. For small bias, $V \to 0$, the transmitted spin for the two lower temperatures should also decrease again, like it does for $T = 0.02\,\mathrm{eV}$. No results are plotted in this regime due to round-off errors in the calculation of the steady-state probabilities.

tunneling of electrons with spin up.

The total spin, that is transmitted from lead α via the molecule into the opposite lead, depends significantly on the initial distribution function $\mathbf{P}_{\mathrm{init}}$ of the molecule and is obtained by integrating the spin current over all times,

$$S[\mathbf{P}_{\mathrm{init}}] = \int_0^\infty dt\; I_s^\alpha(t). \tag{3.34}$$

Results for the bias dependence of the transmitted spin with initial state $|0, 2\rangle$ are shown Fig. 3.5. Varying the bias voltage we observe four different regimes: (i) For small bias voltages we are in the Coulomb blockade regime with a very small steady-state current. However, we find that the total transmitted spin is exponentially large in a characteristic energy barrier ΔE over temperature. In our example ΔE is the difference between the energy $\epsilon^-(1, 3/2) - \epsilon(0, 2)$ necessary for a *spin-down* electron to tunnel in and the available energy $eV/2$ of an incoming electron, which is smaller. While all transitions are thermally activated, the ones necessary to relax the spin have a much higher energy than the transition between $|0, 2\rangle$ and $|1, 5/2\rangle$, which dominates the current. However, the transmission takes exponentially long since this transition is also thermally activated.

(ii) For larger bias we find the most interesting regime. The spin relaxation rate is still small while the current is large. The bias is too small to overcome the energy barrier between spin up and down, see Fig. 3.4(b). If the system starts in state $|0,2\rangle$, the only transition with a large rate is to state $|1,5/2\rangle$, while the transitions to the states $|1,3/2\rangle^{\pm}$ are thermally suppressed in this regime [note that they are higher in energy in Fig. 3.4(b)]. Thus a *spin-up* electron has to enter since the process increases the total spin from $m = 2$ to $m = 5/2$. This electron can leave the molecule through the other lead, returning it to the initial state. On the other hand, a second electron cannot enter the molecule since this would cost a high Coulomb energy U. Therefore, the current is fully spin polarized until a transition to state $|1,3/2\rangle^{-}$ occurs. This thermally suppressed transition happens with a small rate proportional to $\exp(-\Delta E/T)$, where $\Delta E = \epsilon^{-}(1,3/2) - \epsilon(0,2) - eV/2$, as above. Consequently, the current is spin-polarized for an exponentially long time leading to an exponentially large transmitted spin, $|\Delta S^{\alpha}|$ [the negative sign in Fig. 3.5 can be understood by considering the transition rates, Eq. (3.20), in detail]. The exponential dependence of the transmitted spin on $\Delta E/T$ is clearly seen in the inset in Fig. 3.5. The average time $T_s^{\alpha} \equiv 1/|I_s^{\alpha}(t=0)|$ for one unit of spin to be transmitted is of the order of τ_0. More precisely, the total transmitted spin for a long time interval $\Delta t \gg \tau_0$ is of the order of $\Delta t/\tau_0$. The tunneling of a single electron is instantaneous in our model. If T_s^R is short compared to the spin relaxation time in the leads, large opposite magnetizations will be accumulated in the leads, similarly to the effect of spin injection studied intensively in recent years [101]. This effect is induced by the breaking of spin symmetry at $t = 0$ only through the polarization of a single quantum spin, and can thus be described as *giant spin amplification*. It is a promising method to *read out* spin information. The magnetization in the leads could be detected with a pickup coil or by the magneto-optical Kerr effect [42; 102]. A strong amplification mechanism could also facilitate the reliable transfer of spin between individual molecules in a device.

(iii) Further increase of the bias leads to a regime where the transmitted spin is nonzero but not exponentially enhanced. Here, both the spin relaxation rate and the current are large. The bias is large enough to overcome the energy barrier. Figure 3.5 shows that the spin transmitted through the left lead is (in absolute value) larger by two than through the right lead. The reason is that the electrons flow from right to left and that the spin of the initial state has to leave the molecule for $t \to \infty$.

(iv) At large bias *all* transitions between states with $n = 0, 1$ are possible. The spin transmitted through the right, incoming lead, ΔS^R, essentially vanishes. The initial spin leaves the molecule through the left lead, leading to $\Delta S^L \cong -2$. This is the nonmagnetic regime.

The pattern seen in Fig. 3.5 is robust under changes of the anisotropy K_2. For $K_2 = 0$ the regime of giant spin amplification is absent but for any $K_2 > 0$ it exists at sufficiently low temperatures, since the only requirement is that the energy of state $|1,5/2\rangle$ is lower than the one of $|1,3/2\rangle^{-}$ states.

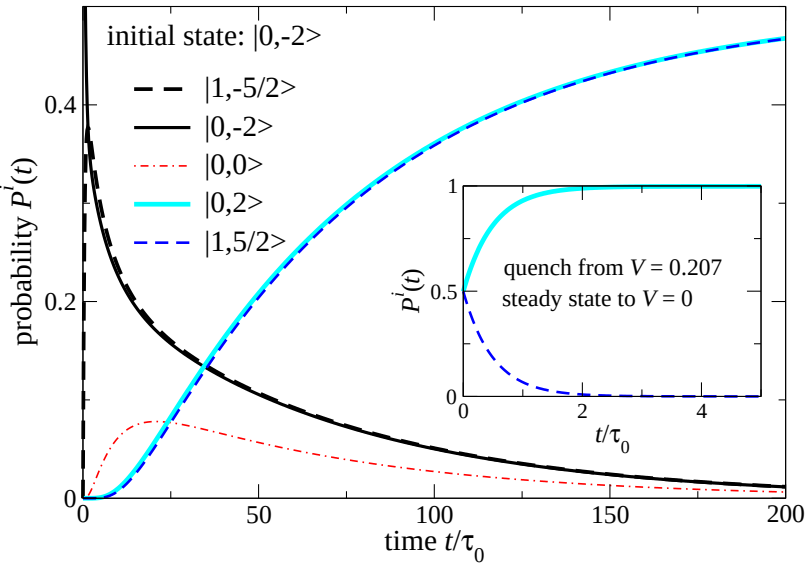

Figure 3.6: Probabilities of molecular states after initial preparation in state $|0,-2\rangle$ as functions of time at the bias voltage $V = 0.207\,\mathrm{V}$. The probabilities of states with extremal spin polarization and of the representative intermediate state $|0,0\rangle$ are shown. A magnetic field ($B = 2\,\mathrm{meV}$) leads to spin relaxation towards larger spin values. The parameters are $T = 0.2\,\mathrm{meV}$ (lower than before), $K_2 = 0.04\,\mathrm{eV}$ and otherwise as in Fig. 3.4(a). Inset: Probabilities after the bias voltage is suddenly switched off in the steady state reached for $V = 0.207\,\mathrm{V}$.

3.3.3 Spin reading and writing

Due to the strong dependence of the transmitted spin on the initial state of the molecule, the spin amplification effect provides an attractive mechanism to read out information through the spin. But for molecular memory applications one also needs the ability to *write* information. In our case, this means that a mechanism is required which enables to switch the molecule to a predetermined spin state. An obvious idea would be to apply a magnetic field to a molecule attached to the nonmagnetic leads considered so far. However, applying a field at zero bias does not work since all transitions remain thermally suppressed so that relaxation to the spin-polarized steady state is exponentially slow.

We find that reliable switching requires a *two-step scheme*. First one applies a magnetic field, which *tilts* the energy levels in Fig. 3.4(b), and a bias voltage that is just large enough to allow transitions in the desired direction but not in the opposite one at sufficiently low temperatures. Since the Zeeman energy B is small, this requires a fine tuning of the bias V on the scale B/e and cooling to temperatures $T \ll B$. Figure 3.6 shows the change of probabilities for all states with $n = 0, 1$ if one starts with state $|0,-2\rangle$ and applies a positive magnetic field to switch the molecule to spin up. The Zeeman energy is chosen as $B = 2\,\mathrm{meV}$. The molecule crosses over from state $|0,-2\rangle$ to a steady state essentially consisting of $|0,2\rangle$ and $|1,5/2\rangle$ on a

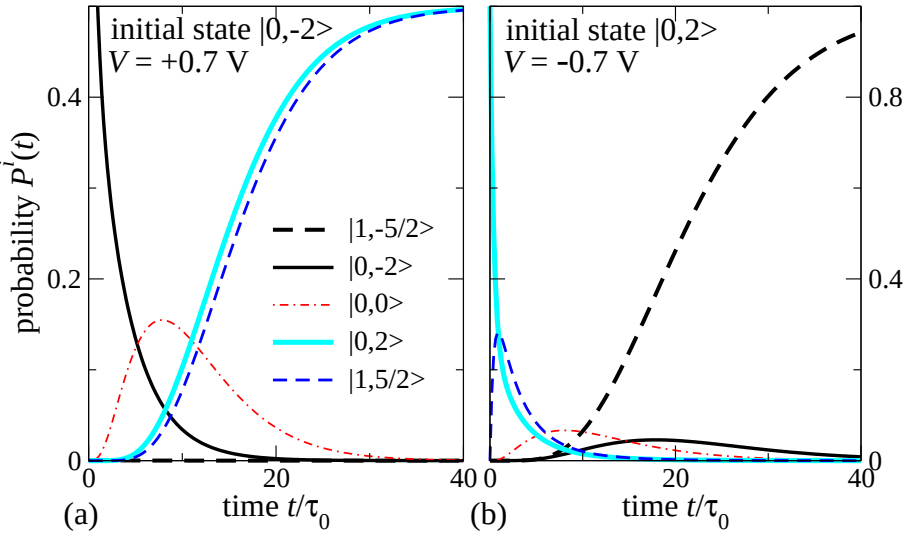

Figure 3.7: Probabilities of molecular states after initial preparation in state (a) $|0,-2\rangle$ and (b) $|0,2\rangle$ as functions of time at the bias voltage (a) $V = 0.7\,\mathrm{V}$ and (b) $-0.7\,\mathrm{V}$. The right lead is ferromagnetic with a ratio of densities of states of $\nu_\downarrow^R/\nu_\uparrow^R = 0.001$. There is no applied magnetic field. The other parameters are as in Fig. 3.6 except for the *much higher* thermal energy $T = 0.02\,\mathrm{eV}$.

time scale of the same order and of the same origin as the spin relaxation times, see Fig. 3.4. The decay of state $|0,2\rangle$ is slow as compared to the typical tunneling time τ_0. Similarly, the occupation and de-occupation of intermediate states with magnetic quantum numbers $m < 2$ happen on a time scale much larger than τ_0. The one-dimensional random walk finally ends in a mixed state with occupation probabilities $1/2$ for the both states $|0,2\rangle$ and $|1,5/2\rangle$.

Note that in a molecular circuit one could apply a magnetic field to many molecules and address a specific one with the bias voltage. In the second step the bias is switched off. The inset of Fig. 3.6 shows that the system then relaxes towards the target state $|0,2\rangle$ on the time scale τ_0. In the nonequilibrium situation, only the two states $|0,2\rangle$ and $|1,5/2\rangle$ are occupied. After switching off the bias, the equilibrium is reached quickly, since it takes only time of the order of one tunneling process for the molecule to be stuck in the ground state $|0,2\rangle$.

However, this writing scheme is problematic because it requires to reverse a large magnetic field between switching events, which is a very slow process. Furthermore, it requires very low temperatures. Our main idea is to overcome these problems by using one ferromagnetic and one nonmagnetic lead. The ferromagnetic lead R is modeled by different densities of states ν_σ^R for up and down ($\sigma = \uparrow, \downarrow$) electrons. We set the spin polarization $\nu_\downarrow^R/\nu_\uparrow^R = 0.001$ so that the lead is essentially a half-metallic ferromagnet such as NiMnSb and CrO_2. For less complete spin polarization in the lead, the reliability of the switching degrades. We note that spin injection from a ferromagnet is not trivial. However, in recent years significant progress has been

made [101]. Nevertheless, the most difficult task in implementing this writing scheme probably is to achieve a high degree of spin polarization of tunneling electrons.

Figure 3.7 shows that one can switch the spin polarization in *both* directions on the time scale of typical spin relaxation times by applying a bias voltage in *vanishing* magnetic field. For $V > 0$ electrons pass through the molecule from right to left, cf. Fig. 3.7(a). Since $\nu_{\downarrow}^{R}$ is small, nearly all electrons have spin up. Due to exchange scattering between the electron spin and the local spin, the latter is increased. Figure 3.7(a) shows that all states except for $|0, 2\rangle$ and $|1, 5/2\rangle$, which have the largest positive magnetization, die out. By switching the bias voltage to $V = 0$ as in Fig. 3.6 we can then make the molecule relax rapidly towards the unique state $|0, 2\rangle$ (not shown). For $V < 0$, electrons flow from left to right, Fig. 3.7(b). Spin-down electrons are essentially trapped on the molecule until they perform a spin exchange with the local spin, which *decreases* the local spin. As the result, the state $|1, -5/2\rangle$ becomes populated at the expense of all other states. Importantly, no fine tuning of the bias voltage is required. Furthermore, the temperature need not be small—the results shown in Fig. 3.7 are calculated with T close to room temperature. Both properties are desirable for molecular-electronics applications.

Note that if one lead is ferromagnetic, the current is generally spin-polarized even in the steady state. Therefore, the total transmitted spin, Eq. (3.34), diverges. However, we can define the *excess* transmitted spin in a certain state relative to the steady state,

$$\Delta S^{\alpha}[\mathbf{P}] = \int_0^{\infty} dt\, [I_s^{\alpha}(t, \mathbf{P}) - I_s^{\alpha}(t = \infty, \mathbf{P})]. \tag{3.35}$$

It is this quantity that exhibits spin amplification as in the case of nonmagnetic leads.

3.4 Transport through anisotropic magnetic molecules with partially ferromagnetic leads

3.4.1 Spin blockade and negative differential conductance

An essential requirement for spintronics devices is the ability to control and detect the spin. In the previous section, we have shown that magnetic anisotropy is crucial for slow spin relaxation in magnetic molecules and leads to the effect of giant spin amplification, which allows one to read out spin information. Furthermore, we have seen that spin writing requires the presence one ferromagnetic lead. For this purpose, we now consider the inelastic transport through an anisotropic magnetic molecule weakly coupled to *one nonmagnetic* and *one ferromagnetic* lead. This configuration is motivated by the possibility to switch the molecule to a predetermined spin state, i.e. to *write* the spin, by applying a bias voltage in zero magnetic field, as discussed above. Our goal is to show that the proposed setup leads to interesting physics going beyond the application of spin writing, including the occurrence of a new spin blockade mechanism and negative differential conductance at room temperature.

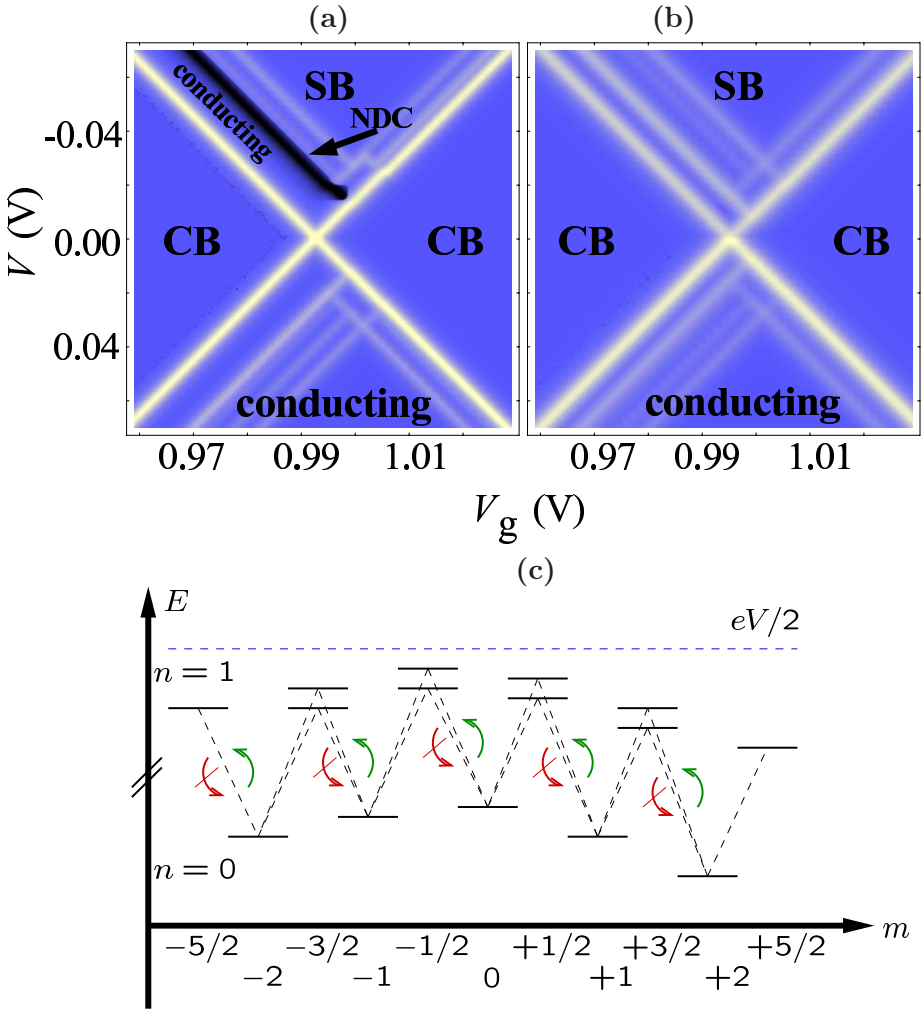

Figure 3.8: Two-dimensional plots of the differential conductance dI/dV in the vicinity of one particular degeneracy point for a magnetic molecule between one nonmagnetic lead, $\nu_\downarrow^L/\nu_\uparrow^L = 1$, and one ferromagnetic lead, $\nu_\downarrow^R/\nu_\uparrow^R \simeq 0$. (a) dI/dV for Zeeman splitting $B = 0.05\,\mathrm{eV}$. (b) dI/dV for vanishing magnetic field. Here we choose $J = K_2 = 5\,\mathrm{meV}$ and zero temperature. When the magnetic field is switched on, the Coulomb blockade regime and the spin blockade regime are separated by a finite window of bias voltage for which the conductance is high. Since the conductance is low (governed by $\nu_\downarrow^R/\nu_\uparrow^R$) in the spin blockade regime, NDC must occur where the conductance drops again. (c) Scheme of the molecular energy levels with all allowed transitions involving the states with $n = 0$ and $n = 1$ electrons in an external magnetic field. In the spin blockade regime all transitions are *energetically* possible if the bias voltage V is large enough. However, the rates for spin-down electrons tunneling from the molecule into the right lead (curved arrows with slash) are strongly suppressed due to the small density of states.

We start by discussing the steady-state transport properties. As noted above, the anisotropy of the local spin partially lifts the degeneracy of the molecular energy levels with respect to the magnetic quantum number m, where m denotes the eigenvalues of the z component of the total spin $\mathbf{S}_{\mathrm{tot}}$ [22; 103]. This leads to a splitting of peaks in the differential conductance dI/dV at low temperatures, as shown in Fig. 3.8 for (a) finite and (b) vanishing magnetic field B. We assume again a spin polarization of $\nu_{\downarrow}^{R}/\nu_{\uparrow}^{R} = 0.001$ for the densities of states of right lead. The complicated fine structure in the vicinity of the degeneracy point V_0 arises from the anisotropy of the local spin and the exchange interaction between the electrons in the molecular orbital and the local spin. This feature has been discussed for the case of two unpolarized leads above and can be explained in an analogous way. Strikingly, dI/dV is *asymmetric* with respect to the bias voltage, i.e., several fine-structure peaks have a significantly different intensity when the bias changes sign. This results from the breaking of spin-rotation symmetry by the ferromagnetic lead together with spin selection rules for the tunneling processes.

The V-V_g map shows three transport regimes: At low bias the current is thermally suppressed due to the Coulomb blockade, except close to the degeneracy point V_0. The electron number on the molecule is constant, i.e., $n = 0$ for $V_g < V_0$ and $n = 1$ for $V_g > V_0$, since all transitions between different molecular charge states are energetically forbidden. At large positive bias the conductivity of the molecule is high, since the electrons in the right lead have enough energy to overcome the energy barrier between the $n = 0$ and $n = 1$ states. This is the conducting regime. However, at large negative bias the conductivity of the molecule is low. This current suppression is due to a spin blockade mechanism which will be explained in the following.

There exist essentially two definitions of spin blockade that are frequently used in the literature on transport through quantum dots. The original definition refers to the phenomenon that transition probabilities for single-electron tunneling vanish between states corresponding to successive electron numbers if the total spins differ by more than $\Delta S = 1/2$ [22; 104–107]. The other, more general definition refers to the situation that the tunneling rate for electrons of one spin direction is strongly suppressed relative to the other, e.g. due to ferromagnetic leads [108; 109] or Zeeman splitting [110]. In this case the system can be stuck in a particular molecular many-body state because the rates for leaving these states are small.

In our case the spin blockade is related to the second mechanism [108–110] but the interaction between the electrons on the molecule and the local anisotropic spin leads to a modified picture. As soon as the bias is sufficiently high, all transitions between the $n = 0$ and the $n = 1$ multiplets are energetically possible, as shown in Fig. 3.8(c). Selection rules for sequential tunneling require $\Delta m = 1/2$. Both spin-up and spin-down electrons hop *onto* the molecule with equal rates, since the densities of states $\nu_{\uparrow}^{L}$ and $\nu_{\downarrow}^{L}$ in the left (incoming) lead are equal for both spin directions. On the other hand, spin-up electrons leave the molecule much faster due to the polarization of the right (out-going) lead. Electrons keep flowing through the molecule until a spin-down electron tunnels in. This spin-down electron can leave

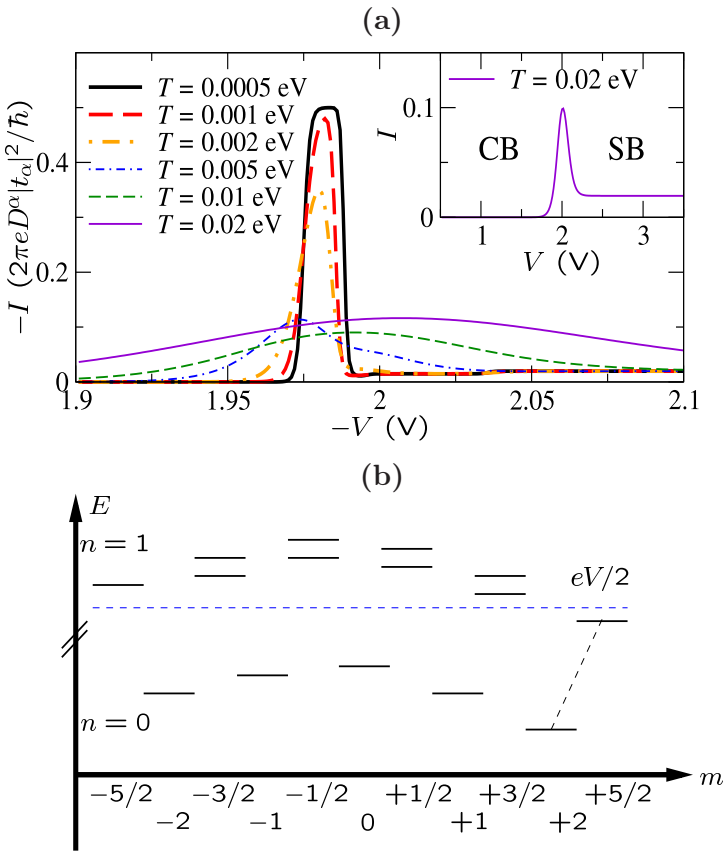

Figure 3.9: (a) Current-voltage characteristics in the vicinity of the Coulomb blockade threshold assuming $K_2 = J = B = 0.05\,\mathrm{eV}$. The inset shows the current over a broader voltage range. (b) Energy level scheme for the $n = 0$ and $n = 1$ spin multiplets as a function of the magnetic quantum number m. The bias voltage is just high enough to allow the transition between the many-particle states with spin $m = S$ and $m = S + 1/2$. The steady-state current is highly spin-polarized, since the tunneling of spin-down electrons is thermally suppressed. This regime corresponds to the *plateau* with enhanced current in (a).

the molecule only with a very small tunneling rate due to the low density of states $\nu_{\downarrow}^{R}$. On the other hand, it can rapidly leave the molecule as a spin-*up* electron if the local spin is simultaneously reduced by unity. However, the number of possible spin flips is limited, depending on the initial spin state and the length S of the local spin. Therefore, the molecule finally ends up in the singly charged state with minimal spin, i.e., $S_{\mathrm{tot}} = -S - 1/2$. Further electronic tunneling is *blocked*, since the left lead is energetically unreachable and the right lead has a low density of states for spin-down electrons, cf. Fig. 3.8(c).

Another interesting feature shown in Fig. 3.8(a) is the appearance of a finite window of bias voltages between the Coulomb blockade and spin blockade regimes, for which the conductivity of the molecule is high. This obviously leads to negative

differential conductance when the spin blockade regime with low conductivity is entered. Figure 3.9(a) shows the current-voltage characteristics in the vicinity of the Coulomb blockade threshold at zero gate voltage for finite magnetic induction. The external field tilts the molecular energy levels with respect to the magnetic quantum number m due to the additional Zeeman energy, as sketched in Fig. 3.9(b). This removes any degeneracies of the spin multiplets entirely. For small bias voltages and low temperatures the current is suppressed due to the Coulomb blockade. But as soon as the transition from the ground state of the $n = 0$ multiplet with maximal spin, $m = S$, to the lowest-energy state of the $n = 1$ multiplet with maximal spin, $m = S + 1/2$, becomes energetically allowed the current increases to the plateau shown in Fig. 3.9(a). These two levels are then equally occupied. Moreover, the current through the molecule is highly spin polarized, since spin-up electrons tunnel rapidly through the molecule, whereas the passage of spin-down electrons is suppressed. When the bias is further increased to allow tunneling also of spin-down electrons, the molecule goes over to the state with $n = 1$ and $m = -S - 1/2$ in several steps and the current is strongly suppressed by the spin blockade mechanism discussed above. The first required transition from $n = 0$ and $m = S$ to $n = 1$ and $m = S - 1/2$ has the highest energy so that all following transitions become active at the same bias. The width ΔV of the bias window with large current corresponds to twice the difference of these two excitation energies and is given by

$$e\Delta V = 2\big[2SK_2 + B - \Delta E(S + 1/2) - \Delta E(S - 1/2)\big], \tag{3.36}$$

where $\Delta E(m) \equiv [K_2(K_2-J)m^2+(J/4)^2(2S+1)^2]^{1/2}$. This holds as long as $\nu_\downarrow^R/\nu_\uparrow^R \ll 1$ and the Zeeman energy B is not too small. For $B \to 0$ we have to take into account that the states with $n = 0$ and $m = \pm S$ become degenerate ground states.

The observation of the current plateau requires the temperature to be small compared to $e\Delta V$, see Fig. 3.9(a). At *high* temperatures the current steps broaden so that the plateau of high current vanishes. Nevertheless, the current remains large at bias voltages close to the transition point from the Coulomb blockade to the spin blockade, as shown in the inset in Fig. 3.9(a). For vanishing magnetic field, $B = 0$, there is no enhanced current at low temperatures, as we will explain below. Nevertheless, at high temperatures a pronounced current maximum develops close to the transition from the Coulomb blockade to the spin blockade, as shown in Fig. 3.10(a). For anisotropy barriers $K_2 > 0$, the peak grows and broadens with increasing temperature. Since the current remains small deep in the spin blockade regime, a broad region of negative differential conductance develops. This is remarkable since negative differential conductance, which has already been observed or predicted for many systems, is usually a low-temperature effect. The high-temperature NDC is a distinct effect, since it appears even when there is no NDC at low temperatures.

Before we explain the high-temperature negative differential conductance we note that the temperature dependence of the I-V curves is qualitatively different for vanishing anisotropy barrier and *large* exchange interaction, $K_2 \ll T \ll J$, as shown in Fig. 3.10(b). Most striking is the fact that the maximum of the peaks stays constant for $T \to 0$. For this situation the energy levels are shown in Fig. 3.10(c).

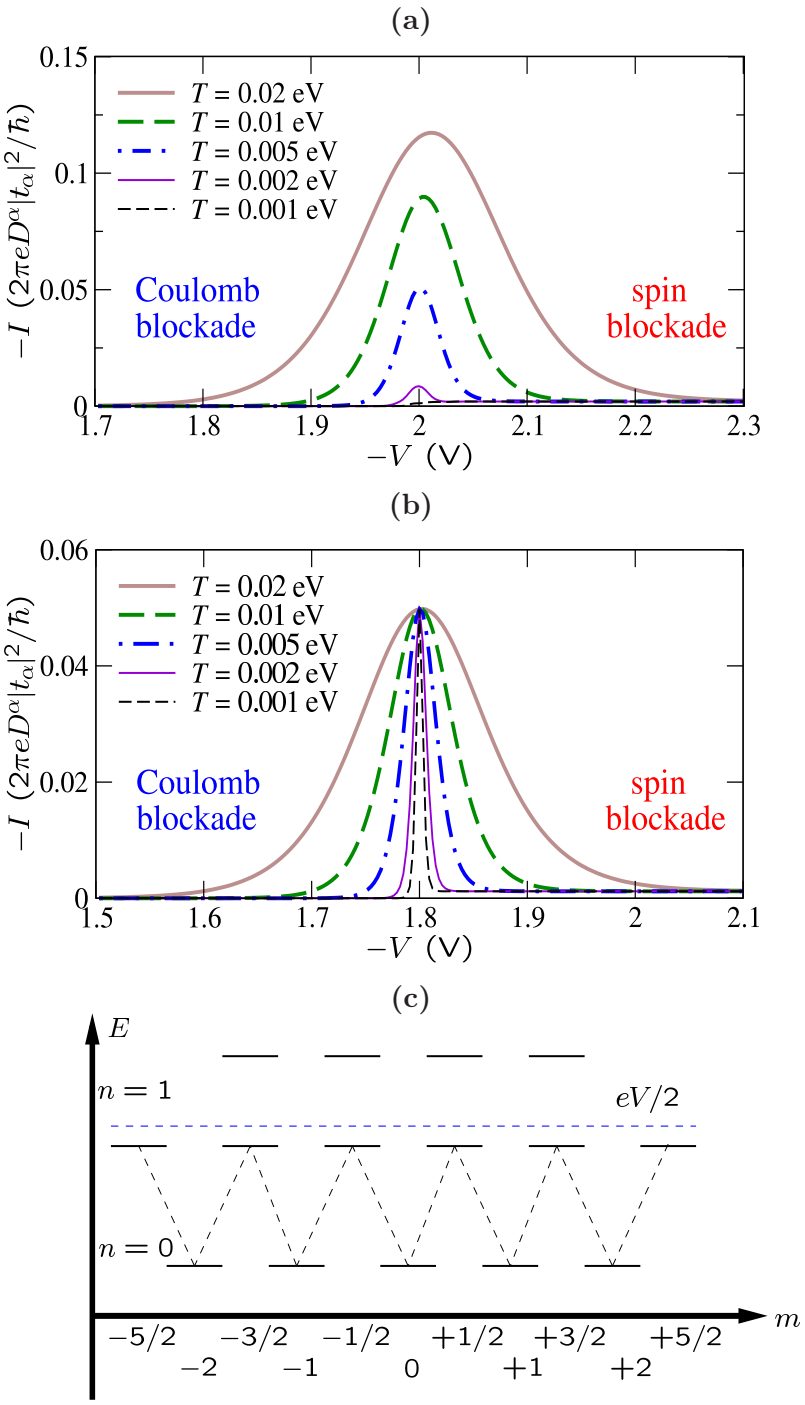

Figure 3.10: (a),(b) Temperature dependence of the current-voltage characteristics exhibiting negative differential conductance. In (a) we assume $K_2 = J = 5\,\text{meV}$ and vanishing magnetic field, corresponding to the spin multiplets schematically shown in Figs. 3.8 and 3.9, except that now $B = 0$. In (b) we assume a large exchange interaction $J = 0.1\,\text{eV}$ and vanishing magnetic anisotropy $K_2 = 0$. (c) Energy level scheme for the $n = 0$ and $n = 1$ multiplets as a function of the magnetic quantum number m for the case in (b).

It is obvious that only a *single* energy difference is relevant as long as the higher $n = 1$ quartet is not occupied. If $eV/2$ exactly equals this transition energy, the Fermi functions in the rates, Eq. (3.20), for these transitions all equal $1/2$ and are thus independent of the temperature. Consequently, the steady-state probabilities and the current are also independent of the temperature at this bias. For lower bias all transitions from states with occupancy $n = 0$ to states with $n = 1$ are thermally suppressed and for higher bias the relevant transitions become fully active (the Fermi functions approach unity) and we enter the spin blockade regime discussed above. In both regimes the current decreases for $T \to 0$. (In fact the current maximum does not occur exactly where $eV/2$ equals the transition energy. Rather, it depends on the balance between the thermally activated transition rates from $n = 0$ to 1 and the spin-down transition rates from $n = 1$ to 0 controlled by $\nu_\uparrow^R/\nu_\downarrow^R$.) In the spin blockade regime this leads to negative differential conductance. It is remarkable that the spin blockade—a quantum effect—leads to large negative differential conductance at room temperature.

For the case of large anisotropy barriers $K_2 > 0$ and, more importantly, small exchange coupling J, cf. Fig. 3.10(a), the current at the maximum increases with temperature since transport through the higher $n = 1$ quartet contributes more and more. For the same reason the current maximum shifts to larger bias voltages. On the other hand, the current maximum vanishes for $T \to 0$. In Fig. 3.10(a) we have assumed vanishing magnetic field and there is no window of enhanced current at low temperatures: At small bias, in the Coulomb blockade regime, the steady state has predominantly $n = 0$ and $m = -S$ due to the asymmetric tunneling rates into the right lead. As the bias is increased the system *directly* crosses over to the spin blockade regime when the bias equals the excitation energy to the state with $n = 1$ and $m = -S - 1/2$.

3.4.2 Super-Poissonian shot noise

In the previous sections we have seen that interesting dynamical transport phenomena such as slow spin relaxation and giant spin amplification are revealed aside from remarkable steady-state properties such as the fine structure of the Coulomb diamonds. For this reason, we now pay more attention to dynamical properties of the system and study the intrinsic noise (also known as shot noise) of a single-molecule magnet due to the stochastic character of electron tunneling. Our motivation is to show that the current suppression originating from the discussed spin blockade mechanism can easily be distinguished experimentally from other blockade mechanisms by characteristic features in the noise spectrum.

The noise spectrum is defined as the Fourier transform of the current-current correlation function [111],

$$S^{\alpha\beta}(\omega) = 2\int_{-\infty}^{\infty} dt\, e^{i\omega t}\langle \delta I^\alpha(t)\, \delta I^\beta(0)\rangle, \tag{3.37}$$

where α and β denote lead indices. The noise of the symmetrized current $I = I^L + I^R$

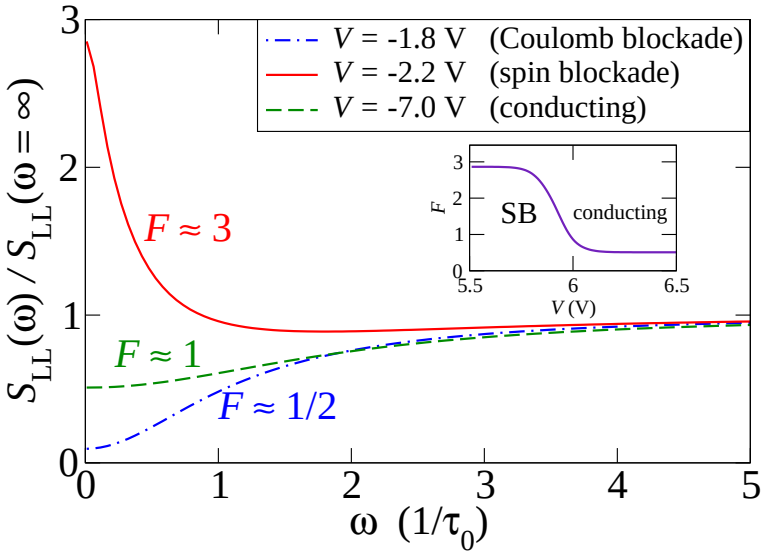

Figure 3.11: Current noise spectrum. Shown are the normalized correlation functions $S_{LL}(\omega)/S_{LL}(\omega = \infty)$ for three different bias voltages representing the three transport regimes: $V = 1.8\,\mathrm{V}$ (Coulomb blockade CB), $V = 2.2\,\mathrm{V}$ (spin blockade SB), and $V = 7.0\,\mathrm{V}$ (conducting regime). The zero-frequency limit gives the Fano factor $F = S(\omega \to 0)/2e|I|$ which tends to 3 in the spin blockade regime, if we assume the one lead to be *halfmetallic*, $\nu_\downarrow^R/\nu_\uparrow^R \to 0$.

reads

$$S(\omega) \equiv \frac{1}{4}\left[S^{LL}(\omega) + S^{LR}(\omega) + S^{RL}(\omega) + S^{RR}(\omega)\right]. \tag{3.38}$$

Nonequilibrium current noise in mesoscopic structures is a consequence of the discreteness of the charge carriers [112]. For conductors with open channels the fermionic statistics of electrons results in a suppression of the shot noise below the classical Schottky limit [113]. This was first noted by Khlus [114] and Lesovik [115] for single-channel conductors and generalized by Büttiker [116] for many-channel conductors. Mesoscopic conductors are often probed by two or more leads. In this case quantum statistics also induces cross-correlations between the currents in different terminals α and β. Since these correlations vanish in the classical limit, even their sign is not obvious *a priori* [110].

An exact solution of the non-stationary rate equations describing the dynamics of the single-electron transistor is obtained in the frequency representation. The low-frequency limit of the noise intensity, which is relevant for the calculation of Fano factors, is considered in detail. The discussion is based on the viewpoint of Korotkov [111]. The time evolution of the occupation probabilities P_n of various many-particle states is obtained as explained in Sec. 3.3.2.

Figure 3.11 shows the current noise spectrum for three different bias voltages representing the Coulomb blockade, spin blockade, and conducting regime. The latter is reached here by applying a large negative bias, which overcomes the spin blockade

by allowing conduction through doubly occupied states. Here we consider the normalized correlation function $S_{LL}(\omega)/S_{LL}(\omega \to \infty)$ which gives information about temporal correlations of tunneling events for the left lead. According to Eq. (3.37), $S_{LL}(\omega)$ is the Fourier transform of the current-current correlation function. The constant part $S_{LL}(\infty)$ comes from the autocorrelation contribution, which is a positive delta-function at vanishing time difference. In the conducting regime the noise spectrum exhibits a minimum at zero frequency since the corresponding contribution to the correlation function is negative. Whenever the molecule is doubly occupied, further electrons cannot tunnel in due to the Pauli principle. This is the usual *antibunching* effect for fermions. The typical frequency scale apparent in Fig. 3.11 for the conducting case is the inverse of the typical time the molecule remains doubly occupied, which is of the order of the typical tunneling time $\tau_0 = (2\pi|t_L|^2\nu^L/\hbar)^{-1}$.

Anticorrelation of subsequent tunneling events is also found for the Coulomb blockade regime. In this case, however, the anticorrelation is due to the Coulomb repulsion, which hinders a second electron from entering the singly occupied molecule. As it is well known, the Fano factor $F \equiv S(\omega = 0)/2e|I|$, which is defined as the ratio of the zero-frequency noise to the classical Schottky result [112], is close to unity in this case, since single electrons tunnel through the system in rare, uncorrelated events.

In contrast, in the spin blockade regime the noise is enhanced at $\omega = 0$. This maximum results from a *bunching* of the charge carriers, which means that several electrons tend to tunnel through the molecule within a short time interval. On the other hand, the average waiting time between such events is comparatively long. Results for the Fano factor reveal super-Poissonian shot noise, $F > 1$, in the spin blockade regime. It reaches the value $F \simeq 3$ for one halfmetallic lead, $\nu^R_\downarrow/\nu^R_\uparrow \to 0$. This factor can be understood by taking into consideration that the Fano factor contains information about the charge of the current-carrying particles and the quantum correlations between them. In the spin blockade regime, the molecule is in the singly occupied state and has minimal spin for most of the time. Electrons from the left lead cannot hop onto the molecule until a spin-down electron is emitted into the right lead. The rate for this process is strongly suppressed. However, if the spin-down electron does leave the molecule, the probability for further tunneling processes is high, since electrons of both spin directions may then tunnel into the molecule. A current is flowing until a spin-down electron occupies the molecule again, which leads to the spin blockade state. Analytical results for the Fano factor can be obtained from the following expression, cf. Ref. [29],

$$F = \langle N\rangle \frac{\langle t^2\rangle - \langle t\rangle^2}{\langle t\rangle^2} + \frac{\langle N^2\rangle - \langle N\rangle^2}{\langle N\rangle^2}. \tag{3.39}$$

Here N denotes the number of electrons tunneling through the molecule in one *bunch* and t the waiting time between such processes. The waiting times t between the tunneling events approximately obey a Poisson distribution. Since the electronic transport is dominated by the three states with $n = 0$, $m = -S$ and $n = 1$, $m = -S \pm 1/2$, one finds a probability of $1/2^N$ for N electrons in the bunch. From this

one can calculate the moments occurring in Eq. (3.39) and obtains $F = 3$. This result is of the same fundamental origin as the super-Poissonian shot noise found for quantum dots in the spin blockade regime in Ref. [110], which considers the case $K_2 = J = 0$ (no local spin) and nonmagnetic leads. In this case the spin blockade is induced by application of a magnetic field [110]. We note that Eq. (3.11) also gives the observed value $F = 1/2$ for the conducting regime.

3.4.3 Spin-charge conversion

As discussed above, slow spin relaxation leads to the effect of giant spin amplification in transport through anisotropic magnetic molecules coupled to two *nonmagnetic* leads. At bias voltages close to the Coulomb blockade threshold the total spin transmitted from one lead to the other can become exponentially large at low temperatures, if the molecule is prepared in a magnetically polarized initial state at time $t = 0$. However, if one lead is *ferromagnetic* the steady-state current is highly spin-polarized so that it is necessary to consider the *excess* transmitted spin instead. Analogously, one can define the *excess transmitted charge*: Assume that the molecule is prepared in a specific state n at time zero and then evolves according to the rate equations (3.19). Since it approaches the steady state exponentially as a function of time, the excess charge

$$\Delta Q_n^\alpha \equiv \int_0^\infty dt\, [I^\alpha(t) - I^\alpha(t=\infty)] \tag{3.40}$$

is finite. Here our main observation is that ΔQ_n^α can depend very strongly on the initial state n if the steady state shows spin blockade behavior. Practically it is much easier to measure the charge accumulation in the leads instead of the excess spin [42; 43; 117], since the accumulated charge is conserved (except for leakage currents), whereas the spin is not. Moreover, it should be easier to employ the excess charge for further data processing.

Results for the excess transmitted charge as a function of bias voltage are shown in Fig. 3.12(a), where an initial state with $n = 0$ and spin $m = S$ is assumed. The fine structure close to the Coulomb blockade threshold basically originates from the anisotropy of the local spin. Most striking is the exponential enhancement of ΔQ_n^α at voltages *above* the Coulomb blockade threshold, where the steady-state current is already nonzero (but small due to the spin blockade). When the bias is just large enough to enable the two transitions from the $n = 0$ state with extremal spin to the $n = 1$ state with extremal spin, $m = \pm S \to \pm(S+1/2)$, the system initially prepared in a state with *maximal* spin, $m = S + 1/2$, for an exponentially long time only performs transitions between the two extremal state connected by a solid line in the level scheme in Fig. 3.12(b). Thus a sizable—and completely spin-polarized—current is flowing until the molecule overcomes the anisotropy barrier by thermal activation. After that it rapidly relaxes towards the spin blockade state, which shows a small steady-state current. On the other hand, if the molecule is prepared in the state with minimal spin, $m = -S - 1/2$, it already starts out in the spin blockade state

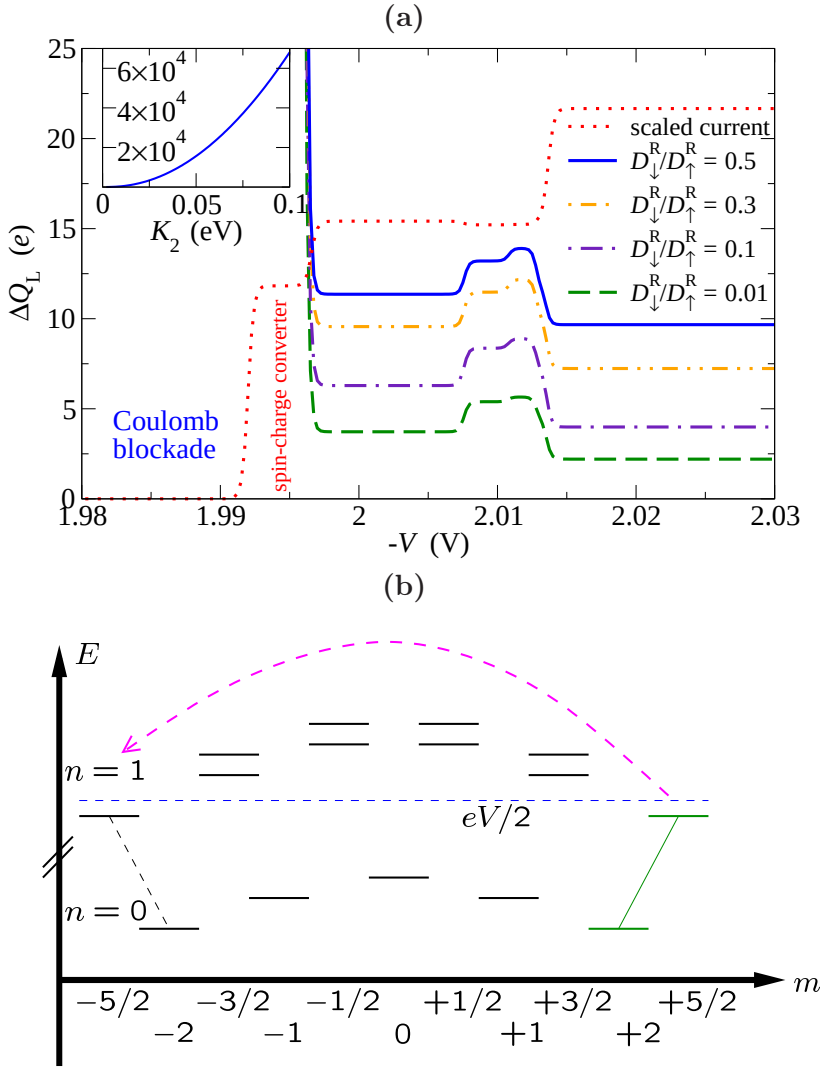

Figure 3.12: (a) Excess transmitted charge ΔQ^L as a function of bias voltage in the vicinity of the first Coulomb blockade step for different polarizations of the right lead: $\nu_\downarrow^R/\nu_\uparrow^R = 0.5,\ 0.3,\ 0.1$, and 0.01. We assume $J = 4\,\mathrm{meV}$, $K_2 = 1\,\mathrm{meV}$, vanishing magnetic field and an initial state with $n = 0$ and $m = 2$. The steady-state current for $\nu_\downarrow^R/\nu_\uparrow^R = 0.1$ is also shown. The inset shows ΔQ^L as a function of the anisotropy constant K_2, where the bias voltage V corresponds to the arithmetic mean of the first two excitation energies. (b) Energy level scheme of the $n = 0$ and $n = 1$ multiplets. The molecule is prepared in the initial state with spin $m = S$.

and the current is always small. Thus in the first case an exponentially large excess charge is accumulated in the leads in addition to the excess spin. In this regime the proposed setup functions as a *spin-charge converter*, i.e., spin information can be read through measurement of the excess transmitted charge.

On the other hand, if the bias is large enough to allow further transitions involving other levels, the system rapidly relaxes back towards spin blockade so that ΔQ_n^α is of the order of the elementary charge e. Note that the excess transmitted charge increases for increasing anisotropy of the local spin, as can be seen from the inset in Fig. 3.12(a).

3.5 Cotunneling and non-equilibrium magnetization in magnetic molecular monolayers

3.5.1 Cotunneling through magnetic molecules

Until now we have restricted ourselves to the regime where the electronic tunneling in and out of the molecule is governed by incoherent, sequential tunneling processes only. However, if these are suppressed due to blockade mechanisms such as the Coulomb blockade or the Franck-Condon blockade [29], cotunneling processes naturally play an important role and may give the dominant contribution to the electronic tunneling. Cotunneling processes are next to leading order in the tunneling Hamiltonian and describe the coherent transfer of an electron from one lead to another in two steps, as discussed in Chapter 2. Importantly, the intermediate state can have an energy much larger than the energy of the initial state. Thus cotunneling is referred to as a virtual process.

In the following we study magnetic molecules under a bias voltage in the Coulomb-blockade regime. Our main result is that, while any features in the differential conductance are very small due to the suppression of the current, there are large changes in the average magnetic moments of the molecules with bias voltage and applied field. The measurement of magnetic moments of submonolayers of molecules has been demonstrated years ago [118; 119]. Even the detection of the spin of a single molecule may be feasible [76; 120]. However, it is not clear how to perform such a measurement in a molecular-junction experiment. A recent experiment suggests that it is possible to employ carbon nanotube superconducting quantum interference devices for the detection of the switching of single magnetic moments [121].

For the most part, we consider here a monolayer of magnetic molecules sandwiched between two metallic electrodes, see Fig. 3.13, since the measurement of the magnetization of a thin film is expected to be easier than that of a single molecule. Furthermore, various molecules form nearly perfect monolayers on metallic substrates [122]. We assume that magnetic interactions between the molecules are negligible and that all molecules have the same spatial orientation relative to the electrodes [122]. In this case it is sufficient to consider the properties of a single molecule. described by the Hamiltonian in Eq. (3.2).

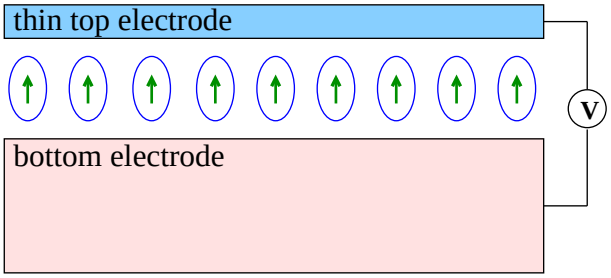

Figure 3.13: Sketch of the geometry. A monolayer of magnetic molecules is adsorbed on a metallic substrate, which serves as a bottom electrode. A thin metallic layer is used as a top electrode.

The leading contribution to the transition rates between molecular many-particle states is of second order in H_t, corresponding to Fermi's Golden Rule. Going beyond the leading order is possible by employing a T-matrix formalism, as discussed in Chapter 2. The T matrix [83] is self-consistently given by

$$T = H_t + H_t \frac{1}{E_i - H_0 + i\eta} T. \tag{3.41}$$

Here E_i is the energy of the initial state $|i\rangle|n\rangle$, where $|i\rangle$ refers to the equilibrium state of the left and right leads (at different chemical potentials) and $|n\rangle$ is a molecular state, and η is a positive infinitesimal ensuring that the Green function in T is retarded. To fourth order, the transition rate from state $|i\rangle|n\rangle$ to $|f\rangle|n'\rangle$ with an electron tunneling from lead α to lead α' is given by

$$\Gamma_{\alpha\alpha'}^{ni;n'f} = \frac{2\pi}{\hbar} \left| \langle f|\langle n'|H_t \frac{1}{E_i - H_0 + i\eta} H_t |n\rangle|i\rangle \right|^2 \delta(E_f - E_i). \tag{3.42}$$

The energies of the initial state $|n\rangle|i\rangle$ and final state $|n'\rangle|f\rangle = |n'\rangle a^\dagger_{\alpha'\mathbf{k}'\sigma'} a_{\alpha\mathbf{k}\sigma}|i\rangle$ are denoted by E_i and E_f, respectively. We only consider the case of infinite U, i.e. double occupancy of the molecule is forbidden, and obtain

$$\begin{aligned} \Gamma_{\alpha\alpha'}^{nn',00} &= \frac{2\pi}{\hbar} t_\alpha^2 t_{\alpha'}^2 \sum_{\sigma\sigma'} \nu_{\alpha\sigma}\nu_{\alpha'\sigma'} \int d\epsilon \left| \sum_{n''} \frac{C^{\sigma'}_{n'n''} C^{\sigma *}_{nn''}}{\epsilon + \epsilon_n - \epsilon_{n''} + i\eta} \right|^2 \\ &\quad f(\epsilon - \mu_\alpha)\,[1 - f(\epsilon + \epsilon_n - \epsilon_{n'} - \mu_{\alpha'})], \end{aligned} \tag{3.43}$$

$$\begin{aligned} \Gamma_{\alpha\alpha'}^{nn',11} &= \frac{2\pi}{\hbar} t_\alpha^2 t_{\alpha'}^2 \sum_{\sigma\sigma'} \nu_{\alpha\sigma}\nu_{\alpha'\sigma'} \int d\epsilon \left| \sum_{n''} \frac{C^{\sigma'}_{n''n} C^{\sigma *}_{n''n'}}{-\epsilon + \epsilon_{n'} - \epsilon_{n''} + i\eta} \right|^2 \\ &\quad f(\epsilon - \mu_\alpha)\,[1 - f(\epsilon + \epsilon_n - \epsilon_{n'} - \mu_{\alpha'})], \end{aligned} \tag{3.44}$$

where $\Gamma_{\alpha\alpha'}^{nn',00}$ ($\Gamma_{\alpha\alpha'}^{nn',11}$) denotes the cotunneling rate describing virtual transitions between two empty (singly occupied) molecular states. To the same order in H_t, one

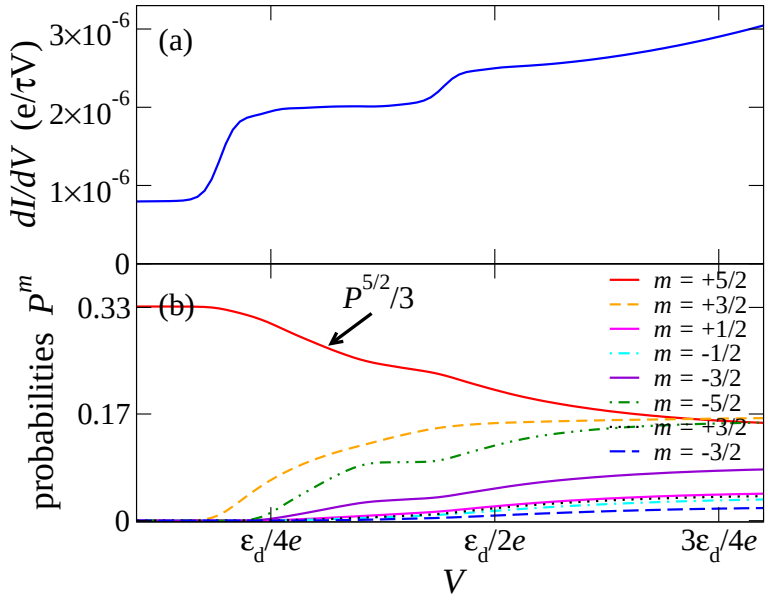

Figure 3.14: (a) Differential conductance dI/dV and (b) probabilities P^n of molecular many-particle states as functions of bias voltage V, for low bias voltages. The probability $P^{5/2}$ of the ground state has been scaled by a factor $1/3$. Here, we assume $S = 2$, $J = K_2 = 5\,\mathrm{meV}$, $\epsilon_d = 10\,J$, $B = 2\,\mathrm{meV}$, and $T = 0.3\,\mathrm{meV}$.

also obtains processes changing the electron number by ± 2. However, for $U \to \infty$ these pair-tunneling processes [123] are suppressed. Note that Eqs. (3.43) and (3.44) contain both elastic and inelastic cotunneling.

Since the above expressions diverge due to second-order poles from the energy denominators, the cotunneling rates cannot be evaluated directly. We apply a regularization scheme that follows Refs. [88–90] and is motivated by the observation that Eqs. (3.43) and (3.44) do not take into account that the intermediate state obtains a finite width Γ due to the coupling to the leads. In the regime of weak tunneling, the width Γ is of second order in the tunneling amplitudes t_α. This width is introduced into the energy denominators replacing η. When the cotunneling rates are expanded in powers of Γ, it turns out that the leading term is of order $1/\Gamma \propto 1/t_\alpha^2$. This cancels two powers of the tunneling amplitude in Eqs. (3.43) and (3.44) so that the result is in fact a *sequential tunneling* contribution. Since we have already included the full sequential-tunneling rates, this new contribution should be dropped. We thus take the next order, Γ^0, for the cotunneling rates.

Both the sequential and cotunneling rates appear in the rate equations for the probabilities to find the molecule in state n,

$$\frac{dP^n}{dt} = \sum_{\alpha m} \left(\Gamma_\alpha^{mn} P^m - \Gamma_\alpha^{nm} P^n\right) + \sum_{\alpha\alpha' m} \left(\Gamma_{\alpha\alpha'}^{mn} P^m - \Gamma_{\alpha\alpha'}^{nm} P^n\right), \tag{3.45}$$

where Γ_{α}^{mn} denotes the sequential tunneling rate and $\Gamma_{\alpha\alpha'}^{mn} \equiv \Gamma_{\alpha\alpha'}^{mn,00} + \Gamma_{\alpha\alpha'}^{mn,11}$ the cotunneling rate. Note that $\Gamma_{\alpha\alpha'}^{mn,00}$ ($\Gamma_{\alpha\alpha'}^{mn,11}$) is non-zero only if both n and m are empty (singly occupied) states. The current through, say, the left lead is given by

$$I^L = -e\sum_{nm}(n_n - n_m)\Gamma_L^{mn}P^m - e\sum_{nm}\left(\Gamma_{LR}^{mn} - \Gamma_{RL}^{mn}\right)P^m, \tag{3.46}$$

where n_m is the occupancy of state m. The steady-state probabilities P^m of the molecular states m are obtained by solving Eq. (3.45) with the time derivatives set to zero. The average magnetization in the z direction per molecule is given by $M = \sum_n m_n P^n$, where m_n denotes the quantum number of the z component of the total spin $\mathbf{s} + \mathbf{S}$ in state n.

We start by discussing our results obtained for the differential conductance dI/dV at low bias voltages. If the system is in the Coulomb blockade regime, sequential tunneling is thermally suppressed and transport is dominated by cotunneling. The magnitude of the current is then small. The conductance at zero bias voltage is finite, see Fig. 3.14(a), due to *elastic* cotunneling. The cotunneling rates are proportional to the bias voltage, if the molecular level is far away from the chemical potentials, leading to ohmic behavior. The rounded steps in dI/dV correspond to the onset of additional *inelastic* cotunneling processes. Selection rules for the spin quantum number require $\Delta m = 0, \pm 1$. For the parameters chosen in Fig. 3.14, the ground state has electron number $n = 1$ and maximum spin, $m = 5/2$. Inelastic cotunneling processes corresponding to the two steps involve the two different final states with $n = 1$, $m = 3/2$ and virtual occupation of the state with $n = 0$, $m = 2$, as illustrated in Fig. 3.15. Further steps in dI/dV are not observed, since the corresponding inelastic cotunneling transitions have smaller energy differences between initial and final states and are therefore activated immediately when the probability of the initial state becomes significant.

Cotunneling steps and sequential tunneling peaks show fundamentally different dependences on the onsite energy ϵ_d. For *single-molecule* junctions it is possible to change ϵ_d by applying a gate voltage, e.g. in molecular-junction experiments. However, for monolayers one does not have this opportunity. We come back to this point below. While the bias voltages at which sequential tunneling peaks occur shift linearly with ϵ_d, the positions of cotunneling steps remain unaffected. This follows directly from evaluating Eqs. (3.43)–(3.44) in the limit of large ϵ_d [83]. For magnetic molecules, the position of the cotunneling steps shifts linearly as a function of the external magnetic field due to the Zeeman effect, as observed for Mn_{12} [23] and $N@C_{60}$ [35].

While dI/dV represents the change of the very small current with bias voltage in the cotunneling regime, changes of the occupation probabilities P^n of molecular states with bias voltage are of order unity, as shown in Fig. 3.14(b). The probability of the lowest-energy state with $m = 5/2$ decreases, whereas the probabilities of other states increase. Cotunneling enables transitions between molecular states with the same electron number but with magnetic quantum numbers differing by $\Delta m = \pm 1$. These transitions are suppressed only as the inverse square of the energy difference

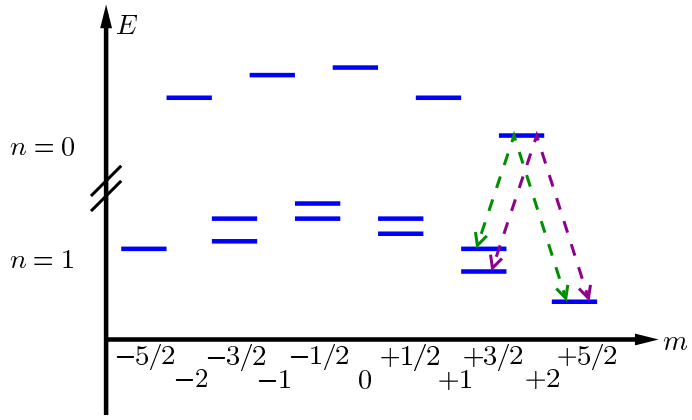

Figure 3.15: Level scheme showing the energies of molecular states as a function of magnetic quantum number m for electron numbers $n = 0, 1$ in the presence of a magnetic field. The dashed double arrows signify inelastic cotunneling between the ground state with $m = 5/2$ and the two states with $m = 3/2$, involving virtual occupation of the state with $n = 0$ and $m = 2$. While sequential tunneling requires a change of the electron number by $\Delta n = \pm 1$ and of the magnetic quantum number by $\Delta m = \pm 1/2$, cotunneling processes obey the selection rules $\Delta n = 0$, $\Delta m = 0, \pm 1$.

between the initial state and the virtual state involved. In sequential tunneling, such transitions are also possible, requiring two consecutive steps, but are exponentially suppressed in the Coulomb blockade regime. In the sequential tunneling approximation the molecule would thus remain in the lowest energy state with essentially unit probability. This approximation is evidently invalid for determining the probabilities in this regime.

Interestingly, the strong effect of cotunneling on the probabilities also leads to observable effects of *sequential* tunneling on transport in the cotunneling regime [124; 125]. While sequential tunneling starting from the lowest-energy state is exponentially suppressed, sequential tunneling from higher-energy states can be possible. With increasing bias voltage, these higher-energy states become increasingly populated due to *cotunneling*, as Fig. 3.14(b) shows. This leads to sidebands in dI/dV in the Coulomb blockade regime that show the linear dependence on the gate voltage characteristic of sequential tunneling [125]. Strong electron-phonon coupling can enhance this effect, since it crucially affects the ratio of the rates for sequential and cotunneling processes [124; 125]. In our case, these sidebands are very weak, since the current is controlled by the small cotunneling rates. However, we will see that the effect on the probabilities P^n of molecular states is significant.

3.5.2 Nonequilibrium magnetization in magnetic molecular monolayers

Figure 3.16(a) shows the average magnetization per molecule as a function of bias voltage over a broad range including both the cotunneling and sequential tunneling regimes. The magnetization is nonzero due to an external magnetic field. At zero

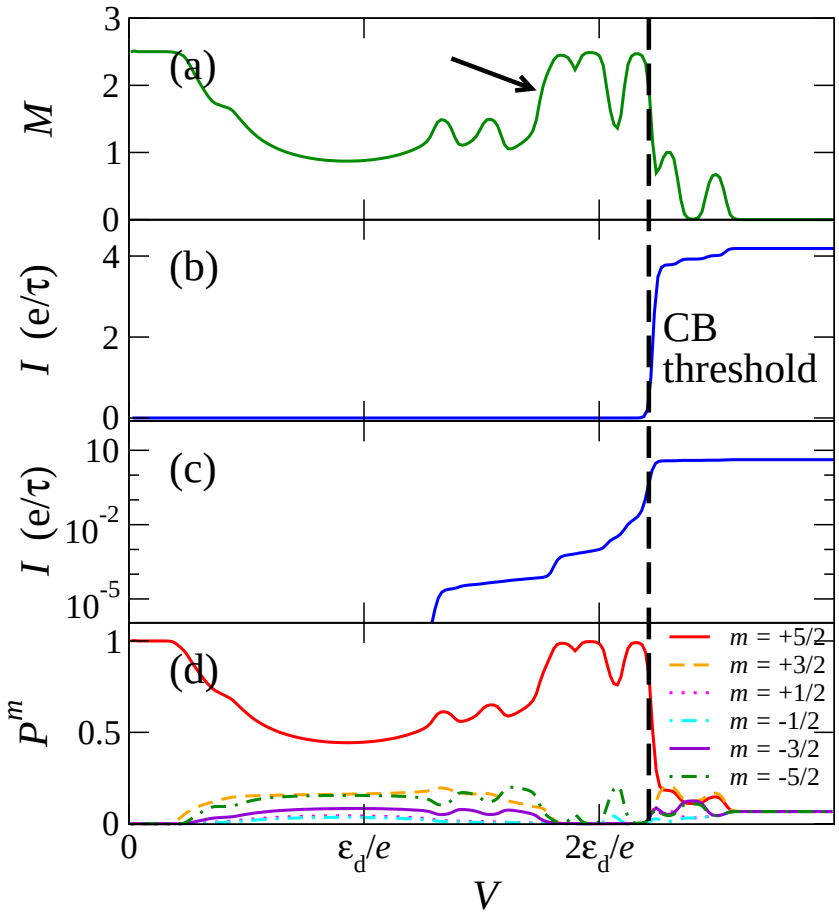

Figure 3.16: (a) Average magnetization M of a single magnetic molecule in units of $\hbar$, (b) linear and (c) logarithmic plot of the current I, and (d) probabilities P^n of various molecular many-particle states as functions of bias voltage V. The parameters are chosen as in Fig. 3.14.

bias, the molecule is in its ground state with $m = 5/2$. The onset of inelastic cotunneling to the two states with $m = 3/2$ leads to a decrease in the magnetization in each case.

The bias voltage dependence of the magnetization for voltages *above* the Coulomb blockade threshold is accompanied by sizeable steps in the current, as seen in Fig. 3.16(b). At each of these fine structure steps an additional inelastic sequential tunneling transition becomes possible. The Coulomb blockade threshold corresponds to the transition with initial state $n = 1$, $m = 5/2$ and final state $n = 0$, $m = 2$. Therefore, the onset of sequential tunneling is accompanied by a *decrease* in the magnetization. At large bias the magnetization drops to zero since all states are occupied with equal probability.

Remarkably, pronounced step-like features are also present *below* the Coulomb

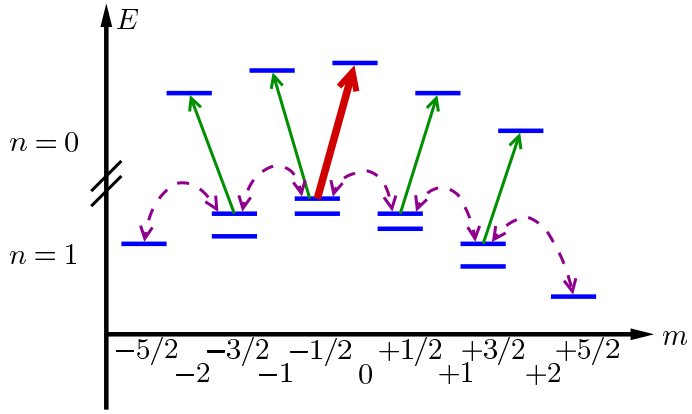

Figure 3.17: Level scheme illustrating the interplay between sequential tunneling (solid arrows) and cotunneling (dashed arrows) in magnetic molecules. Even below the Coulomb-blockade threshold sequential tunneling processes starting from higher-energy states populated by cotunneling may cause the depopulation of these states and drastically affect the average magnetization. At the step denoted by an arrow in Fig. 3.16(a), the excitation of the transition with $m = -1/2 \to 0$ (heavy solid arrow) gives rise to a redistribution of the probabilities P^n. Note that exothermal transitions with $\Delta m = \pm 1/2$ are always possible.

blockade threshold in Fig. 3.16(a), where the current is due to cotunneling and thus very small, cf. Figs. 3.16(b)–(c). This can be understood from the bias voltage dependence of the relevant probabilities P^n in Fig. 3.16(d). As an example, consider the step marked by an arrow in Fig. 3.16(a). The physics leading to the drastic change of the probabilities is illustrated in Fig. 3.17: The sequential tunneling processes with $m = -3/2 \to -2$, $m = -1/2 \to -1$, $m = 3/2 \to 2$, and $m = 1/2 \to 1$, starting at the higher-energy level of each pair (thin arrows in Fig. 3.17), are already energetically possible at lower bias voltages causing the partial depopulation of the initial states. However, the probabilities of these states are non-zero mainly due to cotunneling processes (dashed arrows in Fig. 3.17). Below the step marked in Fig. 3.16(a), the half-integer spin states with positive and negative m are *not connected* by sequential tunneling processes. As soon as the transition with $m = -1/2 \to 0$ (bold arrow in Fig. 3.17) becomes possible, the states with positive and negative m are connected and fast, sequential tunneling processes depopulate all states except for the ground state, which has $m = 5/2$. Consequently, the average magnetization again approaches its maximum value. Similarly, one can attribute each step to a particular molecular transition. As Fig. 3.16(c) shows, the onsets of some of these sequential tunneling processes can also be seen in the current, which is, however, tiny in the cotunneling regime.

The above discussion shows that quantities that depend strongly on the probabilities of molecular states, such as the magnetization, are much more sensitive to changes of the bias voltage in the Coulomb blockade regime than the conductance. This suggests to use the *magnetization-voltage* characteristics, i.e., the magnetization as a function of bias voltage, instead of the current-voltage characteristics to extract

the excitation spectrum of magnetic molecules. In order to distinguish magnetic transitions from, e.g. vibrational excitations, one should analyze their dependence on the magnetic field. Furthermore, for a monolayer there is no gate voltage that can serve as an independent parameter. The magnetic field can assume this role.

Figure 3.18(a) shows a density plot of the magnetization as a function of bias voltage and magnetic field. The magnetization is an odd function of the field. The transition energies shift linearly with the field, $\Delta E = \Delta m\, B$, if the initial and final states have magnetic quantum numbers differing by Δm.

Complementary to conventional dI/dV plots, the density plots in Fig. 3.18 can serve as fingerprints of the internal degrees of freedom of the molecules. The Zeeman splitting of the molecular levels due to the external magnetic field gives rise to triangular plateaus with a tip at $B = 0$. These plateaus are bounded by two sequential tunneling transitions. In each case, these two transitions differ in the sign of the magnetic quantum number m of both initial and final molecular states. For the chosen parameters, the plateaus can be attributed to the following transitions from empty to singly occupied states, starting at low bias voltage (cf. Fig. 3.17): $|m| = 3/2 \to 2$, $|m| = 1/2 \to 1$, $|m| = 1/2 \to 0$, $|m| = 3/2 \to 2$, $|m| = 3/2 \to 1$, $|m| = 1/2 \to 1$, $|m| = 5/2 \to 2$ (this is the first transition starting from the ground state and thus represents the Coulomb blockade threshold), $|m| = 1/2 \to 0$, and $|m| = 3/2 \to 1$. Several transitions appear twice because there are two states with magnetic quantum numbers $\pm 3/2$ and $\pm 1/2$, respectively. For a local spin $S = 2$ there exist nine transitions obeying the selection rule $\Delta m = \pm 1/2$, as can be seen from Fig. 3.17, in accordance with the nine plateaus shown in Fig. 3.18(a). Note again that the signal is similar on both sides of the Coulomb blockade threshold.

The origin of the plateaus is schematically illustrated in Fig. 3.18(e) for the transition $|m| = 1/2 \to 0$. In the absence of an external Zeeman field the excitation energies for both transitions is equal. However, the excitation energies differ by the Zeeman energy as soon as a magnetic field is switched on. This leads to the occurrence of a finite bias voltage window, where the excitation of one of the two transitions is energetically possible whereas the other one is not. Inside this window, only the spin-down state is depopulated by sequential tunneling, leading to a large positive magnetization.

3.5.3 Interplay of cotunneling and spin relaxation

So far, we have restricted ourselves to the situation where the relaxation of the local molecular spin is dominated by electron tunneling, i.e. the spin is *conserved* between tunneling events. However, there are other processes that also contribute to spin relaxation: (i) Magnetic molecules containing transition-metal ions, such as Mn_{12} clusters, show strong spin-orbit interaction, which leads to spin relaxation. (ii) Hyperfine interactions with nuclear magnetic moments in the molecule can also lead to spin relaxation. However, in molecules one has the chance to essentially remove this mechanism by choosing isotopes with vanishing nuclear spins. (iii) Dipolar interactions with spins of other molecules in the monolayer or with impurity spins

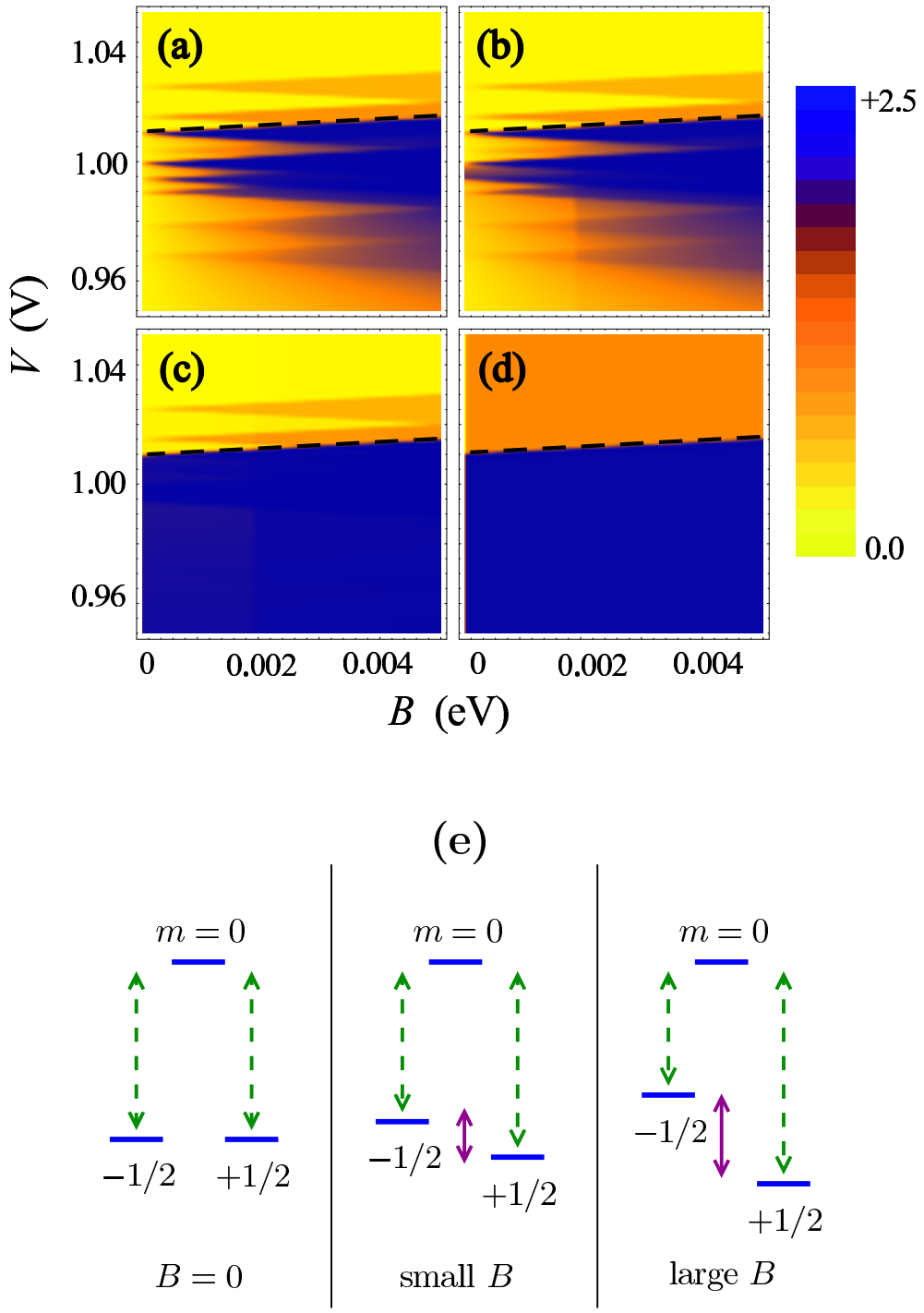

Figure 3.18: Average magnetization M of a single magnetic molecule in units of $\hbar$ as a function of bias voltage V and magnetic field B for different spin relaxation times: (a) $t_{\mathrm{rel}} = \infty$, (b) $t_{\mathrm{rel}} = 10^6\tau_0$, (c) $t_{\mathrm{rel}} = 10^2\tau_0$, and (d) $t_{\mathrm{rel}} = 0$. Here τ_0 denotes the typical electronic tunneling time. All other parameters are chosen as above. The dashed lines denote the Coulomb-blockade threshold. (e) Level schemes illustrating the origin of the magnetization plateaus.

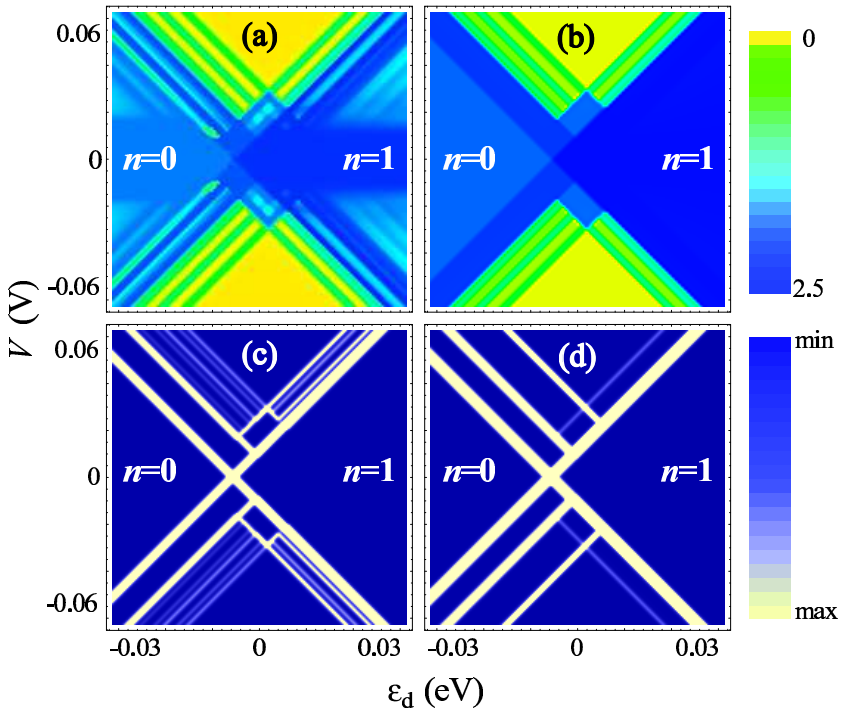

Figure 3.19: (a),(b) Magnetization M and (c),(d) differential conductance of a single magnetic molecule as a function of V and ϵ_d for (a),(c) slow spin relaxation, $t_{\rm rel} = 10^{10}\tau_0$, and (b),(d) fast spin relaxation, $t_{\rm rel} = \tau_0$. We assume $S = 2$, $J = K_2 = 5\,\text{meV}$, $T = 0.1\,\text{meV}$, and $B = 2\,\text{meV}$.

in the electrodes contribute to spin relaxation. (iv) Small non-uniaxial magnetic anisotropies lead to tunneling between the eigenstates of $H_{\rm mol}$. This mechanism has recently been discussed in the context of transport through magnetic molecules [22; 103; 126].

All these processes change the magnetic quantum number while keeping the electron number constant ($\Delta n = 0$). The dominant transitions are the ones with $\Delta m = \pm 1$. These are the same selection rules as for cotunneling, indicating that one should include additional spin relaxation for consistency when studying cotunneling.

The effect of spin relaxation on electronic transport is included in the formalism by a phenomenological rate $\propto 1/t_{\rm rel}$ which forces the system to approach the equilibrium distribution on the time scale $t_{\rm rel}$. We include additional transition rates between states i and j with selection rules $\Delta n = 0$ for the occupancy and $\Delta m = \pm 1$ for the spin,

$$\Gamma_{ij}^{\rm rel} = \frac{1}{t_{\rm rel}} \exp\left(\frac{\epsilon_i - \epsilon_j}{T}\right), \qquad \text{for } \epsilon_i < \epsilon_j, \tag{3.47}$$

$$\Gamma_{ij}^{\rm rel} = \frac{1}{t_{\rm rel}}, \qquad \text{otherwise.} \tag{3.48}$$

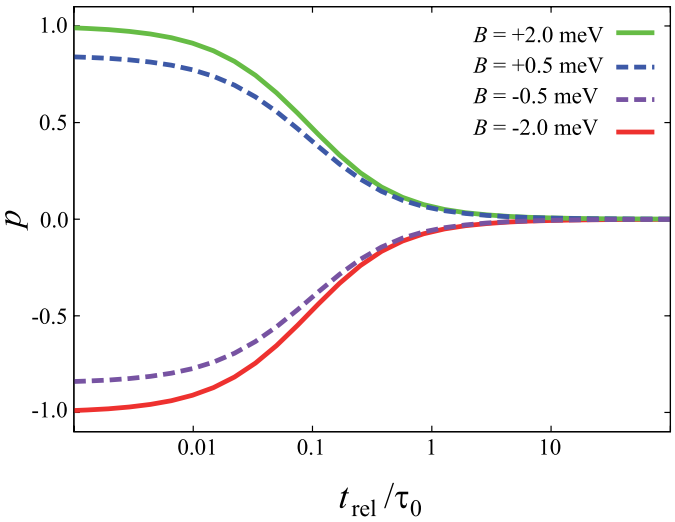

Figure 3.20: Polarization of the current, $p = (I^L_\uparrow - I^L_\downarrow)/(I^L_\uparrow + I^L_\downarrow)$, as a function of spin relaxation time $t_{\rm rel}$ in units of the typical tunneling time τ_0 for different values of the magnetic field.

The additional rates obey detailed balance, ensuring relaxation towards equilibrium in the absence of tunneling.

Effects of spin relaxation on the bias-voltage dependence of the magnetization are illustrated in Figs. 3.18(a)–(d). For small $t_{\rm rel}$ (fast relaxation), the number of transitions appearing as steps in the magnetization-voltage characteristics is reduced, since spin relaxation depopulates higher-energy states that serve as initial states for these transitions.

The magnetization plateaus start to occur when the relaxation time $t_{\rm rel}$ becomes significantly larger than the typical sequential-tunneling time τ_0. (The *sequential*-tunneling time enters because the relevant process is the depopulation of states by sequential tunneling.) Then the time spent by the electron on the molecule is smaller than the spin relaxation time so that magnetic excitations survive between tunneling events.

So far, we have considered a monolayer of magnetic molecules, mostly because the measurement of the magnetization is easier for larger numbers of molecules. As mentioned previously, even the detection of a *single* molecular spin might be feasible [76; 120]. Using a single molecule allows one to introduce a gate electrode in order to tune the molecular energy levels by shifting ϵ_d, see Eq. (3.2). In the following, we briefly discuss results obtained for varying gate voltage. To increase the magnetization signal while retaining the gate electrode, one might also consider a one-dimensional array of magnetic molecules or even a large number of such arrays aligned in parallel.

The plot of the magnetization and the differential conductance as functions of bias

voltage and onsite energy ϵ_d presented in Figs. 3.19(a),(c) shows two striking features. First, the magnetization shows steps indicating the onset of inelastic cotunneling which are almost independent of ϵ_d. The corresponding steps in dI/dV are very small in absolute units, see Fig. 3.14(a).

Second, the magnetization shows strong additional magnetic sidebands in the Coulomb blockade regime. These sidebands are the consequence of sequential tunneling transitions depopulating molecular states that are populated by cotunneling, as discussed above. In the differential conductance the corresponding features are completely hidden by the low-bias tail of the large peak at the Coulomb blockade threshold (not shown). The observation of these sidebands in the Coulomb blockade regime requires spin relaxation times long compared to the typical tunneling time. For fast spin relaxation, fine structure peaks are only present in the sequential tunneling regime, see Fig. 3.19(b), since sequential tunneling is still faster than spin relaxation, even though cotunneling is slower. As shown in Fig. 3.19(d), the absence of such sidebands is accompanied by suppressed fine structure peaks in the sequential tunneling regime.

Finally, we note that sufficiently fast spin relaxation leads to *spin-polarized* stationary currents in the presence of a magnetic field. If the spin of the magnetic molecule relaxes fast compared to the typical tunneling times, which is essentially determined by the current, the system is essentially always in its ground state. Due to the Zeeman effect the ground state has maximum magnetic quantum number; $m = 5/2$ for our example. Thus only spin-down electrons can tunnel onto the molecule, resulting in a spin-polarized current. Note that this argument is not restricted to low-order perturbation theory in H_t. As shown in Fig. 3.20, the degree of spin polarization is basically determined by the ratio of the spin relaxation rate and the typical electronic tunneling rate.

3.6 Conclusions

In conclusion, we have studied the inelastic charge and spin transport through an anisotropic magnetic molecule weakly coupled to metallic leads. The three processes crucial for molecular memory applications—writing, storing, and reading information—can be implemented in such a device. The information storage is affected by spin relaxation, which can be very slow for large easy-axis anisotropy. Also due to the anisotropy, application of a bias voltage to a molecule in a spin-polarized state can lead to the transfer of a large amount of spin or magnetic moment from one lead to the other. This transmitted spin increases exponentially for low temperatures. We have proposed that this giant spin amplification could be used to read out spin information and have discussed a scheme to write the information, which does not require a magnetic field but uses one ferromagnetic lead.

In this context, we have investigated transport through a single anisotropic magnetic molecule coupled to one *ferromagnetic* and one nonmagnetic lead. Two types of negative differential conductance occur. One appears at *low* temperatures in an

external magnetic field. Here the Coulomb blockade and spin blockade regimes are separated by a finite window of bias voltages for which the current is strongly enhanced. This is due to the interplay of bias voltage, magnetic field, and magnetic anisotropy, which allows only transitions between two specific molecular many-body states and prevents the spin flips necessary for spin blockade. The other negative differential conductance effect appears at *high* temperatures in the vicinity of the Coulomb blockade threshold. Interestingly, this predicted effect is a manifestation of quantum effects (the Pauli principle and spin selection rules) at room temperature. We have further shown that spin blockade is accompanied by super-Poissonian shot noise, as found earlier for nonmagnetic quantum dots. Furthermore, the total charge transmitted through the molecule can depend strongly on its initial spin state. The difference in transmitted charge can become exponentially large at low temperatures. This spin-charge conversion presents an elegant method to read out the spin.

Finally, we have considered the interplay of electronic transport through magnetic molecules and their nonequilibrium magnetic moment beyond the sequential tunneling approximation. We have focused mostly on monolayers, which should give a better chance to measure the magnetization than single molecules would.

While the excitation of inelastic tunneling processes in the Coulomb blockade regime only leads to a very small absolute change in the current, the changes in the probabilities of finding the molecule in various many-particle states are significant. This manifests itself in a strong bias voltage dependence of the magnetization. The magnetization of a molecular monolayer can be switched by an amount of the order of the saturation magnetization by a small change of bias voltage, and without causing the flow of a large current.

We find steps in the differential conductance due to inelastic cotunneling, which have been observed in recent experiments on Mn_{12} [23]. These steps are accompanied by much larger changes in the magnetization. Another interesting effect is the appearance of additional sidebands in the Coulomb-blockade regime that can be ascribed to *de*-excitations by sequential tunneling of states populated by cotunneling. These sidebands are very prominent in the magnetization. We suggest that the magnetization, or any measurable quantity that strongly differs between molecular states, can be employed to study molecular transitions that are hidden in the Coulomb blockade regime.

For spintronics applications, the ability to control the persistence of the stored information is crucial. In this context, we have also discussed effects of spin relaxation due to the coupling of the molecule to its environment, by introducing a phenomenological spin relaxation rate in the formalism. Our results have shown that for sufficiently fast spin relaxation the peaks in the differential conductance and the steps in the magnetization are washed out, as expected. At the same time, the degree of polarization of the steady-state current contains information about the ratio of the spin relaxation rate and the typical electronic tunneling rate. Fast spin relaxation, while in general undesirable, can lead to a highly polarized current in the presence of a magnetic field.

4 Asymmetric Coulomb blockade and Kondo temperature of single-molecule transistors

In the following we pay attention to a very prominent spin-related transport phenomenon known as the Kondo effect. The build-up of Kondo correlations requires a system with a spin-degenerate ground state such as a singly-charged molecule with total spin 1/2. In this context, we are particularly interested in the interplay of magnetic and vibrational degrees of freedom. Recent experiments for single-molecule transistors have shown that the gate voltage dependence of the Kondo temperature is much weaker as compared to conventional nanostructures such as quantum dots. This phenomenon is accompanied by the occurrence of strongly asymmetric Coulomb blockade peaks in the differential conductance. These experimental observations are explained within a generic model that considers the coupling between the electronic and vibrational degrees of freedom of the molecule, taking into account anharmonic vibrational potentials.

4.1 Motivation

The occurrence of the Kondo effect in transport through artificial nanostructures such as quantum dots was predicted long ago [5; 6]. Its experimental observation [127] has generated considerable interest in recent years leading to a number of fascinating experimental and theoretical works [7; 32; 128–131]. An important question addressed by these works is the fate of the Kondo effect out of equilibrium due to the presence of a bias voltage [132–134].

In quantum dots a quantitative description of the build-up of Kondo correlations is possible in terms of the single-impurity Anderson model,

$$H_0 = \sum_{\alpha\mathbf{k}\sigma} \epsilon_k a^\dagger_{\alpha\mathbf{k}\sigma} a_{\alpha\mathbf{k}\sigma} + \epsilon_d(n_\uparrow + n_\downarrow) + U n_\uparrow n_\downarrow + \sum_{\alpha\mathbf{k}\sigma} \left[t_{\alpha\mathbf{k}} a^\dagger_{\alpha\mathbf{k}\sigma} d_\sigma + t^*_{\alpha\mathbf{k}} d^\dagger_\sigma a_{\alpha\mathbf{k}\sigma} \right], \quad (4.1)$$

where $d^\dagger_\sigma$ ($a^\dagger_{\alpha\mathbf{k}\sigma}$) creates an electron with energy ϵ_d (with energy $\epsilon_\mathbf{k}$ and momentum $\mathbf{k}$ in lead α) and spin σ on the dot (in the reservoir), U is the local Coulomb repulsion of the electrons and $n_\sigma = d^\dagger_\sigma d_\sigma$. For single occupation of the molecular level, the exchange between the localized spin of the molecule and the spin of the conduction electrons is obtained from a Schrieffer-Wolff transformation and yields

$$J = 2t^2 \left(\frac{1}{\epsilon_d} - \frac{1}{\epsilon_d + U} \right), \quad (4.2)$$

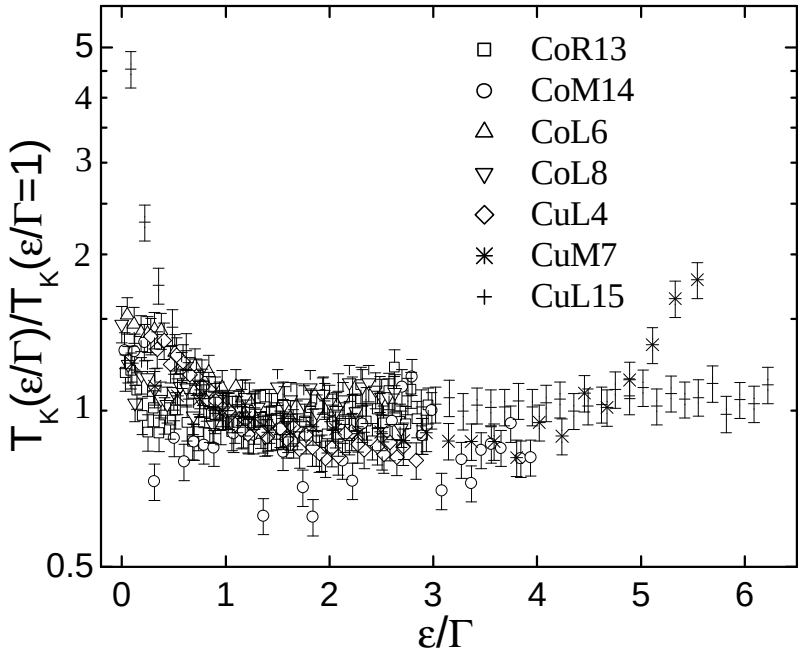

Figure 4.1: Experimental data for the Kondo temperature T_K as a function of gate voltage V_g for several devices, taken from Ref. [20]. The Kondo temperature is normalized with respect to the Coulomb blockade charge degeneracy point. Values of Γ inferred for these devices are, top down, 22.6, 11.5, 18, 3.3, 12.6, 14.2, and 26.8 meV.

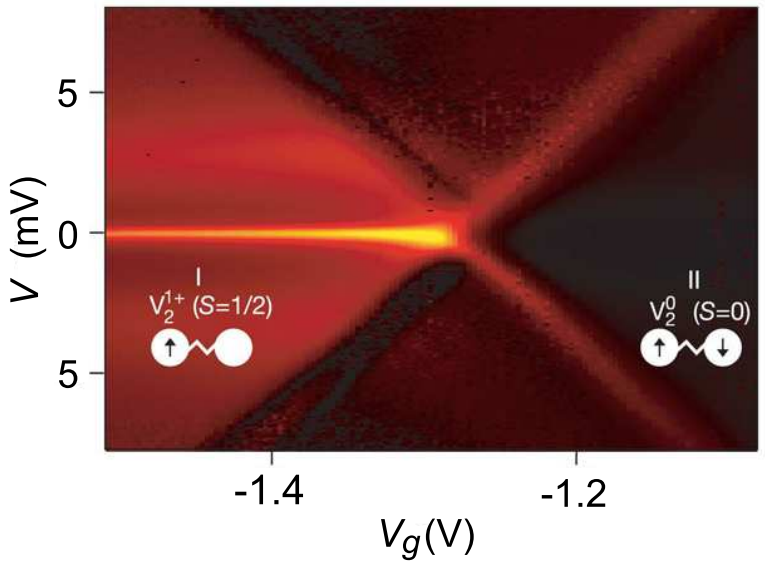

Figure 4.2: Experimental data for the differential conductance dI/dV as a function of bias voltage V and gate voltage V_g obtained from a single-V_2 transistors, taken from Ref. [19].

for $\epsilon_{\mathbf{k}} \ll \epsilon_d, U$ and $t_{\alpha\mathbf{k}} \simeq t$. In single-electron transistors the onsite energy ϵ_d can be effectively shifted by applying an additional gate voltage, V_g. Employing *poor man's scaling* one can derive an expression which describes the experimentally observed gate voltage dependence of the Kondo temperature $T_K \sim e^{-1/\nu_0 J}$ in quantum dots [135],

$$T_K = \frac{\sqrt{\Gamma U}}{2} e^{\pi\epsilon_d(\epsilon_d+U)/\Gamma U}, \tag{4.3}$$

where Γ is the coupling to the leads.

Surprisingly, recent experiments by Yu *et al.* have revealed that Eq. (4.3) does not work in certain single-molecule junctions, composed of transition metal complexes [di-(di-pyridyl-pyrrolato)cobalt] [20]. Instead the gate dependence of the Kondo temperature is found to be much weaker, cf. Fig. 4.1. Interestingly, this observation is coupled to strongly asymmetric Coulomb blockade peaks, cf. Fig. 4.2. Measurements of the differential conductance as a function of bias and gate voltage show Coulomb diamonds with drastically different peak intensities at the two opposite sides of the crossing point [19; 20; 77; 78]. The persistence of these unusual features in different single-molecule devices suggests that their explanation can be ascribed to the presence of specific molecular degrees of freedom such as vibrations.

In two recent works, Balseiro *et al.*[136; 137] suggested that strong electron-vibron interactions could explain the weak dependence $T_K(V_g)$. The principal idea is that for strong electron-vibron coupling the dominant contribution to the kinetic exchange stems from virtual charge fluctuations involving higher-excited vibrational states. In this case, the energy denominators in Eq. (4.2) are modified to include the vibrational excitation energy of the intermediate states for which the Franck-Condon overlap with the vibrational ground state is maximal. As a result the dependence of J, and hence T_K, on the gate voltage is suppressed as compared to the situation of weak or no electron-vibron coupling. These authors also show numerical results, based on the numerical renormalization group technique, which are consistent with the asymmetric Coulomb blockade.

The purpose of this chapter is to point out that strong electron-vibron coupling may also naturally account for the observation of a pronounced asymmetry of the Coulomb blockade diamonds in an *alternative* manner. Indeed, strong electron-vibron coupling implies that tunneling of electrons onto or off the molecule is accompanied by significant molecular deformations. This suggests that one should go beyond the common assumption of harmonic vibrations by including *anharmonicities* of the molecular potential surfaces. Our central result is that these anharmonicities can lead to strongly asymmetric Coulomb blockade diamonds.

4.2 Model and Methods

Our results are based on a model which considers a single molecule weakly coupled to two metallic leads. Relaxation in the leads is assumed to be sufficiently fast so that their electron distributions can be described by Fermi functions. We assume

transport to be dominated by a single molecular level with onsite energy ϵ_d and local Coulomb repulsion U. In addition to H_0, the full Hamiltonian contains a vibrational contribution,

$$H = H_0 + \frac{P^2}{2\mu} + V_n(X), \tag{4.4}$$

describing the kinetic and potential energy for the collective vibrational mode X. The variables P and μ denote the momentum and the reduced mass of the nuclear motion. Due to the electron-phonon coupling, the potential energy $V_n(X)$ depends on the molecular charge state n.

This dependence is included through a global shift of the potential surface, $V_n(X) = \sum_n v(X - \sqrt{2}n\lambda l)|n\rangle\langle n|$, where $|n\rangle$ denotes the electronic state with charge n, λ the dimensionless electron-phonon coupling strength and $l = (\hbar/\mu\omega_0)^{1/2}$ the oscillator length. The anharmonic shape $v(X)$ of the potential surface is described by a Morse potential [138],

$$v(X) = D\left[e^{-2\beta X} - 2e^{-\beta X}\right]. \tag{4.5}$$

The curvature of $v(X)$ is given by $\omega_0 = \beta^2\sqrt{2D}/\mu$. The energies of bound states of the Morse oscillator are given by

$$E_q = \hbar\omega_0(q + 1/2) - \chi\hbar\omega_0(q + 1/2)^2, \tag{4.6}$$

cf. Ref. [138]. The parameter $\chi = \hbar\beta/2\sqrt{2D\mu}$ determines the asymmetry of the Morse potential in comparison with the harmonic potential and the number of bound states which is given by $j = \lfloor(1/\chi - 1)/2\rfloor$.

The occupation probabilities P_q^n of the molecular eigenstates $|n, q\rangle$ with electronic occupancy n and phonon number q are obtained by solving rate equations,

$$\frac{dP_q^n}{dt} = \sum_{n'q'}(P_{q'}^{n'}W_{q'\to q}^{n'\to n} - P_q^n W_{q\to q'}^{n\to n'}) - \frac{1}{\tau}(P_q^n - P^{\rm eq}\sum_{q'}P_{q'}^n). \tag{4.7}$$

Here $W_{q\to q'}^{n'\to n}$ is the rate for a transition from state $|n, q\rangle$ to $|n', q'\rangle$. The last term describes the fact that phonons relax towards the equilibrium distribution $P_q^{\rm eq} = e^{-\hbar\omega_0/kT}[1-e^{-\hbar\omega_0/kT}]$ on the phenomenological time scale τ. Here we always assume fast vibrational relaxation, i.e. $\tau \approx 0$. Effects of nonequilibrium for anharmonic molecular vibrations have been considered in Ref. [139].

Second-order perturbation theory in the tunneling Hamiltonian yields a *Golden-Rule* expression for the transition rates, for the transition rates,

$$\begin{aligned} W_{q\to q',\alpha}^{n\to n'} =& 2\pi t^2\nu \left|M_{q\to q'}^{n\to n'}\right|^2 \Big\{ f(-\Delta_{nn'}^c + (q'-q)\hbar\omega_0 - \mu_\alpha) \\ &+ [1 - f(\Delta_{nn'}^c + (q-q')\hbar\omega_0 - \mu_\alpha)]\Big\}, \end{aligned} \tag{4.8}$$

where f denotes the Dirac-Fermi function, ν the local density of states in the leads, μ_α the chemical potential of lead α, $\Delta_{nn'}^c \equiv \epsilon_d(n'-n) + Un'(n'-1)/2 - Un(n-1)/2$,

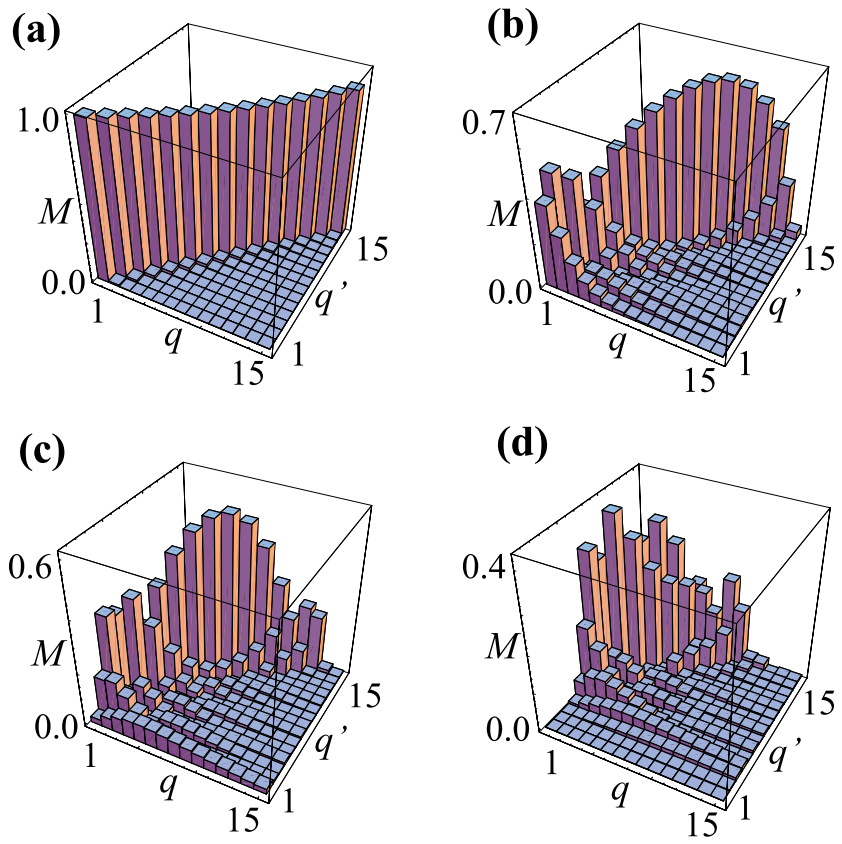

Figure 4.3: Franck-Condon matrix elements, $M_{q\to q'}^{0\to 1}$, of the Morse oscillator for (a) $\lambda = 0.1$, (b) $\lambda = 1.0$, (c) $\lambda = 2.0$, and (d) $\lambda = 4.0$.

and $M_{q\to q'}^{n\to n'} = \int_{-\infty}^{\infty} dx\, \phi_{n,q}^*(x)\phi_{n',q'}(x)$ the Franck-Condon matrix element of two eigenfunctions of the Morse oscillator [138],

$$\phi_{n,q}(\xi) = \sqrt{\frac{\beta q! 2(j-q)}{\Gamma(2j-q+1)}} e^{-\xi/2}\xi^{j-q} L_q^{2(j-q)}(\xi + \sqrt{2}n\lambda l). \tag{4.9}$$

Here $\xi = (2j+1)\exp(-\beta X)$ is the Morse coordinate, L the generalized Laguerre polynomial, and Γ denotes the Gamma function. The total tunneling rate is $W_{q\to q'}^{n\to n'} = \sum_\alpha W_{q\to q',\alpha}^{n\to n'}$. In the sequential tunneling regime, the steady-state current is given by $I_\alpha = e\sum_{nqq'} P_q^n [W_{q\to q',\alpha}^{n\to n-1} - W_{q\to q',\alpha}^{n\to n+1}]$, where the bias voltage is $V = (\mu_L - \mu_R)/e$.

4.3 Results and Discussion

We will analyze the consequences of the model for both the Kondo temperature and the Coulomb blockade. In both cases, important ingredients are the Franck-

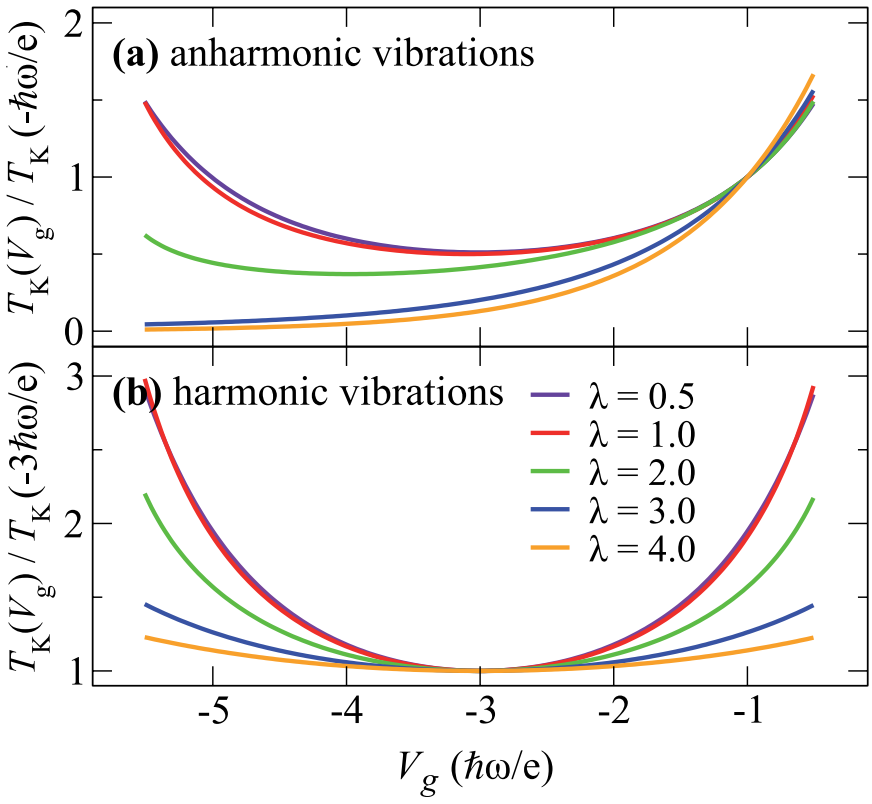

Figure 4.4: Kondo temperature as a function of gate voltage for (a) anharmonic and (b) harmonic vibrations. Here we assume $U = 6\,\hbar\omega_0$, $\Gamma \equiv 2\pi|t_\alpha|^2\nu_\alpha = \pi\hbar\omega_0$.

Condon matrix elements of the Morse potential. Corresponding numerical results are plotted in Fig. 4.3, which reveal two striking features: (i) The diagonal matrix elements decrease exponentially with increasing λ, whereas off-diagonal elements increase simultaneously, giving rise to the Franck-Condon blockade [29]. (ii) The Franck-Condon matrix is no longer symmetric under parity transformations. The direction of the relative shift of the potential surfaces of neutral and charged states, as determined by the sign of λ, is relevant for the overlap of two vibrational wave functions, and hence $M_{n\to n'}^{q\to q'} \neq M_{n\to n'}^{q'\to q}$ [138]. For a given sign of λ, the Franck-Condon elements $M_{n\to n'}^{q\to q'}$ with $q' < q$ are strongly suppressed in comparison with those with $q' > q$.

We first address the gate voltage dependence of the Kondo temperature within our model. Performing a Schrieffer-Wolff transformation in the presence of anharmonic

potential surfaces, we obtain

$$J = 2t^2 \sum_{m=0}^{\infty} \left[\frac{|M_{0\to m}^{0\to 1}|^2}{\epsilon_d - \hbar\omega_0[m - \chi(m+1/2)^2 + \chi/4]} - \frac{|M_{0\to m}^{2\to 1}|^2}{\epsilon_d + U + \hbar\omega_0[m - \chi(m+1/2)^2 + \chi/4]} \right] \tag{4.10}$$

for the exchange coupling. Implications for the Kondo temperature as a function of gate voltage (setting $V_g = \epsilon_d$ for simplicity) are shown in Fig. 4.4(a) for different values of λ. Similar to the case of harmonic vibrations [136], which is presented in Fig. 4.4(b) for comparison, the gate voltage dependence becomes weaker with increasing electron-vibron interaction λ. The origin of this suppression is that due to the Franck-Condon matrix elements $M_{0\to m}^{n\to n'}$, the dominant contribution to the exchange coupling in Eq. (4.10) for large λ stems from virtual charge fluctuations involving highly excited vibrational states with $m \approx \lambda^2$. Indeed, these states have maximal overlap $M_{0\to m}^{n\to n'}$ with the vibronic ground state. As a result, the energy denominators in Eq. (4.10) are dominated by the vibrational energy of the intermediate state, suppressing the dependence of the exchange coupling and consequently T_K on the gate voltage V_g.

The anharmonicity of the molecular potential surfaces results in an asymmetric dependence $T_K(V_g)$, which is most pronounced in the regime of strong electron-vibron coupling. For the symmetric case, the function $\ln T_K(V_g)$ is approximately a parabola, which can essentially be described by only taking into account the term with $q = \lambda^2$ in the expression for the exchange coupling in Eq. (4.10), i.e. $\ln T_K \propto (\epsilon_d - \hbar\omega_0\lambda^2)(\epsilon_d + U + \hbar\omega_0\lambda^2)/(U + 2\lambda^2\hbar\omega_0)$. For strong electron-vibron coupling, this parabola is flattened out by increasing λ. In contrast, for the asymmetric case, the gate voltage dependence is approximately given by

$$\ln T_K \propto \frac{(\epsilon_d - \hbar\omega_0\lambda^2)(\epsilon_d + U + \hbar\omega_0\lambda^2)}{U + \alpha\lambda^2\hbar\omega_0 + \gamma\epsilon_d}, \tag{4.11}$$

in the regime of weak electron-vibron coupling, where $\alpha \equiv (M_{0\to 1}^{0\to\lambda^2} + M_{2\to 1}^{0\to\lambda^2})/M_{0\to 1}^{0\to\lambda^2}$ and $\gamma \equiv (M_{0\to 1}^{0\to\lambda^2} - M_{2\to 1}^{0\to\lambda^2})/M_{0\to 1}^{0\to\lambda^2}$, For stronger electron-vibron coupling, only one of the two energy denominators of the term with $q \approx \lambda^2$ in Eq. (4.10) is large, whereas the other one is negligible. Therefore, the parabolic gate voltage dependence $\ln T_K(V_g)$ crosses over into a linear dependence, as can be seen from Fig. 4.4.

Next, we address the asymmetry in the Coulomb blockade peaks about the charge degeneracy point (marking the transition from the non-Kondo to the Kondo valley) which accompanies the quenching of the gate dependence of T_K in experiment. To this end, we have computed the Coulomb blockade behavior in the presence of anharmonic vibronic potentials within the sequential tunneling approximation. (Of course, this approximation will not capture the Kondo physics at small biases.) Corresponding two-dimensional plots of the differential conductance as a function of bias voltage V and gate voltage V_g are shown in Fig. 4.5. We observe a fine structure in

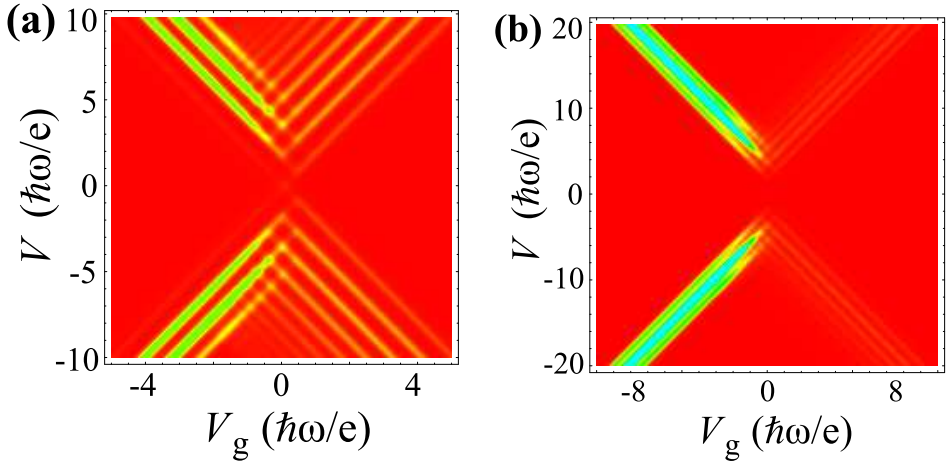

Figure 4.5: Differential conductance dI/dV as a function of V and V_g for $\lambda = 2.0$, and temperatures (a) $T = 0.1\,\hbar\omega_0$ and (b) $T = 0.2\,\hbar\omega_0$. We assume $\chi \simeq 0.03$, $j = 18$ and strong Coulomb interaction ($U \to \infty$).

the vicinity of the Coulomb blockade peaks [cf. Fig. 4.5a] which results from excitations of bound states of the Morse oscillator, once the bias voltage exceeds the limits of the the Coulomb blockade.

Interestingly, the number of visible peaks and the peak heights changes drastically about the charge degeneracy point, where two molecular charge states become degenerate. While there occur only very few, but strongly pronounced peaks on one side, there are several consecutive weaker peaks on the other side.

The underlying physics behind this behavior is illustrated in Fig. 4.6. Due to the coupling of the electrons and the vibrations, the oscillator potential surfaces of the charged and uncharged state are shifted with respect to each other. As a consequence, the overlap of two wave functions with occupancy differing by unity depends strongly on their vibrational quantum numbers.

If the neutral state is energetically *below* the singly charged one [as shown in Fig. 4.6(a)], the spatial overlap of the state with $n = 0$, $q = 0$ and several states with charge $n = 1$ and higher vibronic states are of the same order of magnitude. The wave functions assume large values in the vicinity of the classical turning points. Since the position of the *left* turning point is similar for a large number of vibronic states, the corresponding inelastic transition rates involving the excitation of vibrons are comparatively large likewise.

On the other hand, if the neutral state is energetically *above* the singly charged state [cf. 4.6(b)], the situation looks qualitatively different. Only the spatial overlaps of the vibronic ground state with $n = 0$, $q = 0$ and very few excited vibronic states with $n = 1$ are significant. Since the position of the right turning point changes drastically as a function of the vibrational quantum number, there are only very few Franck-Condon matrix elements which are of the same order of magnitude, so that

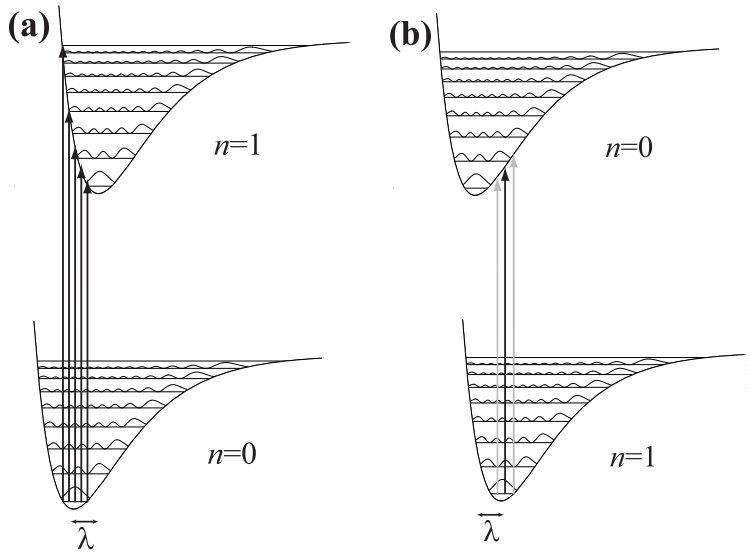

Figure 4.6: Level schemes showing the relevant vibrational excitations for a ground state with occupancy (a) $n = 0$ and (b) $n = 1$.

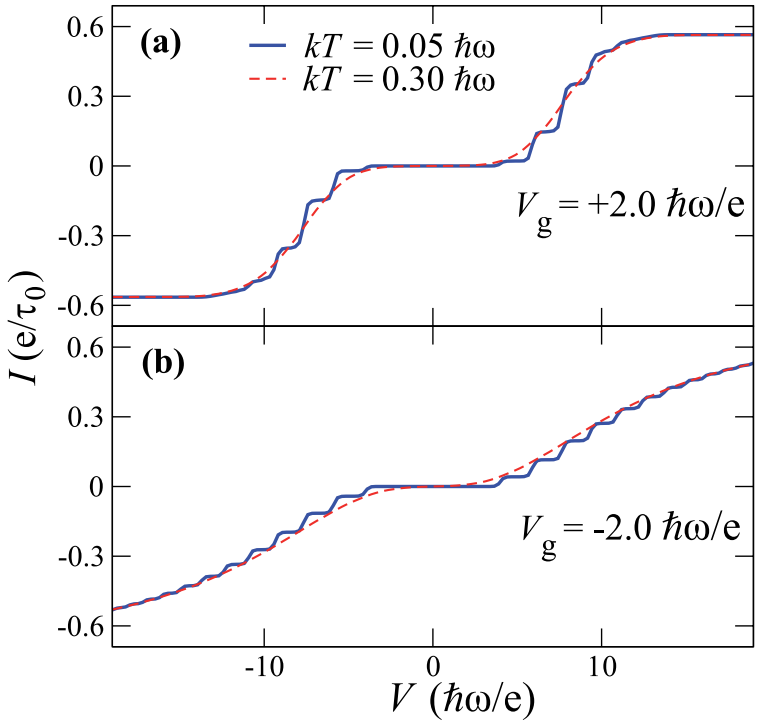

Figure 4.7: Current-voltage characteristics for (a) positive and (b) negative gate voltage in units of e/τ_0, where $1/\tau_0 = (2\pi/\hbar)|t_\alpha|^2\nu_\alpha$. Here, we assume $\lambda = 2.0$, $\chi \simeq 0.03$, $j = 18$, strong Coulomb interaction ($U \to \infty$) and temperatures $T = 0.05\,\hbar\omega_0$ (solid curves) and $T = 0.3\,\hbar\omega_0$ (dashed curves), respectively.

the number of peaks in dI/dV is small, whereas the corresponding peak heights are large.

We note in passing that the saturation value of the current does not depend on the gate voltage, so that the sum of all differential-conductance peak heights is equal for both sides of the degeneracy point, cf. Fig. 4.7.

Our crucial observation with regard to the experimentally observed asymmetry of the Coulomb blockade peaks involves the effect of thermal broadening at finite temperature. As shown in Fig. 4.5(b), thermal broadening washes out the fine structure with the characteristic temperature scale given by the vibrational frequency $\hbar\omega_0$ (with a rather small numerical prefactor). Due to the asymmetry in the number and strength of vibrational sidebands on both sides of the charge degeneracy point, this induces a pronounced asymmetry of the Coulomb blockade which is quite reminiscent of the experimental data. In fact, due to the thermal broadening, the closely spaced peaks on one side of the charge degeneracy point effectively merge into one peak, while the more widely spaced peaks on the other side are merely suppressed. We want to emphasize that this feature is characteristic of the regime of strong (and intermediate) electron-vibron interaction, whereas it disappears entirely in the weak coupling limit.

4.4 Summary and Conclusions

In summary, we have analyzed the effects of anharmonic potential surfaces on Coulomb blockade and Kondo physics in single-molecule transistors. Our study was motivated by recent measurements for single-molecule devices which have reported the simultaneous occurrence of two striking features: First, the observed gate voltage dependence of the Kondo temperature is much weaker in comparison with quantum dots. Second, the differential conductance reveals peaks with drastically different intensities at the two opposite sides of the charge degeneracy point. We argue that strong electron-vibron coupling which favors anharmonic potential surfaces can explain both observations within a single generic model.

Our explanation is alternative to previous suggestions, also relying on strong electron-vibron coupling, but relating the asymmetry in the Coulomb blockade to the influence of Kondo correlations. Possible experimental signtures which can distinguish between the two explanations include: (i) Anharmonic potential surfaces should lead to a nonparabolic dependence of the Kondo temperature on gate voltage. (ii) In our model, the suppressed Coulomb blockade peaks can, in principle, occur on either side of the charge degeneracy point, dependent on the specific molecule under consideration and independent of whether one is concerned with a Kondo or non-Kondo valley. We hope that future experiments will investigate these issues.

5 Current-induced conformational switching in single-molecule junctions

Current-induced conformational switching in single-molecule junctions constitutes a fundamental process in molecular electronics. Motivated by recent experiments on azobenzene derivatives, we study this process for molecules which exhibit two (meta)stable conformations in the neutral state, but only a single stable conformation in the ionic state. We derive and analyze appropriate Fokker-Planck equations, obtained from a density-matrix formalism starting from a generic model, and present comprehensive analytical and numerical results for the switching dynamics in general and the quantum yield in particular.

5.1 Introduction

An essential requirement for electric circuits of nanoscale dimensions is a molecular device that can be switched between two distinct conductive states. Because of intrinsic bistabilities many single-molecule junctions reveal switching behavior, e.g. involving cis and trans isomers of a molecule [50–60].

In this context, various types of switching mechanisms that stimulate changes of the chemical conformation have been discussed in the literature [51]. Consider a molecule that is either in the cis or in the trans configuration modeled by a double-well potential as shown in Fig. 5.1(a). The potential surface is characterized by an energy barrier W between the two minima and an attempt frequency ω_0, which is determined by the curvature at the local minimum. This energy barrier can be overcome by (i) thermal activation. The rate for this process is given by

$$\Gamma_{\text{thermal}} \simeq \frac{\omega_0}{2\pi} \exp\left(-\frac{W}{T}\right). \tag{5.1}$$

For thermal energies T larger than the vibrational energy $\hbar\omega_0$, thermal activation dominates over (ii) quantum tunneling, cf. Fig. 5.1(b). Switching due to quantum

tunneling is also exponentially suppressed,[1]

$$\Gamma_{\text{quantum}} \simeq \frac{\omega_0}{2\pi} \exp\left(-\frac{W}{\hbar\omega_0/2\pi}\right). \tag{5.2}$$

Both thermal and quantum tunneling do not require the molecule to be out of equilibrium and, in principle, occur even at zero bias voltage. In addition, conformational switching can also be induced by the applied current, which drives the molecule out of equilibrium. (iii) Such *current-induced* switching can be triggered by tunneling events into and out of the molecule which are accompanied by the emission of a single vibron, as illustrated in Fig. 5.1(c). Assuming that all relevant charge states exhibit the same conformational bistability and ohmic response,

$$\Gamma_{\text{cur-ind}}(V) \simeq \frac{\lambda G}{e} \left(|V| - \hbar\omega_0/e\right) \Theta\left(|V| - \hbar\omega_0/e\right), \tag{5.3}$$

i.e. the rate for such processes is proportional to the phase space volume of electrons energetically available in the reservoirs determined by the bias voltage V. Here G is the conductance and λ the effective electron-vibron coupling strength. Equation (5.3) can be derived treating the electron-vibron coupling perturbatively [57]. (iv) The switching may also require several subsequent inelastic tunneling events to overcome the energy barrier between the cis and trans state, cf. Fig. 5.1(d). If the critical oscillator state where the transition becomes possible is given by n, the switching rate acquires the form [57]

$$\Gamma_{\text{cur-ind},n}(I) \sim I^n. \tag{5.4}$$

In order to observe such a power-law dependence on the current I the excitation of vibrons has to be induced by the current, whereas vibrational de-excitation has to be dominated by *dissipative* rather than *current-induced* processes. The discussed switching mechanisms (i)–(iv) have been found to play an important role in oligophenylenevinylene (OPV3) derivatives, which have recently been investigated by Danilov *et al.* [51] in a molecular junction.

In the present chapter we consider molecules which exhibit conformational bistability only in the neutral state, while the potential surface of the ionic state has a single minimum. Due to an avoided level crossing this minimum is typically in between the two minima of the double well, cf. Fig. 5.1(e), e.g. as approximately realized in azobenzene [140]. Our main focus is on the regime of strongly asymmetric couplings to the leads, corresponding to the experimental setup of a scanning tunneling microscope (STM) conductance measurement. Here the molecule is strongly coupled to the substrate, while the coupling to the tip is much weaker. This asymmetry has important consequences for the conductance and for the dynamics of the passage of

[1] In the expression for the switching rate due to quantum tunneling, the frequency in the exponential is actually determined by the curvature of the potential surface at the local maximum. However, since it is usually of the same order of magnitude as the attempt frequency ω_0, we do not distinguish between the two frequencies.

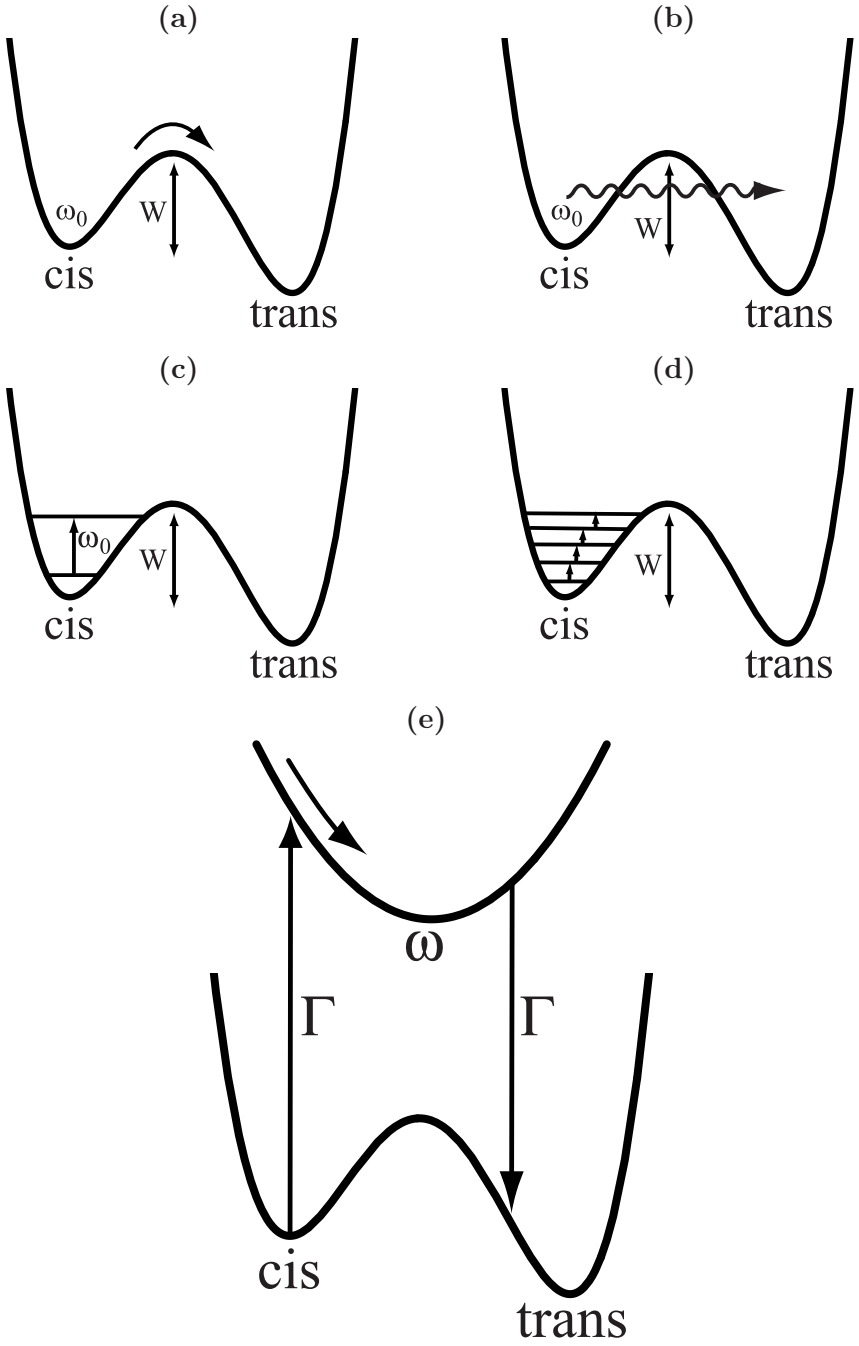

Figure 5.1: Switching process induced by thermal activation (a), quantum tunneling (b), vibrational-assisted tunneling involving the emission of a single phonon (c), and the emission of several phonons (d). The switching process studied in the present work is sketched in (e).

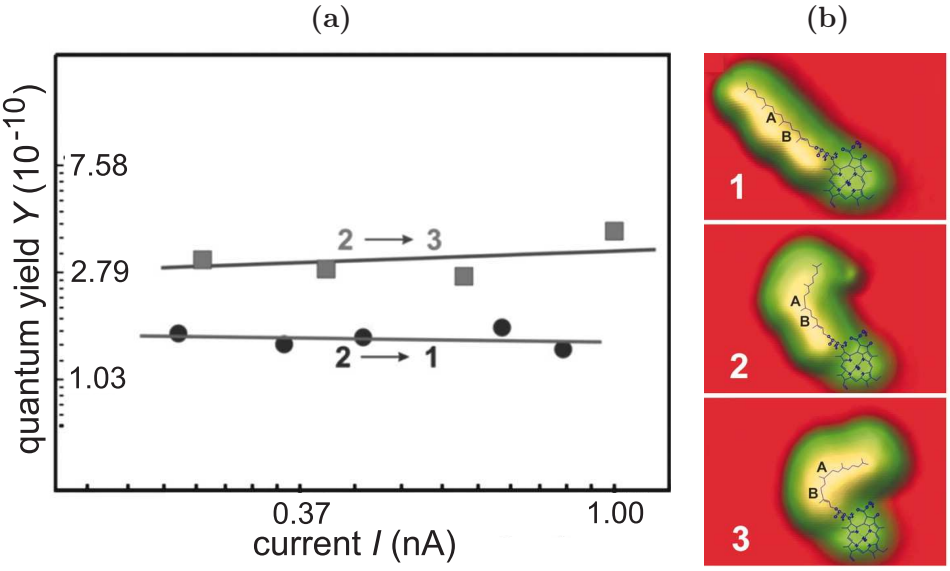

Figure 5.2: (a) Experimental data for the quantum yield of a molecular switch in scanning tunneling microscope manipulation of single chlorophyll-a derivatives, taken from Ref. [141]. The two curves describe the switching dynamics involving the molecular conformations shown in (b). The data sets used for the plots are recorded with constant bias voltage.

charge carriers. For thermal energies large compared to the level-broadening due to the coupling to the leads, the stationary current is

$$I \sim e \frac{\Gamma_{\text{tip}}\Gamma_{\text{sub}}}{\Gamma_{\text{tip}} + \Gamma_{\text{sub}}}, \tag{5.5}$$

where Γ_{tip} and Γ_{sub} are the tunneling-induced level widths due to the coupling to the tip and to the substrate, respectively. Thus, the current passing through an asymmetric junction is, to a good approximation, governed by the smaller rate only. The molecule spends most of the time in the neutral state, i.e. whenever an electron tunnels from the tip onto the molecule, it continues into the substrate almost instantaneously, while the average waiting time until the next tunneling event from the tip is long.

The basic mechanism of current-induced switching now follows from the Franck-Condon principle, which states that the vibrational state does not change during the much faster electronic tunneling processes in and out of the molecule. The switching process is initiated by a first transition from one of the two conformational states into the charged state. After the molecule evolves on the potential surface of the charged state, it eventually undergoes a second tunneling transition from the charged state into a conformational state, cf. Fig. 5.1(e). Clearly, the switching probability strongly depends on the ratio of the vibrational frequency in the charged state, ω,

and $\Gamma = \Gamma_{\rm tip} + \Gamma_{\rm sub}$. For $\omega \gg \Gamma$ the molecule oscillates many times between the two tunneling events, and the probabilities for transitions from the charged state into the two conformational states of the neutral molecule are of the same order. In contrast, for $\omega \ll \Gamma$ the ionic state survives for much less than a full vibration period. Thus, the molecule returns to its original conformation with high probability, and conformational switching occurs rarely. Such low-quantum-yield switching has been observed in recent experiments [50; 141; 142], cf. Fig. 5.2. For instance, STM measurements on azobenzene and chlorophyll-a derivatives show that only one out of 10^{10} tunneling electrons induces a switching event.

It is this regime of low-quantum-yield switching in asymmetric molecular junctions which is the principal focus of the this chapter. We focus on the regime of sequential tunneling relevant to STM experiments on passivated surfaces [143]. We present a fully analytical treatment of the quantum yield within a generic model system. Specifically, we show that the temperature dependence reflects a sensitive interplay of vibrational frequency, tunneling rates, and charge-induced vibrational deformation. Our results are obtained from a Fokker-Planck equation which incorporates the molecule-tip and molecule-substrate tunneling as well as dissipation of the vibrational degree of freedom. A crucial assumption in our approach is the quasi-classical treatment of the vibrations. In this respect, our approach is related to the formalism used for the description of transport through nanoelectromechanical systems (NEMS) that have recently received much attention [144–146].

5.2 Model

We consider a vibrating single molecule which is coupled to two reservoirs, which serve as source and drain electrodes. The vibrational potential surface of the neutral molecule is assumed to have the form of a double well representing the cis and the trans state, whereas the potential surface of the charged state is assumed to be harmonic.

Vibrational relaxation in the neutral state is assumed to be sufficiently fast so that tunneling events always start from one of the minima of the double well. This permits one to approximate the double well potential by two separate harmonic oscillators. The resulting three-level system with states $|\text{cis}\rangle$, $|\text{trans}\rangle$, $|1\rangle$ is described by the molecular Hamiltonian

$$H_{\rm mol} = H_{\rm cis}|\text{cis}\rangle\langle\text{cis}| + H_{\rm trans}|\text{trans}\rangle\langle\text{trans}| + H_1|1\rangle\langle 1|, \tag{5.6}$$

where

$$H_s = \epsilon_s + \frac{p^2}{2m_s} + V_s(x) \tag{5.7}$$

denotes the vibrational Hamiltonian of subspace $s = \text{cis, trans, 1}$. The variables x, p, and m_s denote the normal coordinate, momentum, and reduced mass of the vibrational modes, and $V_s(x)$ denotes the corresponding potential within the harmonic approximation, $V_s(x) = m_s\omega_s^2(x - x_s)^2/2$, with oscillator frequency ω_s and

local minimum x_s. The parameter ϵ_s denotes the energies of the relevant electronic states.

The full system is modeled by the Hamiltonian

$$H = H_{\text{mol}} + H_{\text{leads}} + H_t, \tag{5.8}$$

where

$$H_{\text{leads}} = \sum_{\alpha\mathbf{k}} \epsilon_{\mathbf{k}} a^\dagger_{\alpha\mathbf{k}} a_{\alpha\mathbf{k}} \tag{5.9}$$

describes the non-interacting electrons in the two leads (α =tip, sub), and

$$H_t = \sum_{\alpha\mathbf{k}} t_\alpha a^\dagger_{\alpha\mathbf{k}} \Big(|\text{cis}\rangle\langle 1| + |\text{trans}\rangle\langle 1| \Big) + \text{h.c.} \tag{5.10}$$

represents the tunneling between the molecule and the leads. We assume that t_α is non-zero for the $|\text{cis}\rangle \leftrightarrow |1\rangle$ ($|\text{trans}\rangle \leftrightarrow |1\rangle$) transitions when $x < x_1$ ($x > x_1$). Here $a^\dagger_{\alpha\mathbf{k}}$ creates an electron with momentum $\mathbf{k}$ and energy $\epsilon_{\mathbf{k}}$ in lead α. We omit the spin index of these operators, since we ignore spin-dependent transport phenomena in the following.

5.3 Boltzmann equation

The dynamics of the system is described by a set of Boltzmann equations, which we derive within a density-matrix formalism. The starting point is the von Neumann equation,

$$\frac{d\rho}{dt} = -\frac{i}{\hbar}\left[H, \rho\right], \tag{5.11}$$

for the time evolution of the density matrix ρ of the system, which has the formal iterative solution [73]

$$\frac{d\rho(t)}{dt} = -\frac{i}{\hbar}\left[H_t(t), \rho(0)\right] - \frac{1}{\hbar^2}\int_0^t dt' \left[H_t(t), \left[H_t(t'), \rho(t')\right]\right]. \tag{5.12}$$

Operators O with an explicit time argument are in the interaction picture, $O(t) = e^{i(H_{\text{mol}}+H_{\text{leads}})t/\hbar} O\, e^{-i(H_{\text{mol}}+H_{\text{leads}})t/\hbar}$. The dynamics of the molecule is described by the reduced density matrix which is obtained by tracing out the degrees of freedom of the leads,

$$\rho_{\text{mol}}(t) = \text{Tr}_{\text{leads}}\, \rho(t). \tag{5.13}$$

As discussed in Chapter 2, solving Eq. (5.12) for ρ relies on making the large-reservoir approximation, which allows us to write the density matrix as a direct product, $\rho(t) \simeq \rho_{\text{mol}}(t) \otimes \rho_{\text{leads}}$, of the density matrices $\rho_{\text{mol}}(t)$ and ρ_{leads} of the molecule and the leads, and the Markov approximation, which allows us to replace $\rho_{\text{mol}}(t') \simeq \rho_{\text{mol}}(t)$ in Eq. (5.12).

Furthermore, we assume $\rho_{\rm mol}(t)$ to be diagonal in the conformational degree of freedom,

$$\rho_{\rm mol} = |{\rm cis}\rangle\,\rho_{\rm cis}\,\langle{\rm cis}| + |{\rm trans}\rangle\,\rho_{\rm trans}\,\langle{\rm trans}| + |1\rangle\,\rho_1\,\langle 1|\,. \tag{5.14}$$

Superpositions of different charge states can be neglected due to superselection rules [147; 148], while superpositions of the cis and the trans state are assumed to decay rapidly due to fast vibrational relaxation in the neutral state.

Tracing out the degrees of freedom of the leads, and opening the double commutator in Eq. (5.12) gives

$$\begin{aligned}\frac{d\rho_{\rm mol}}{dt} = &-\frac{i}{\hbar}\,[H_{\rm mol},\rho_{\rm mol}] - \sum_{\alpha\mathbf{k}}\frac{|t_\alpha|^2}{\hbar^2}\sum_{s={\rm cis,trans}}\int_0^\infty d\tau \\ &\times(|s\rangle\langle s| - |1\rangle\langle 1|)\Big\{e^{i\epsilon_{\mathbf{k}}\tau/\hbar}\Big(f_\alpha(\epsilon_{\mathbf{k}})e^{-iH_1\tau/\hbar}e^{iH_s\tau/\hbar}\rho_s \\ &-[1-f_\alpha(\epsilon_{\mathbf{k}})]\,\rho_1 e^{-iH_1\tau/\hbar}e^{iH_s\tau/\hbar}\Big) + {\rm h.c.}\Big\}.\end{aligned} \tag{5.15}$$

Going to the Wigner representation of the density matrix,

$$W_s(x,p) = \int\frac{dy}{2\pi\hbar}\;e^{-ipy/\hbar}\langle x+\frac{y}{2}|\rho_s|x-\frac{y}{2}\rangle, \tag{5.16}$$

allows for a semiclassical description of the vibrational modes, where, in the quasiclassical limit, the Wigner function $W_s(x,p)$ describes the probability of finding the oscillator in state $s = $ cis, trans, 1 at position x with momentum p.

The Wigner transform of the terms in Eq. (5.15) is evaluated for the slow-resonator limit, $\omega_s \ll \Gamma$, and the sequential tunneling limit, $T \gg \hbar\Gamma$. Details on the calculation are explained in the footnote.[2] One finally arrives at the following set of Boltzmann

[2] We assume that the oscillators of the cis, trans, and charged states centered at $x_{\rm cis}$, $x_{\rm trans}$, and $x_1 = 0$, respectively, all have the same reduced mass m and frequency ω, which allows all calculations to be done explicitly. It is evident that the underlying arguments also extend to the more general case.

Projecting Eq. (5.15) on, say, the cis state (the derivation for the two other states proceeds analogously), we obtain

$$\begin{aligned}\frac{d\rho_{\rm cis}}{dt} &= -\frac{i}{\hbar}\,[H_{\rm cis},\rho_{\rm cis}] - \sum_{\alpha\mathbf{k}}\frac{|t_\alpha|^2}{\hbar^2}\int_0^\infty d\tau\Big\{e^{i\epsilon_{\mathbf{k}}\tau/\hbar}\Big(f_\alpha(\epsilon_{\mathbf{k}})e^{-iH_1\tau/\hbar}e^{iH_{\rm cis}\tau/\hbar}\rho_{\rm cis} \\ &\quad -[1-f_\alpha(\epsilon_{\mathbf{k}})]\,\rho_1 e^{-iH_1\tau/\hbar}e^{iH_{\rm cis}\tau/\hbar}\Big) + {\rm h.c.}\Big\}.\end{aligned} \tag{5.17}$$

The Wigner transform of this equation reads

$$\begin{aligned}\frac{\partial}{\partial t}W_{\rm cis}(x,p) &= \{\mathcal{H}_{\rm cis}(x,p),W_{\rm cis}(x,p)\} - 2\sum_{\alpha\mathbf{k}}\frac{|t_\alpha|^2}{\hbar^2}{\rm Re}\int_0^\infty d\tau e^{\frac{i}{\hbar}[(\epsilon_{\mathbf{k}}+\epsilon_{\rm cis}-\epsilon_1)\tau - p\tilde{x}_\tau - \left(x-\frac{x_{\rm cis}}{2}\right)\tilde{p}_\tau]} \\ &\quad\times\left\{f_\alpha(\epsilon_{\mathbf{k}})W_{\rm cis}\left(x-\frac{\tilde{x}_\tau}{2},p+\frac{\tilde{p}_\tau}{2}\right) - [1-f_\alpha(\epsilon_{\mathbf{k}})]\,W_1\left(x+\frac{\tilde{x}_\tau}{2},p-\frac{\tilde{p}_\tau}{2}\right)\right\}\end{aligned} \tag{5.18}$$

with $\tilde{x}_\tau = x_{\rm cis}\,[\cos(\omega\tau)-1]$ and $\tilde{p}_\tau = m\omega x_{\rm cis}\sin(\omega\tau)$. The first term in the right-hand side in

equations,

$$\frac{\partial W_s}{\partial t} = \{\mathcal{H}_s, W_s\} + R_{1\to s}W_1 - R_{s\to 1}W_s, \tag{5.20a}$$

$$\frac{\partial W_1}{\partial t} = \{\mathcal{H}_1, W_1\} + \sum_s \left(R_{s\to 1}W_s - R_{1\to s}W_1\right), \tag{5.20b}$$

for $s = \text{cis}, \text{trans}$, with transition rates which are equivalent to Fermi's Golden Rule,

$$R_{s\to 1}(x,p) = \sum_\alpha \Gamma_\alpha f_\alpha\big(\mathcal{H}_1(x,p) - \mathcal{H}_s(x,p)\big), \tag{5.21a}$$

$$R_{1\to s}(x,p) = \sum_\alpha \Gamma_\alpha \left[1 - f_\alpha\big(\mathcal{H}_1(x,p) - \mathcal{H}_s(x,p)\big)\right]. \tag{5.21b}$$

Here $\mathcal{H}_s(x,p) = \epsilon_s + p^2/2m_s + V_s(x)$ is the Wigner transform of the harmonic-oscillator Hamiltonian and $\Gamma_\alpha = 2\pi|t_\alpha|^2\nu_\alpha/\hbar$, where ν_α denotes the density of states in lead α, which we take as a constant. The Poisson bracket appearing in Eq. (5.20) is defined as

$$\{\mathcal{H}_s, W_s\} = \frac{\partial \mathcal{H}_s}{\partial x}\frac{\partial W_s}{\partial p} - \frac{\partial \mathcal{H}_s}{\partial p}\frac{\partial W_s}{\partial x}. \tag{5.22}$$

Note that all rates in Eq. (5.21) depend only on x and not on p if one assumes equal reduced masses m_s for all vibrational modes.

5.4 Fokker-Planck equation

The set of Boltzmann equations derived in the previous section does not have a unique stationary solution in the absence of electronic tunneling. In this case Eq. (5.20) is solved by any function W_s that depends on $\mathcal{H}_s$ only, since the Poisson brackets then vanish exactly. However, a unique solution is obtained if we add the coupling to a bath, which takes into account the damping of the vibrations such that the system is driven back towards (local) equilibrium. The relaxation of the molecular

(5.18) denotes the Poisson bracket between the classical Hamiltonian and the Wigner function of the cis state.

Computing the sum over momenta $\mathbf{k}$ in the wide-band limit, one realizes that the integrand in (5.18) decays exponentially with the temperature. Since we are considering the slow-vibration limit ($\omega \ll \Gamma$) and the sequential-tunneling regime ($\hbar\Gamma \ll T$), we can therefore expand (5.18) for $\omega\tau \ll 1$ to obtain

$$\begin{aligned}\frac{\partial}{\partial t}W_{\text{cis}}(x,p) \;\simeq\; & \{\mathcal{H}_{\text{cis}}(x,p), W_{\text{cis}}(x,p)\} - 2\sum_{\alpha\mathbf{k}} \frac{|t_\alpha|^2}{\hbar^2}\text{Re}\int_0^\infty d\tau e^{\frac{i}{\hbar}\left[\epsilon_{\mathbf{k}}+\epsilon_{\text{cis}}-\epsilon_1-m\omega^2 x_{\text{cis}}(x-x_{\text{cis}}/2)\right]\tau} \\ & \times \left\{f_\alpha(\epsilon_{\mathbf{k}})W_{\text{cis}}(x,p) - \left[1 - f_\alpha(\epsilon_{\mathbf{k}})\right]W_1(x,p)\right\}. \end{aligned} \tag{5.19}$$

The remaining integral over τ is easily evaluated and guarantees energy conservation for the rates entering the Boltzmann equation (5.20).

vibron due to the presence of a bosonic bath can be modeled by the Caldeira-Leggett Hamiltonian [149; 150],

$$H_{\mathrm{CL}} = H_{\mathrm{vib}} + H_{\mathrm{bath}} + H_{\mathrm{coupling}}, \tag{5.23}$$

where

$$H_{\mathrm{vib}} = \hbar\omega b^{\dagger} b \tag{5.24}$$

describes the vibron,

$$H_{\mathrm{bath}} = \sum_{q} \hbar\omega_q b_q^{\dagger} b_q \tag{5.25}$$

a bath of harmonic oscillators, and

$$H_{\mathrm{coupling}} = \hbar g(b^{\dagger} + b) \sum_{q} (b_q^{\dagger} + b_q) \tag{5.26}$$

the linear coupling between them. Here $b_q^{\dagger}$ creates a phonon in the reservoir with frequency ω_q and g determines the coupling strength. Treating both the bosonic and fermionic coupling to the leads perturbatively, we obtain a set of Fokker-Planck equations [149; 150],

$$\begin{aligned}
\frac{\partial W_s}{\partial t} =& \{\mathcal{H}_s, W_s\} + R_{1\to s} W_1 - R_{s\to 1} W_s \\
&+ \gamma_s \frac{\partial}{\partial p} p W_s + \frac{\gamma_s}{2} m_s \hbar\omega_s \coth\left(\frac{\hbar\omega_s}{2T}\right) \frac{\partial^2}{\partial p^2} W_s, \qquad (5.27a) \\
\frac{\partial W_1}{\partial t} =& \{\mathcal{H}_1, W_1\} + \sum_{s} \left(R_{s\to 1} W_s - R_{1\to s} W_1\right) \\
&+ \gamma_1 \frac{\partial}{\partial p} p W_1 + \frac{\gamma_1}{2} m_1 \hbar\omega_1 \coth\left(\frac{\hbar\omega_1}{2T}\right) \frac{\partial^2}{\partial p^2} W_1, \qquad (5.27b)
\end{aligned}$$

to lowest non-vanishing order in $\hbar g$. The damping rate $\gamma_s = 2\pi g^2 \sum_q \delta(\omega_s - \omega_q)$ determines the magnitude of the drift (terms proportional to the first derivative with respect to the momentum) and diffusive motion (terms proportional to the second derivative). Note that our calculation ignores any effects of dissipation on the tunneling rates.

In the absence of electronic tunneling, the stationary solutions of Eq. (5.27) reduce to Gaussian distribution functions,

$$W_s \sim \exp\left[-\frac{\mathcal{H}_s(x,p)}{\hbar\omega_s \coth\left(\hbar\omega_s/2T\right)/2}\right], \tag{5.28}$$

where $s =$ cis, trans, 1. If the vibrational energy is larger than the thermal energy, $\hbar\omega_s \gg T$, one obtains the occupation probabilities of the ground state wave function of the harmonic oscillator, whereas for the reverse case, $\hbar\omega_s \ll T$, one obtains Boltzmann distribution functions.

5.5 Quantum yield

The Fokker-Planck equation derived in Sec. 5.4 allows us to investigate the current-induced conformational switching dynamics of the molecule. Specifically, we are interested in the *quantum yield* which is the probability for a single electron tunneling through the system to switch the molecule. We calculate this quantity as the conditional probability for the molecule to go, say, into the trans state in the first tunneling event after excitation from the cis state into the charged state at time $t = 0$.

We are interested in the regime where the molecule spends almost all the time in the neutral state, i.e. either in the cis or in the trans conformation, due to very asymmetric couplings to the leads. The rate for electronic tunneling from the molecule into the leads is assumed to be much higher than all vibrational frequencies, $\omega_s \ll \Gamma$. Shortly after a transition from the cis state to the charged state, the two Wigner functions $W_{\rm cis}$ and $W_{\rm trans}$ are equal to zero. In this case the equations of motion (5.27) simplify to

$$\begin{aligned}
\frac{\partial W_{\rm cis}}{\partial t} &= \{\mathcal{H}_{\rm cis}, W_{\rm cis}\} + R_{1\to\rm cis} W_1 + \gamma_{\rm cis}\frac{\partial}{\partial p} p W_{\rm cis} \\
&\quad + \frac{\gamma_{\rm cis}}{2} m_{\rm cis}\hbar\omega_{\rm cis}\coth\left(\frac{\hbar\omega_{\rm cis}}{2T}\right)\frac{\partial^2}{\partial p^2} W_{\rm cis}, \qquad (5.29)\\
\frac{\partial W_{\rm trans}}{\partial t} &= \{\mathcal{H}_{\rm trans}, W_{\rm trans}\} + R_{1\to\rm trans} W_1 + \gamma_{\rm trans}\frac{\partial}{\partial p} p W_{\rm trans} \\
&\quad + \frac{\gamma_{\rm trans}}{2} m_{\rm trans}\hbar\omega_{\rm trans}\coth\left(\frac{\hbar\omega_{\rm trans}}{2T}\right)\frac{\partial^2}{\partial p^2} W_{\rm trans}, \qquad (5.30)\\
\frac{\partial W_1}{\partial t} &= \{\mathcal{H}_1, W_1\} - \left(R_{1\to\rm cis} + R_{1\to\rm trans}\right) W_1. \qquad (5.31)
\end{aligned}$$

We need not include any rates out of the cis and trans states, since we are only interested in the first out-scattering event. The drift and diffusion terms in Eq. (5.31) for the charged state have been neglected. This is justified since the switching dynamics is controlled by times $t \sim 1/\omega_s$ beyond which $W_1(t)$ is exponentially suppressed. In contrast, dissipation becomes relevant for much later times of order $1/\gamma_s$. Note also that the dissipative terms in the other two equations do not change the overall probability to be in one of the charge states, but only the detailed form of the distribution function within each charge states. Consequently, dissipation affects the quantum yield only through the initial vibrational distribution function after an electron tunnels from the tip to the molecule.

It is convenient to introduce action and angle variables (S and θ) for the charged state,

$$x = -\sqrt{\frac{2S}{m_1\omega_1}}\cos\theta, \qquad p = \sqrt{2m_1\omega_1 S}\sin\theta, \qquad (5.32)$$

since this transformation generates a cyclic variable and reduces the Poisson bracket

to the simple form

$$\{\mathcal{H}_1, W_1\} = -\omega_1 \frac{\partial W_1}{\partial \theta}. \tag{5.33}$$

Since Eq. (5.31) does not contain W_{cis} and W_{trans}, it can thus be solved independently,

$$W_1(\theta, S, t) = W_1(\theta - \omega_1 t, S, t = 0) \exp\left[- \int_0^t dt' \sum_s R_{1\to s}(\theta - \omega_1 t', S) \right]. \tag{5.34}$$

We can now insert this result into Eq. (5.30). Integrating over phase space yields

$$\begin{aligned} \int d\theta\, dS\, W_{\text{trans}}(\theta, S, t) = & \int d\theta\, dS\, R_{1\to\text{trans}}(\theta, S) \\ & \times \int_0^t dt' W_1(\theta - \omega_1 t', S, t = 0) \exp\left[- \int_0^{t'} dt'' \sum_s R_{1\to s}(\theta - \omega_1 t'', S) \right], \end{aligned} \tag{5.35}$$

where we made use of the fact that the integral of the Poisson bracket over phase space vanishes.

The quantum yield is the total probability of going into *any* trans state with position x and momentum p at any time $t > 0$,

$$Y = \lim_{t\to\infty} \int d\theta\ dS\ W_{\text{trans}}(\theta, S, t). \tag{5.36}$$

First we calculate the *partial quantum yield*, $y(\theta_0, S_0)$, which is obtained if one assumes a delta function in phase space for the initial distribution function of the charged molecule, $W_1(\theta, S, t = 0) = \delta(S - S_0)\, \delta(\theta - \theta_0)$. Then the total quantum yield Y can be computed as an average over all possible initial conditions $W_1(\theta, S, t = 0)$,

$$Y = \int d\theta dS\, W_1(\theta, S, t = 0) y(\theta, S). \tag{5.37}$$

For the partial quantum yield we obtain

$$y(\theta, S) = \int_0^\infty dt'\, R_{1\to\text{trans}}\left(\theta + \omega_1 t', S\right) \exp\left[- \int_0^{t'} dt'' \sum_s R_{1\to s}\left(\theta + \omega_1 t'', S\right) \right]. \tag{5.38}$$

Note that it depends on both x_{cis} and x_{trans} because of the position dependence of the rates $R_{1\to\text{cis}}$ and $R_{1\to\text{trans}}$. Making use of the periodicity of the rates in θ we can perform the integrations over complete periods, $T_1 = 2\pi/\omega_1$, and obtain

$$y(\theta, S) = \int_0^{T_1} dt'\, R_{1\to\text{trans}}\left(\theta + \omega_1 t', S\right) \frac{\exp\left[- \int_0^{t'} dt'' \sum_s R_{1\to s}\left(\theta + \omega_1 t'', S\right) \right]}{1 - \exp\left[- \int_0^{T_1} dt'' \sum_s R_{1\to s}\left(\theta + \omega_1 t'', S\right) \right]}. \tag{5.39}$$

In the regime of our interest, where the tunneling rate is large compared to the oscillation frequency, $\omega_1 \ll \Gamma$, the exponential in the denominator is very close to zero and can be neglected, such that

$$y(\theta, S) \simeq \int_0^{T_1} dt'\, R_{1\to\text{trans}}\left(\theta + \omega_1 t', S\right) \exp\left[-\int_0^{t'} dt'' \sum_s R_{1\to s}\left(\theta + \omega_1 t'', S\right)\right]. \tag{5.40}$$

This result has a clear physical interpretation. The exponential describes the conditional probability that the molecule starting at phase space point S and θ at time $t'' = 0$ is still in the charged state at time $t'' = t'$.

5.6 Results and discussion

In what follows, we assume for simplicity that the three oscillators of the cis, trans, and charged states centered at x_{cis}, x_{trans}, and $x_1 = 0$, respectively, all have the same reduced mass m and frequency ω. The damping rate is thus the same for all vibrational states and we denote it as γ.

The regime of interest is characterized by the inequalities

$$\Gamma_{\text{tip}} \ll \omega \ll \Gamma_{\text{sub}}. \tag{5.41}$$

Moreover, we will assume that the tip-to-molecule tunneling is sufficiently weak,

$$\Gamma_{\text{tip}} \ll \gamma \ll \omega, \tag{5.42}$$

so that the vibrational mode thermally equilibrates in both the cis and trans conformation after each tunneling event. The nonequilibrium regime $\Gamma_{\text{tip}} \gg \gamma$ is clearly interesting but beyond the scope of the present work.

It is natural to assume that the asymmetric molecule-electrode coupling goes along with asymmetric voltage drops (although the latter are determined by capacitive couplings rather than tunnel amplitudes). To be specific, we will assume that the voltage $V = V_{\text{tip}} - V_{\text{sub}}$ drops entirely between tip and molecule,

$$V_{\text{tip}} \simeq V, \qquad V_{\text{sub}} \simeq 0. \tag{5.43}$$

This has important consequences for the electronic transport. Energy conservation for the electronic tunneling from the cis state into the charged state requires

$$\epsilon_1 - \epsilon_{\text{cis}} + V_1(x) - V_{\text{cis}}(x) < V_{\text{tip}}. \tag{5.44}$$

In the vicinity of $x \simeq x_{\text{cis}}$ this condition reduces to

$$\epsilon_1 - \epsilon_{\text{cis}} + \frac{1}{2} m\omega^2 x_{\text{cis}}^2 < V_{\text{tip}}, \tag{5.45}$$

which defines a threshold voltage beyond which tunneling from tip to molecule becomes possible. For voltages not too far below this threshold, tunneling from the

molecule into the substrate is always energetically possible, since the corresponding condition for energy conservation,

$$\epsilon_1 - \epsilon_{\mathrm{cis}} + V_1(x) - V_{\mathrm{cis}}(x) > V_{\mathrm{sub}}, \tag{5.46}$$

is always satisfied for sufficiently large values of $\epsilon_1 - \epsilon_{\mathrm{cis}}$ and $V_{\mathrm{sub}} \simeq 0$.

When the bias exceeds the threshold value $V_{\mathrm{c}} = \epsilon_1 - \epsilon_{\mathrm{cis}} + m\omega^2 x_{\mathrm{cis}}^2/2$, the steady-state current through the molecule is given by

$$I_{\mathrm{cis}} \simeq e\,\Gamma_{\mathrm{tip}}, \tag{5.47}$$

i.e. it is essentially governed by the slower tip-to-molecule tunneling. Due to the Franck-Condon principle, the vibrational distribution function in the cis state will be left unaltered during the tunneling process. Due to the assumption $\Gamma_{\mathrm{tip}} \ll \gamma$ and for thermal energies $T \gg \hbar\omega$, the stationary solution of Eq. (5.27) in absence of tunneling reduces to a Boltzmann distribution function, cf. Eq. (5.28). Thus the initial distribution function of the charged state is

$$W_1(\theta, S, t=0) = \frac{\omega}{2\pi T} \exp\left[-\frac{\mathcal{H}_{\mathrm{cis}}(\theta, S) - \epsilon_{\mathrm{cis}}}{T}\right]. \tag{5.48}$$

Notice that if the bias voltage is in the vicinity of the threshold voltage V_{c}, the distribution function becomes truncated during tunneling due to energetic restrictions. Apart from the initial distribution function, the switching dynamics is mostly determined by tunneling processes from the molecule into the substrate. Since these processes are not affected by energetic restrictions, their rates are essentially constant, independent of temperature and bias.

We begin our analytical analysis by deriving the partial quantum yield $y(\theta, S)$. We approximate $R_{1\to\mathrm{trans}}(\theta, S) = \Gamma_{\mathrm{sub}}$ for $|\theta| > \pi/2$ and zero otherwise. Similarly, we take $R_{1\to\mathrm{cis}}(\theta, S) = \Gamma_{\mathrm{sub}}$ for $|\theta| < \pi/2$. Then, we find for $\omega \ll \Gamma_{\mathrm{sub}}$

$$y(\theta) \simeq \exp\left[-\frac{\Gamma_{\mathrm{sub}}}{\omega}\left(\frac{\pi}{2} - \theta\right)\right]. \tag{5.49}$$

Note that the quantum yield depends only on the phase space angle θ and not on the action coordinate S. This is a direct consequence of the harmonic potential surface. Phase space angles $\theta > 0$ correspond to positive initial velocities and thus lead to a higher quantum yield as compared to $\theta < 0$. Plots of the partial quantum yield for different values of $\Gamma_{\mathrm{sub}}/\omega$ are shown in Fig. 5.3.

For $\theta = 0$ the partial quantum yield is approximately $\exp(-\Gamma_{\mathrm{sub}}\pi/2\omega)$. This result has a simple physical interpretation, since $\pi/2\omega$ is just a quarter period of the harmonic motion on the potential surface.

For the case where the initial distribution function $W_1(\theta, S, t = 0)$ is given by Eq. (5.48), i.e. the thermal distribution in the cis state, the total quantum yield is

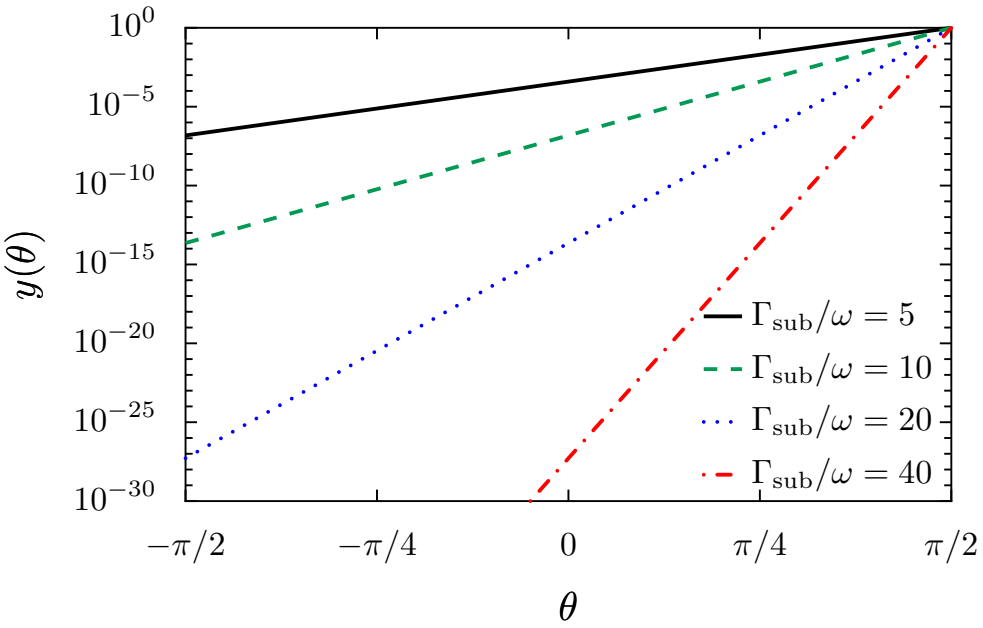

Figure 5.3: Partial quantum yield $y(\theta)$ as a function of phase space angle θ for different ratios of the electronic tunneling rate $\Gamma_{\rm sub}$ and the vibrational frequency ω.

readily obtained from Eqs. (5.38) and (5.40),

$$Y = \frac{\omega}{2\pi T} \exp\left(-\frac{m\omega^2 x_{\rm cis}^2}{2T}\right) \int_{-\pi/2}^{\pi/2} d\theta \exp\left[-\frac{\Gamma_{\rm sub}}{\omega}\left(\frac{\pi}{2} - \theta\right)\right] \times \int_0^\infty dS \exp\left(-\frac{\omega S}{T} + \frac{m\omega^2 |x_{\rm cis}|}{T}\sqrt{\frac{2S}{m\omega}}\cos\theta\right). \tag{5.50}$$

We now change the action variable to $J = \omega S/T$ and introduce the large parameter $L = m\omega^2 x_{\rm cis}^2/2T$. Moreover, it is useful to write the second large parameter $\Gamma_{\rm sub}/\omega = \alpha L$, where α denotes the ratio of the two large parameters. Note that α increases with temperature and can be interpreted as a measure of temperature. With these definitions, we find

$$Y = \frac{\exp(-L)}{2\pi} \int_{-\pi/2}^{\pi/2} d\theta \exp\left[-\alpha L\left(\frac{\pi}{2} - \theta\right)\right] \int_0^\infty dJ \exp\left(-J + 2\sqrt{LJ}\cos\theta\right). \tag{5.51}$$

If the dominant contribution to the θ-integral comes from a region which does not include $\theta \simeq \pi/2$, the integration over J can be performed by saddle-point integration due to $L \gg 1$. This can be made explicit by introducing $x = J/L$. Doing so and performing the saddle-point integration over x, we obtain

$$Y = \sqrt{\frac{L}{\pi}} \int_{-\pi/2}^{\pi/2} d\theta \cos\theta \exp\left\{-L\left[\alpha\left(\frac{\pi}{2} - \theta\right) + \sin^2\theta\right]\right\}. \tag{5.52}$$

Finally, at sufficiently low temperatures, $\alpha < 1$, we can also perform the angular integration by the saddle-point method. Finding the saddle point, we obtain that the optimal θ is given by

$$\theta_0 = \frac{1}{2}\arcsin\alpha. \tag{5.53}$$

The existence of an optimal θ reflects the competition between the following trends: The larger the initial θ, the smaller is its weight in the initial distribution function, but the larger is the corresponding partial yield. Performing the saddle-point integration, we obtain our central analytical result for the quantum yield,

$$Y \simeq \left(\frac{1+\sqrt{1-\alpha^2}}{2\sqrt{1-\alpha^2}}\right)^{1/2} \exp\left\{-\frac{L}{2}\left[\alpha\left(\pi - \arcsin\alpha\right) + 1 - \sqrt{1-\alpha^2}\right]\right\}. \tag{5.54}$$

It is instructive to analyze various limits of this equation. At very low temperatures, $\alpha \ll 1$, the expression (5.54) for the quantum yield takes the form

$$Y \simeq \exp\left(-\frac{\pi}{2}\frac{\Gamma_{\rm sub}}{\omega}\right). \tag{5.55}$$

This reflects the fact that at low temperatures, the initial distribution function is very narrow and is well approximated by $\delta(S - m\omega x_{\rm cis}^2/2)\delta(\theta)$. Thus, switching requires that the system stays for a quarter oscillation period in the charged state. At larger temperatures where α is close to but still smaller than one, we find

$$Y \simeq \frac{1}{\sqrt{2}(1-\alpha^2)^{1/4}} \exp\left[-L\left(\frac{\pi}{4}+\frac{1}{2}\right)\right]. \tag{5.56}$$

This result is remarkable in that the exponential suppression is stronger than what one would expect for thermal activation, namely $\exp(-L)$. This suggests that there exists a "critical" temperature where there is a *sharp crossover* between current-induced switching and processes closely related to thermal activation, originating from $\theta \simeq \pi/2$.

Indeed, it is straightforward to compute the contribution to the quantum yield Y in Eq. (5.51) from angle variables θ in the vicinity of $\pi/2$ which were previously neglected. To do so, we start with Eq. (5.51), expand the exponent for $\theta \simeq \pi/2$, and obtain

$$Y_{\pi/2} \simeq \frac{L}{2\pi}\exp\left(-L\right)\int_0^\infty d\tilde{\theta}\int_0^\infty dJ \exp\left[-L\left(\alpha\tilde{\theta} + J - 2\sqrt{J}\tilde{\theta}\right)\right]. \tag{5.57}$$

Changing integration variables to $t = L\tilde{\theta}$ and $j = LJ$, we note that the last term in the exponent can be neglected in the limit of large L. Then, the integration becomes elementary and we obtain

$$Y_{\pi/2} \simeq \frac{\omega}{2\pi\Gamma_{\rm sub}}\exp\left(-L\right). \tag{5.58}$$

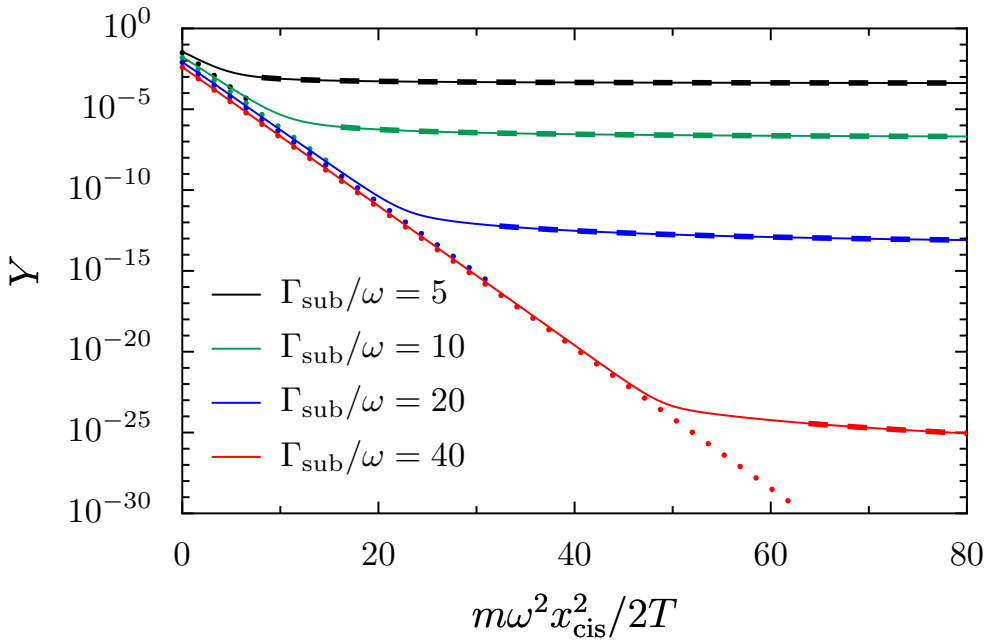

Figure 5.4: Total quantum yield Y as a function of the inverse temperature $1/T$ for different ratios of the electronic tunneling rate $\Gamma_{\rm sub}$ and the vibrational frequency ω. Solid lines: numerical integration of Eq. (5.50). Dashed lines: quantum yield for $T < T_{\rm c}$, Eq. (5.54). Dotted lines: quantum yield for $T > T_{\rm c}$, Eq. (5.58).

Thus, we indeed confirm that for α close to unity, the dominant contribution is no longer current-induced switching, but rather thermal-activation processes. Since $L \gg 1$ there is a sharp crossover between both behaviors when the exponents in Eqs. (5.54) and (5.58) coincide. This happens for a critical $\alpha_{\rm c}$ determined by

$$\frac{\alpha_{\rm c}}{2}(\pi - \arcsin \alpha_{\rm c}) = \sqrt{1-\alpha_{\rm c}^2}, \tag{5.59}$$

which yields $\alpha_{\rm c} \simeq 0.63$.

The critical $\alpha_{\rm c}$ translates into a critical temperature

$$T_{\rm c} = \alpha_{\rm c}\,\frac{\omega}{\Gamma_{\rm sub}}\,\frac{m\omega^2 x_{\rm cis}^2}{2}. \tag{5.60}$$

For $T < T_{\rm c}$, cis-trans switching is dominated by current-induced switching while thermal activation takes over for $T > T_{\rm c}$. Since L is typically a large parameter, this crossover will typically be sharp. It is important to note that this crossover occurs long before the thermal broadening of the initial distribution function becomes comparable to $|x_{\rm cis}|$.

These analytical results are compared to numerical evaluations of Eq. (5.50) in Fig. 5.4 (solid lines) where the quantum yield is shown as a function of temperature.

For $T < T_c$, the yield can be approximated by the expression for current-induced switching [dashed lines, Eq. (5.54)] while for $T > T_c$, it is mostly thermally activated [dotted lines, Eq. (5.58)]. The existence of a sharp transition for T close to T_c can be clearly seen in the figure.

5.7 Summary and conclusions

We have analyzed the current-induced conformational switching in single-molecule junctions. Our study is motivated by recent STM experiments on azobenzene derivatives, which we model as having two stable conformations in the neutral state (cis and trans), while the potential surface of the charged molecule only exhibits a single minimum [Fig. 5.1(e)]. Current flow through such a conformational switch is characterized by telegraph noise, since the two conformations will in general be characterized by different conductances and switching between the conformations occurs rarely.

As appropriate for STM setups, we consider a molecular junction with strongly asymmetric coupling to tip and substrate and treat current flow within the sequential tunneling approximation. The latter is justified in setups with passivated substrates. Our central finding is that there exists a rather sharp crossover between two qualitatively different switching mechanisms as a function of temperature. For low temperatures, the switching process is induced by tunneling electrons when the vibrational coordinate is close to the minimum of the cis state. We call this process current-induced switching. Beyond a critical temperature, switching is strongly dominated by tunneling processes which occur close to the maximum of the barrier between the cis and the trans states. We refer to this process as thermally activated. Remarkably, this happens long before the temperature becomes of the order of the barrier height.

Experimentally, the two switching mechanisms are readily distinguished by their different temperature dependences. While the current-induced switching exhibits only weak temperature sensitivity, thermal activation processes follow Arrhenius behavior, see Fig. 5.4. Moreover, our results predict that the quantum yield depends exponentially on the tunneling rate to the substrate which makes it highly sensitive to the level of passivation of the substrate.

Our results leave several avenues for future research. It would be interesting to analyze the quantum yield as a function of voltage for voltages in the vicinity of the threshold for tip-to-molecule tunneling. Most important would be an extension to include the resonant broadening of the molecular orbital by the molecule-substrate coupling, which would make our results applicable to experiments with non-passivated substrates.

Conclusions and Outlook

In the present thesis, we have investigated the coupling of electronic degrees of freedom to (i) vibrations, (ii) spins, and (iii) chemical conformations in transport through single-molecule devices. Our work is motivated by a number of recent experiments which show that the presence of internal molecular degrees of freedom leads to numerous novel quantum transport phenomena that go beyond the physics observed in larger nanostructural objects such as quantum dots or carbon nanotubes.

Transport through magnetic molecules has been discussed in the context of *molecular spintronics*, i.e. the idea of integrating the promising concepts of molecular electronics and spintronics. We have found that magnetic anisotropy is crucial for slow spin relaxation and allows one to read out and write the spin of a single molecule connected to two metallic electrodes. Interestingly, current-induced spin switching to a predetermined state only requires a finite bias voltage and is also possible in the absence of a magnetic field. Furthermore, we have shown that the proposed setup leads to interesting physics beyond the effect of spin writing, including the occurrence of large negative differential conductance (NDC) at high temperatures and a new *spin blockade* mechanism.

The Kondo effect in single-molecule transistors has been investigated for the case of a vibrational mode which is coupled to the electronic degree of freedom. Our main findings are the quenching of the gate voltage dependence of the Kondo temperature in the regime of strong electron-phonon coupling and the occurrence of a strongly asymmetric Coulomb blockade. Experimental evidence for these two unusual features has been obtained in recent transport experiments on organic complexes.

Because of intrinsic bistabilities many single-molecule junctions reveal current-induced switching behavior, e.g. involving cis and trans isomers of a molecule. We have studied this process for molecules which exhibit two (meta)stable conformations in the neutral state, but only a single stable conformation in the ionic state. While other recent works in this field consider switching processes which are stimulated by thermal tunneling or vibrational-assisted tunneling from one minimum of the double well to the other, we have shown that the switching may also be induced by the current involving two subsequent sequential tunneling processes. We have found that the transport dynamics can be described by a set of Fokker-Planck equations for the Wigner distribution function of the molecule. Our main result is that the average number of switching events per time becomes extremely small compared to the average electronic tunneling rate determined by the current. In other words, the time that the molecule is in one of the two conformations is long compared to the average time between subsequent tunneling events.

Our results leave several avenues for future research. (i) In the context of molecular

spintronics, it would be interesting to investigate spin-dependent transport through one-dimensional and two-dimensional arrays of magnetic molecules. Due to the long lifetime of the magnetic state, spin-crossover molecules promise to be particularly suitable as switches [151]. At low temperatures spin-crossover materials reveal a transition from the low-spin to the high-spin state, where the energy difference between the two states relies on the interplay between crystal field splitting of the d-orbitals of the metal ions and Hund's rule. We expect the conductances of the spin states to be significantly different, which should be related to a large magnetoresistance, i.e. changes of the conductance in response to an external magnetic field. Furthermore, inelastic spin scattering might play a crucial role and affect most transport properties. For instance, spin might be accumulated on the molecules as a consequence of spin-polarized tunneling currents. However, if the molecular array is sufficiently long, the amount of spin transferred from the lead into the junction may reach a macroscopic magnitude and may thus be easily detected. Presumably, investigating the spin dynamics of spin-crossover chains requires one to go beyond the rate-equation approach used in the present work. In particular, interesting physics could be hidden in the off-diagonal matrix elements of the density-matrix describing superpositions of various spin states.

(ii) Transport through single-molecule magnets has only been studied in the regime of weak molecule-lead coupling, so far. However, a large number of experiments is based on a scanning tunneling microscope (STM) setup, where the molecule is weakly coupled to the tip electrode but strongly coupled to the substrate. As a consequence, the resonances in the spectral function of molecule reveal strong broadenings due to quantum fluctuations, which is expected to manifest itself as a broadening of the peaks in the differential conductance for thermal energies small compared to the hybridization energy. Obviously, this cannot be understood within the sequential tunneling approximation. One possibility would be to study transport through magnetic molecule within the Keldysh formalism, in order to take into account all order of the self-energy in the hybridization.

(iii) While the present work has shown that interesting results for current-induced conformational switching can be obtained from semi-classical Fokker-Planck equations in the high-temperature limit, only little attention has been paid to effects in the low-temperature regime. One important question would be to investigate the switching behavior including the broadening of the molecular levels due to the coupling to the leads. Furthermore, interesting physics might be revealed taking into account higher-order tunneling processes such as cotunneling. The discussed switching dynamics should also lead to characteristic features in the noise spectrum of the system, as mentioned previously. Another question would be to include a more realistic model for the description of vibrational dissipation than the Caldeira-Leggett model used in the present work.

Acknowledgments

In carrying out the work contained in this thesis, I have profited greatly from discussions with a number of people. Some of them I would like to mention in the following:

- I would like to thank Felix von Oppen for enabling me to work in his broadly interested and very active research group over the past few years, for supporting and supervising my PhD thesis, and for many inspirational and valuable discussions. I benefited from his creativity and his physical intuition in various situations.

- I would like to thank Carsten Timm for a very fruitful and productive collaboration over the past few years. I appreciate his physical intuition, constructive criticism and advice along the way, and I thank him for many enlightning discussions. The success of this work relies on his participation in a substantial way.

- Furthermore, I would like to thank Jose Pascual (FU Berlin), Jens Koch (Yale University), Maarten Wegewijs (Forschungszentrum Jülich), Alexander Pikovski (FU Berlin), Karsten Flensberg (University of Copenhagen), Jens Paaske (University of Copenhagen), and Wolfgang Harneit (FU Berlin) for helpful discussions.

- I would like to thank Ingo Peschel for reviewing the present work and for his helpfulness in various situations.

Financial support by the Deutsche Forschungsgemeinschaft through Sonderforschungsbereich 658 is gratefully acknowledged.

Publications

- F. Elste and C. Timm, *Theory for transport through a single magnetic molecule: Endohedral* N@C_{60}, Phys. Rev. B **71**, 155403 (2005).

- C. Timm and F. Elste, *Spin Amplification, Reading, and Writing in Transport through Anisotropic Magnetic Molecules*, Phys. Rev. B **73**, 235304 (2006).

- F. Elste and C. Timm, *Transport through anisotropic magnetic molecules with partially ferromagnetic leads: spin-charge conversion and negative differential conductance*, Phys. Rev. B **73**, 235305 (2006).

- F. Elste and C. Timm, *Cotunneling and non-equilibrium magnetization in magnetic molecular monolayers*, Phys. Rev. B **75**, 195341 (2007).

- F. Elste, G. Weick, C. Timm, and F. von Oppen, *Current-induced conformational switching in single-molecule junctions*, submitted to Appl. Phys. A (2008).

- F. Elste and F. von Oppen, *Asymmetric Coulomb blockade and Kondo temperature of single-molecule junctions*, submitted to New J. Phys. (2008).

Bibliography

[1] A. Aviram and M. Ratner, *Molecular Rectifiers,* Chem. Phys. Lett. **29**, 277 (1974).

[2] G. E. Moore, *Cramming more components onto integrated circuits,* Electronics **38**, 114 (1965).

[3] R. P. Feynman, *There's Plenty of Room at the Bottom,* Engineering and Science **23**, 22 (1960).

[4] P. Vettiger, M. Despont, U. Drechsler, U. Dürig, W. Häberle, M. I. Lutwyche, H. E. Rothuizen, R. Stutz, R. Widmer, and G. K. Binnig, *The "Millipede"—More than one thousand tips for future AFM data storage,* IBM J. Res. Develop. **40**, 323 (2000).

[5] L. I. Glazman and M. E. Raikh, *Resonant Kondo transparency of a barrier with quasilocal impurity states,* JETP Lett. **47**, 452 (1988).

[6] T. K. Ng and P. A. Lee, *On-Site Coulomb Repulsion and Resonant Tunneling,* Phys. Rev. Lett. **61**, 1768 (1988).

[7] S. M. Cronenwett, T. H. Oosterkamp, and L. P. Kouwenhoven, *A tunable Kondo effect in quantum dots,* Science **281**, 540 (1998).

[8] C. Joachim, J. K. Gimzewski, and A. Aviram, *Electronics using hybrid-molecular and mono-molecular devices,* Nature **408**, 541 (2000).

[9] E. G. Emberly and G. Kirczenow, *Molecular spintronics: spin-dependent electron transport in molecular wires,* Chem. Phys. **281**, 311 (2002).

[10] E. G. Emberly and G. Kirczenow, *The Smallest Molecular Switch,* Phys. Rev. Lett. **91**, 188301 (2003).

[11] S. A. Wolf, D. D. Awschalom, R. A. Buhrman, J. M. Daughton, S. von Molnár, M. L. Roukes, A. Y. Chtchelkanova, and D. M. Treger, *Spintronics: A Spin-Based Electronics Vision for the Future,* Science **294**, 1488 (2001).

[12] H. Park, J. Park, A. K. L. Lim, E. H. Anderson, A. P. Alivisatos, and P. L. McEuen, *Nanomechanical oscillations in a single-*C_{60} *transistor,* Nature **407**, 57 (2000).

[13] J. Park, A. N. Pasupathy, J. I. Goldsmith, C. Chang, Y. Yaish, J. R. Petta, M. Rinkoski, J. P. Sethna, H. D. Abruña, P. L. McEuen, and D. C. Ralph, *Coulomb blockade and the Kondo effect in single-atom transistors,* Nature **417**, 722 (2002).

[14] A. Mitra, I. Aleiner and A. J. Millis, *Phonon effects in molecular transistors: Quantum and classical treatment,* Phys. Rev. B **69**, 245302 (2004).

[15] Y. Xue and M. A. Ratner, *Microscopic study of electrical transport through individual molecules with metallic contacts. I. Band lineup, voltage drop, and high-field transport,* Phys. Rev. B **68**, 115406 (2003).

[16] Y. Xue and M. A. Ratner, *Microscopic study of electrical transport through individual molecules with metallic contacts. II. Effect of the interface structure,* Phys. Rev. B **68**, 115407 (2003).

[17] Y. Xue and M. A. Ratner, *Molecular Electronics: From Physics to Computing,* Nanotechnology: Science and Computation (Springer-verlag, berlin, 2006).

[18] M. A. Reed, C. Zhou, C. J. Muller, T. P. Burgin, and J. M. Tour, *Conductance of a Molecular Junction,* Science **278**, 252 (1997).

[19] W. Liang, M. P. Shores, M. Bockrath, J. R. Long, and H. Park, *Kondo Resonance in a Single-Molecule Transistor,* Nature **417**, 725 (2002).

[20] L. H. Yu, Z. K. Keane, J. W. Ciszek, L. Cheng, J. M. Tour, T. Baruah, M. R. Pederson, and D. Natelson, *Kondo Resonances and Anomalous Gate Dependence in the Electrical Conductivity of Single-Molecule Transistors,* Phys. Rev. Lett. **95**, 256803 (2005).

[21] H. B. Weber, J. Reichert, F. Weigend, R. Ochs, D. Beckmann, M. Mayor, R. Ahlrichs, and H. von Löhneysen, *Electronic transport through single conjugated molecules,* Chem. Phys. **281**, 113 (2002).

[22] H. B. Heersche, Z. de Groot, J. A. Folk, H. S. J. van der Zant, C. Romeike, M. R. Wegewijs, L. Zobbi, D. Barreca, E. Tondello, and A. Cornia, *Electron Transport through Single* Mn_{12} *Molecular Magnets,* Phys. Rev. Lett. **96**, 206801 (2006).

[23] M.-H. Jo, J. E. Grose, K. Baheti, M. M. Deshmukh, J. J. Sokol, E. M. Rumberger, D. N. Hendrickson, J. R. Long, H. Park, and D. C. Ralph, *Signatures of Molecular Magnetism in Single-Molecule Transport Spectroscopy,* Nano Lett. **6**, 2014 (2006).

[24] A. Nitzan and M. A. Ratner, *Electron Transport in Molecular Wire Junctions,* Science **300**, 1384 (2003).

[25] M. Galperin, M. A. Ratner, and A. Nitzan, *Molecular transport junctions: vibrational effects,* J. Phys.: Condens. Matter **19**, 103201 (2007).

[26] J. Reichert, R. Ochs, H. B. Weber, M. Mayor, and H. von Löhneysen, *Low-temperature conductance measurements on single molecules,* Appl. Phys. Lett. **82**, 4137 (2003).

[27] R. H. M. Smit, Y. Noat, C. Untiedt, N. D. Lang, M. C. van Hemert, and J. M. van Ruitenbeek, *Measurement of the conductance of a hydrogen molecule,* Nature **419**, 906 (2002).

[28] T. Dadosh, Y. Gordin, R. Krahne, I. Khivrich, D. Mahalu, V. Frydman, J. Sperling, A. Yacoby, and I. Bar-Joseph, *Measurement of the conductance of single conjugated molecules,* Nature **436**, 677 (2005).

[29] J. Koch and F. von Oppen, *Franck-Condon Blockade and Giant Fano Factors in Transport through Single Molecules,* Phys. Rev. Lett. **94**, 206804 (2005).

[30] S. Braig and P. W. Brouwer, *Rate equations for Coulomb blockade with ferromagnetic leads,* Phys. Rev. B **71**, 195324 (2005).

[31] G. A. Kaat and K. Flensberg, *Rectification in single molecular dimers with strong polaron effect,* Phys. Rev. Lett. **71**, 155408 (2005).

[32] J. Paaske and K. Flensberg, *Vibrational Sidebands and the Kondo Effect in Molecular Transistors,* Phys. Rev. Lett. **94**, 176801 (2005).

[33] D. Porath, A. Bezryadin, S. de Vries, and C. Dekker, *Direct measurement of electrical transport through DNA molecules,* Nature **403**, 635 (2000).

[34] J. J. Parks, A. R. Champagne, G. R. Hutchison, S. Flores-Torres, H. D. Abruna, and D. C. Ralph, *Tuning the Kondo effect with a mechanically controllable break junction,* Phys. Rev. Lett. **99**, 026601 (2007).

[35] J. E. Grose, E. S. Tam, C. Timm, M. Scheloske, B. Ulgut, J. J. Parks, H. D. Abruña, W. Harneit, and D. C. Ralph, *Tunneling Spectra of Individual Magnetic Endofullerene Molecules,* submitted to Science (2008).

[36] J. Koch, *Quantum transport through single-molecule devices,* PhD Thesis, Freie Universität Berlin, 2006.

[37] Intel's webpage http://www.intel.com.

[38] S. Sanvito and A. R. Rocha, *Molecular-Spintronics: the art of driving spin through molecules,* J. Comput. Theor. Nanosci. **3**, 624 (2006).

[39] P. Grünberg, R. Schreiber, Y. Pang, M. B. Brodsky, and H. Sowers, *Layered Magnetic Structures: Evidence for Antiferromagnetic Coupling of Fe Layers across Cr Interlayers,* Phys. Rev. Lett. **57**, 2442 (1986).

[40] M. N. Baibich, J. M. Broto, A. Fert, F. Nguyen Van Dau, F. Petroff, P. Eitenne, G. Creuzet, A. Friederich, and J. Chazelas, *Giant Magnetoresistance of (001)Fe/(001)Cr Magnetic Superlattices,* Phys. Rev. Lett. **61**, 2472 (1988).

[41] I. Žutić, J. Fabian, and S. Das Sarma, *Spintronics: fundamentals and applications,* Rev. Mod. Phys. **76**, 323 (2004).

[42] Y. K. Kato, R. C. Myers, A. C. Gossard, and D. D. Awschalom, *Observation of the Spin Hall Effect in Semiconductors,* Science **306**, 1910 (2004).

[43] J. Wunderlich, B. Kaestner, J. Sinova, and T. Jungwirth, *Experimental Observation of the Spin-Hall Effect in a Two-Dimensional Spin-Orbit Coupled Semiconductor System,* Phys. Rev. Lett. **94**, 047204 (2005).

[44] S. J. Blundell and F. L. Pratt, *Organic and molecular magnets,* J. Phys.: Condens. Matter **16**, R771 (2004).

[45] T. Lis, *Preparation, structure, and magnetic properties of a dodecanuclear mixed-valence manganese carboxylate,* Acta Crystallogr. B **36**, 2042 (1980).

[46] D. Gatteschi, R. Sessoli, and A. Cornia, *Single-molecule magnets based on iron(III) oxo clusters,* Chem. Commun. 725 (2000).

[47] T. Almeida Murphy, T. Pawlik, A. Weidinger, M. Höhne, R. Alcala, and J.-M. Spaeth, *Observation of Atomlike Nitrogen in Nitrogen-Implanted Solid* C_{60}*,* Phys. Rev. Lett. **77**, 1075 (1996).

[48] W. Harneit, *Fullerene-based electron-spin quantum computer,* Phys. Rev. A **65**, 032322 (2002).

[49] L. A. Bumm, J. J. Arnold, M. T. Cygan, T. D. Dunbar, T. P. Burgin, L. Jones II, D. L. Allara, J. M. Tour, and P. S. Weiss, *Are Single Molecular Wires Conducting?,* Science **271**, 1705 (1996).

[50] N. Henningsen, K. J. Franke, I. F. Torrente, G. Schulze, B. Priewisch, K. Rück-Braun, J. Dokic, T. Klamroth, P. Saalfrank, and J. I. Pascual, *Inducing the rotation of a single phenyl ring with tunneling electrons,* J. Phys. Chem. C **111**, 14843 (2007).

[51] A. V. Danilov, S. E. Kubatkin, S. G. Kafanov, K. Flensberg, and T. Bjørnholm, *Electron Transfer Dynamics of Bistable Single-Molecule Junctions,* Nano Lett. **6**, 2184 (2006).

[52] A. Donarini, M. Grifoni, and K. Richter, *Dynamical Symmetry Breaking in Transport through Molecules,* Phys. Rev. Lett. **97**, 166801 (2006).

[53] J. Gaudioso, L. J. Lauhon, and W. Ho, *Vibrationally-Mediated Negative Defferential Resistance in a Single Molecule,* Phys. Rev. Lett. **85**, 1918 (2000).

[54] X. H. Qiu, G. V. Nazin, and W. Ho, *Mechanisms of Reversible Conformational Transitions in a Single Molecule,* Phys. Rev. Lett. **93**, 196806 (2004).

[55] M. Alemani, M. V. Peters, S. Hecht, K. H. Rieder, F. Moresco, and L. Grill, *Electric Field-Induced Isomerization of Azobenzene by STM,* J. Am. Chem. Soc. **128**, 14446 (2006).

[56] J. Henzl, T. Bredow, and K. Morgenstern, *Irreversible isomerization of the azobenzene derivate Methyl Orange on Au(111),* Chem. Phys. Lett. **435**, 278 (2007).

[57] S. Gao, M. Persson, and B. I. Lundqvist, *Theory of atom transfer with a scanning tunneling microscope,* Phys. Rev. B **55**, 4825 (1997).

[58] W. H. A. Thijssen, D. Djukic, A. F. Otte, R. H. Bremmer, and J. M. van Ruitenbeek, *Vibrationally Induced Two-Level Systems in Single-Molecule Junctions,* Phys. Rev. Lett. **97**, 226806 (2006).

[59] B.-Y. Choi, S.-J. Kahng, S. Kim, H. Kim, H. W. Kim, Y. J. Song, J. Ihm, and Y. Kuk, *Conformational Molecular Switch of the Azobenzene Molecule: A Scanning Tunneling Microscopy Study,* Phys. Rev. Lett. **96**, 156106 (2006).

[60] M. del Valle, R. Gutiérrez, C. Tejedor, and G. Cuniberti, *Tuning the conductance of a molecular switch,* Nature Nanotechnology **2**, 176 (2007).

[61] K. S. Novoselov, A. K. Geim, S. V. Morozov, D. Jiang, Y. Zhang, S. V. Dubonos, I. V. Grigorieva, and A. A. Firsov, *Electric Field Effect in Atomically Thin Carbon Films,* Science **306**, 666 (2004).

[62] A. K. Geim and K. S. Novoselov, *The Rise of Graphene,* Nature Materials **6**, 183 (2007).

[63] W. Kohn and L. J. Sham, *Self-Consistent Equations Including Exchange and Correlation Effects,* Phys. Rev. **140**, A1133 (1965).

[64] K. Burke, J. Werschnik, and E. K. U. Gross, *Time-dependent density functional theory: Past, present, and future,* J. Chem. Phys. **123**, 062206 (2005).

[65] M. Di Ventra, N. D. Lang, and S. T. Pantelides, *Electronic transport in single molecules,* Chem. Phys. **281**, 189 (2002).

[66] R. U. I. Liu, S.-H. Ki, H. Baranger, and W. Yang, *Intermolecular Effect in Molecular Electronics,* J. Chem. Phys. **122**, 044703 (2005).

[67] F. Evers, F. Weigend, and M. Koentopp, *Conductance of molecular wires and transport calculations based on density-functional theory,* Phys. Rev. B **69**, 235411 (2004).

[68] E. Runge and E. K. U. Gross, *Density-Functional Theory for Time-Dependent Systems,* Phys. Rev. Lett. **52**, 997 (1984).

[69] P. Hohenberg and W. Kohn, *Inhomogeneous Electron Gas,* Phys. Rev. **136**, B864 (1964).

[70] S. Kurth, G. Stefanucci, C.-O. Almbladh, A. Rubio, and E. K. U. Gross, *Time-dependent quantum transport: A practical scheme using density functional theory,* Phys. Rev. B **72**, 035308 (2005).

[71] L. V. Keldysh, *Ionization in the Field of a Strong Electromagnetic Wave,* Zh. Éksp. Teor. Fiz. **47**, 1945 (1964).

[72] J. Rammer and H. Smith, *Quantum field-theoretical methods in transport theory of metals,* Rev. Mod. Phys. **58**, 323 (1986).

[73] K. Blum, *Density Matrix Theory and Applications,* Plenum Press, New York, 1981.

[74] K. G. Wilson, *Renormalization Group and Critical Phenomena. I. Renormalization Group and the Kadanoff Scaling Picture,* Phys. Rev. B **4**, 3174 (1971).

[75] S. Takei, Y. B. Kim, and A. Mitra, *Enhanced Fano factor in a molecular transistor coupled to phonons and Luttinger-liquid leads,* Phys. Rev. B **72**, 075337 (2005).

[76] C. Durkan and M. E. Welland, *Electronic spin detection in molecules using scanning-tunneling- microscopy-assisted electron-spin resonance,* Appl. Phys. Lett. **80**, 458 (2002).

[77] L. H. Yu and D. Natelson, *Kondo physics in* C_{60} *Single-Molecule Transistors,* Nano Lett. **4**, 79 (2004).

[78] L. H. Yu, Z. K. Keane, J. W. Ciszek, L. Cheng, M. P. Stewart, J. M. Tour, and D. Natelson, *Inelastic electron tunneling via molecular vibrations in single-molecule transistors,* Phys. Rev. Lett. **93**, 266802 (2004).

[79] Y. Meir and N. S. Wingreen, *Landauer formula for the current through an interacting electron region,* Phys. Rev. Lett. **68**, 2512 (1992).

[80] T. Ando, Y. Arakawa, K. Furuya, S. Komiyama, and H. Nakashima, *Mesoscopic Physics and Electronics,* Springer Berlin, 1998.

[81] J. Kondo, *Resistance Minimum in Dilute Magnetic Alloys,* Prog. Theor. Phys. **32**, 37 (1964).

[82] A. C. Hewson, *The Kondo Problem to Heavy Fermions,* Cambridge University Press, Cambridge, England, 1993.

[83] H. Bruus and K. Flensberg, *Many-body Quantum Theory in Condensed Matter Physics,* Oxford University Press, Oxford, 2004.

[84] C. W. Gardiner, *Quantum Noise,* Springer-Verlag, Berlin, 1991.

[85] F. Elste, *Transport durch endohedrale Fullerene,* Diplomarbeit, Freie Universität Berlin, 2005.

[86] F. Elste and C. Timm, *Theory for transport through a single magnetic molecule: Endohedral* N@C_{60}*,* Phys. Rev. B **71**, 155403 (2006).

[87] C. Timm, *Tunneling through magnetic molecules with arbitrary angle between easy axis and magnetic field,* Phys. Rev. B **76**, 014421 (2007).

[88] D. V. Averin, *Periodic conductance oscillations in the single-electron tunneling transistor,* Physica B **194**, 979 (2003).

[89] M. Turek and K. A. Matveev, *Cotunneling thermopower of single electron transistors,* Phys. Rev. B **65**, 115332 (2002).

[90] J. Koch, F. von Oppen, Y. Oreg, and E. Sela, *Thermopower of single-molecule devices,* Phys. Rev. B **70**, 195107 (2004).

[91] F. von Oppen, private communication.

[92] J. R. Schrieffer and P. A. Wolff, *Relation between the Anderson and Kondo Hamiltonians,* Phys. Rev. **149**, 491 (1966).

[93] P. W. Anderson, *A poor man's derivation of scaling laws for the Kondo problem,* J. Phys. C **3**, 2436 (1970).

[94] M. Pustilnik and L. I. Glazman, *Kondo effect in quantum dots,* J. Phys. Condens. Matter **16**, R513 (2004).

[95] F. Meier, V. Cerletti, O. Gywat, D. Loss, D. D. Awschalom, *Molecular spintronics: Coherent spin transfer in coupled quantum dots,* Phys. Rev. B **69**, 195315 (2004).

[96] K. Tsukagoshi, B. W. Alphenaar, and H. Ago, *Coherent transport of electron spin in a ferromagnetically contacted carbon nanotube,* Nature **401**, 572 (1999).

[97] Z. H. Xiong, D. Wu, Z. Valy Vardeny and J. Shi, *Giant Magnetoresistance in Organic Spin-Valves,* Nature **427**, 821 (2004).

[98] V. Dediu, M. Murgia, F.C. Matacotta, C. Taliani, and S. Barbanera, *Room temperature spin polarized injection in organic semiconductor,* Solid State Commun. **122**, 181 (2002).

[99] J. R. Petta, S. K. Slater and D. C. Ralph, *Spin-dependent transport in molecular tunnel junctions,* Phys. Rev. Lett. **93**, 136601 (2004).

[100] M. Ouyang and D. D. Awschalom, *Coherent Spin Transfer between Molecularly Bridged Quantum Dots,* Science **301**, 1074 (2003).

[101] G. Schmidt, *Concepts for spin injection into semiconductors—a review,* J. Phys. D: Appl. Phys. **38**, R107 (2005).

[102] J. A. C. Bland and B. Heinrich, *Ultrathin Magnetic Structures,* Springer Berlin, 1994.

[103] C. Romeike, M. R. Wegewijs, W. Hofstetter, and H. Schoeller, *Quantum-Tunneling-Induced Kondo Effect in Single Molecular Magnets,* Phys. Rev. Lett. **96**, 196601 (2006).

[104] C. Romeike, M. R. Wegewijs, M. Ruben, W. Wenzel, and H. Schoeller, *Charge-switchable molecular magnet and spin blockade of tunneling,* Phys. Rev. B **75**, 064404 (2008).

[105] D. Weinmann, *Spin blockade in non-linear transport through quantum dots,* Europhys. Lett. **26**, 467 (1994).

[106] H. Imamura, H. Aoki, and P. A. Maksym, *Spin blockade in single and double quantum dots in magnetic fields: A correlation effect,* Phys. Rev. B **57**, R4257 (1998).

[107] A. K. Hüttel, H. Qin, A. W. Holleitner, R. H. Blick, K. Neumaier, D. Weinmann, K. Eberl, and J. P. Kotthaus, *Spin blockade in ground-state resonance of a quantum dot,* Europhys. Lett **62**, 712 (2003).

[108] M. Ciorga, A. S. Sachrajda, P. Hawrylak, C. Gould, P. Zawadski, S. Jullian, Y. Feng, and Z. Wasilewski, *Addition spectrum of a lateral dot from Coulomb and spin-blockade spectroscopy,* Phys. Rev. B **61**, R16315 (2000).

[109] A. Cottet, W. Belzig, and C. Bruder, *Positive Cross Correlations in a Three-Terminal Quantum Dot with Ferromagnetic Contacts,* Phys. Rev. Lett. **92**, 206801 (2004).

[110] A. Cottet and W. Belzig, *Dynamical spin-blockade in a quantum dot with paramagnetic leads,* Europhys. Lett. **66**, 405 (2004).

[111] A. N. Korotkov, *Intrinsic noise of the single-electron transistor,* Phys. Rev. B **49**, 10381 (1994).

[112] Y. M. Blanter and M. Büttiker, *Shot noise in mesoscopic conductors,* Phys. Rep. **336**, 2000 (2000).

[113] W. Schottky, *Über spontane Stromschwankungen in verschiedenen Elektrizitätsleitern,* Ann. Phys. **57**, 541 (1918).

[114] V. A. Khlus, *Current and voltage fluctuations in microjunctions between normal metals and superconductors,* Sov. Phys. JETP **66**, 1243 (1987).

[115] G. B. Lesovik, *Excess quantum noise in 2D ballistic point contacts,* JETP Lett. **49**, 592 (1989).

[116] M. Büttiker, *Scattering theory of thermal and excess noise in open conductors,* Phys. Rev. Lett. **65**, 2901 (1990).

[117] V. Sih, R. C. Myers, Y. K. Kato, W. H. Lau, A. C. Gossard, and D. D. Awschalom, *Spatial imaging of the spin Hall effect and current-induced polarization in two-dimensional electron gases,* Nature Phys. **1**, 31 (2005).

[118] M. Zomack and K. Baberschke, *Electron spin resonance study of* NO_2 *adsorbed on* Kr/Ag(110) *at 20 K,* Surf. Sci. **178**, 618 (1986).

[119] M. Zomack and K. Baberschke, *Submonolayers of paramagnetic* NO_2 *adsorbed on argon and xenon films,* Phys. Rev. B **36**, 5756 (1987).

[120] D. Rugar, R. Budakian, H. J. Mamin, and B. W. Chui, *Single spin detection by magnetic resonance force microscopy,* Nature **430**, 329 (2004).

[121] J.-P. Cleuziou, W. Wernsdorfer, V. Bouchiat, T. Ondarçuhu, and M. Monthioux, *Carbon nanotube superconducting quantum interference device,* Nature Nanotechnology **1**, 53 (2006).

[122] C. Zhou, M. R. Deshpande, M. A. Reed, L. Jones II, and J. M. Tour, *Nanoscale metal/self-assembled monolayer/metal heterostructures,* Appl. Phys. Lett. **71**, 611 (1997).

[123] J. Koch, M. E. Raikh, and F. von Oppen, *Pair tunneling through single molecules,* Phys. Rev. Lett. **96**, 056803 (2006).

[124] B. LeRoy, S. Lemay, J. Kong, and C. Dekker, *Electrical generation and absorption of phonons in carbon nanotubes,* Nature **432**, 371 (2004).

[125] J. Koch, F. von Oppen, and A. V. Andreev, *Theory of the Franck-Condon blockade regime,* Phys. Rev. B **74**, 205438 (2006).

[126] C. Romeike, M. R. Wegewijs, and H. Schoeller, *Spin Quantum Tunneling in Single Molecular Magnets: Fingerprints in Transport Spectroscopy of Current and Noise,* Phys. Rev. Lett. **96**, 196805 (2006).

[127] D. Goldhaber-Gordon, H. Shtrikman, D. Mahalu, D. Abusch-Magder, U. Meirav, M. A. Kastner, *Kondo effect in a single-electron transistor,* Nature **391**, 156 (1998).

[128] W. G. van der Wiel, S. De Franceschi, T. Fujisawa, J. M. Elzerman, S. Tarucha, L. P. Kouwenhoven, *The Kondo effect in the unitary limit,* Science **289**, 2105 (2000).

[129] E. Sela, Y. Oreg, F. von Oppen, and J. Koch, *Fractional Shot Noise in the Kondo Regime,* Phys. Rev. Lett. **97**, 060501 (2006).

[130] M. Galperin, A. Nitzan, M. A. Ratner, *Inelastic effects in molecular junctions in the Coulomb and Kondo regimes: Nonequilibrium equation-of-motion approach,* Phys. Rev. B **76**, 035301 (2007).

[131] L. I. Glazman and M. Pustilnik, *Low-temperature transport through a quantum dot,* Nanophysics: Coherence and Transport, Elsevier, Amsterdam, 2005.

[132] A. Rosch, J. Kroha, and P. Wölfle, *Kondo Effect in Quantum Dots at High Voltage: Universality and Scaling,* Phys. Rev. Lett. **87**, 156802 (2001).

[133] P. Coleman, C. Hooley, and O. Parcollet, *Is the quantum dot at large bias a weak coupling problem?,* Phys. Rev. Lett. **86**, 4088 (2001).

[134] A. Kaminski, Y. V. Nazarov, and L. I. Glazman, *Universality of the Kondo effect in a quantum dot out of equilibrium,* Phys. Rev. B **62**, 8154 (2000).

[135] F. D. M. Haldane, *Scaling Theory of the Asymmetric Anderson Model,* Phys. Rev. Lett. **40**, 416 (1978).

[136] C. A. Balseiro, P. S. Cornaglia, and D. R. Grempel, *Electron-phonon correlation effects in molecular transistors,* Phys. Rev. B **74**, 235409 (2006).

[137] P. S. Cornaglia, Gonzalo Usaj, and C. A. Balseiro, *Electronic Transport through Magnetic Molecules with Soft Vibrating Modes,* Phys. Rev. B **76**, R241403 (2007).

[138] P. M. Morse, *Diatomic Molecules According to the Wave Mechanics. II. Vibrational Levels,* Phys. Rev. **34**, 57 (1929).

[139] J. Koch and F. von Oppen, *Effects of charge-dependent vibrational frequencies and anharmonicities in transport through molecules,* Phys. Rev. B **72**, 113308 (2005).

[140] G. Füchsel, T. Klamroth, J. Dokic, P. Saalfrank, *On the Electronic Structure of Neutral and Ionic Azobenzenes and Their Possible Role as Surface Mounted Molecular Switches,* J. Phys. Chem. **110**, 16337 (2006).

[141] V. Iancu and S.-W. Hla, *Realization of a four-step molecular switch in scanning tunneling microscope manipulation of single chlorophyll-a molecules,* Proc. Natl. Acad. Sci. **103**, 13718 (2006).

[142] J. Henzl, M. Mehlhorn, H. Gawronski, K. H. Rieder, and K. Morgenstern, *Reversible cis-trans Isomerization of a Single Azobenzene Molecule,* Angew. Chem. Int. Ed. **45**, 603 (2006).

[143] X. H. Qiu, G. V. Nazin, and W. Ho, *Vibrationally Resolved Fluorescence Excited with Submolecular Precision,* Science **299**, 542 (2003).

[144] L. Y. Gorelik, A. Isacsson, M. V. Voinova, B. Kasemo, R. I. Shekhter, and M. Jonson, *Shuttle Mechanism for Charge Transfer in Coulomb Blockade Nanostructures,* Phys. Rev. Lett. **80**, 4526 (1998).

[145] T. Novotny, A. Donarini, and A.-P. Jauho, *Quantum Shuttle in Phase Space,* Phys. Rev. Lett. **90**, 256801 (2003).

[146] T. Novotny, A. Donarini, C. Flindt, and A.-P. Jauho, *Shot Noise of a Quantum Shuttle,* Phys. Rev. Lett. **92**, 248302 (2004).

[147] W. H. Zurek, *Environment-induced superselection rules,* Phys. Rev. D **26**, 1862 (1982).

[148] D. Giulini, C. Kiefer, and H. D. Zeh, *Symmetries, superselection rules, and decoherence,* Phys. Lett. A **199**, 291 (1995).

[149] A. O. Caldeira and A. J. Leggett, *Influence of Dissipation on Quantum Tunneling in Macroscopic Systems,* Phys. Rev. Lett. **46**, 211 (1981).

[150] A. O. Caldeira and A. J. Leggett, *Path integral approach to quantum brownian motion,* Physica A **121**, 587 (1983).

[151] O. Kahn and C. J. Martinez, *Spin-Transition Polymers: From Molecular Materials Toward Memory Devices,* Science **279**, 44 (1998).

Quantentransport durch einzelne Moleküle:
Spin- und Schwingungsfreiheitsgrade

Deutsche Kurzfassung

Im Zuge des vorherrschenden Optimismus im jungen Forschungsgebiet der Molekularen Elektronik hat die Untersuchung des elektronischen Transports durch einzelne Moleküle während der letzten Jahre besondere Beachtung erfahren. Dies ist nicht nur die Folge vielversprechender technologischer Anwendungen. Auch hat sich gezeigt, dass die Anwesenheit spezifischer molekularer Freiheitsgrade zu neuartigen Quantentransportphänomenen führt, deren Beschreibung über die in größeren Nanostrukturen zu beobachtende Physik hinausgeht. In der vorliegenden Arbeit untersuchen wir die Kopplung zwischen elektronischen Freiheitsgraden und (i) Schwingungsfreiheitsgraden, (ii) Spins, (iii) Konformationsfreiheitsgraden im Transport durch Einzelmolekültransistoren.

Der Transport durch magnetische Moleküle wird mit Bezug auf *molekulare Spintronik* diskutiert, der Idee Konzepte molekularer Elektronik und Spintronik mit einander zu kombinieren. Eine der Hauptvoraussetzungen für Spintronik-Bauelemente stellt die Fähigkeit der Manipulation und Detektion von Spins dar. In diesem Zusammenhang finden wir, dass magnetische Anisotropie verantwortlich ist für langsame Spinrelaxation.

Die Spinmenge, die von einer Zuleitung des Einzelmolekültransistors zur anderen transmittiert wird, hängt stark von der Orientierung des anfänglichen molekularen Spins ab und kann sehr viel größer als dieser werden. Dieser Effekt der Spinverstärkung gestattet es effektiv Spininformationen auszulesen. Es sei darauf hingewiesen, dass die Zuleitungen nicht spin-polarisiert zu sein brauchen. Andererseits erfordert das Schreiben des Spins einen Aufbau, der aus einer ferromagnetischen und einer nicht-magnetischen Zuleitung besteht. Interessanterweise ist für das strominduzierte Schalten des Spins in einen vorgegebenen Zustand lediglich eine endliche Spannung, jedoch kein Magnetfeld erforderlich.

Darüberhinaus führt der vorgeschlagene Aufbau zu interessanter Physik über den Effekt des magnetischen Schreibens hinaus, wie dem Auftreten großer negativer differentieller Widerstände bei hohen Temperaturen. Dieser Effekt ist die Konsequenz eines neuartigen Spinblockade-Mechanismus. Damit meinen wir die Unterdrückung der Tunnelraten für Elektronen einer bestimmten Spinrichtung aufgrund unterschiedlicher Zustandsdichten der Zuleitungen.

Das Wechselspiel zwischen magnetischen Freiheitsgraden und Vibrationsfreiheitsgraden untersuchen wir im Transport durch schwingende Einzelmolekültransistoren im Kondo-Regime. Wir finden, dass die Abhängigkeit der Kondo-Temperatur von der Gate-Spannung für starke Elektron-Phonon-Kopplung sehr viel schwächer ist als in konventionellen Nanostrukturen wie Quantenpunkten. Außerdem ist die Coulombblockade stark asymmetrisch in der Nähe der Entartungspunkte in der differentiellen

Leitfähigkeit, d. h. Peaks in der differentiellen Leitfähigkeit sind stark ausgeprägt auf der einen Seite des Entartungspunktes, hingegen sehr schwach auf der anderen. Ein experimenteller Nachweis dieser ungewöhnlichen Transporteigenschaften gelang in kürzlich veröffentlichten Messungen an organischen Molekülkomplexen.

Die Hauptvoraussetzung für einen elektrischen Schaltkreis auf der Nanoskala sind molekulare Bauelemente, die sich zwischen zwei Zuständen mit deutlich unterschiedlichen Leitwerten hin- und herschalten lassen. Aufgrund intrinsischer Bistabilität zeigen viele Einzelmolekültransistoren strom-induziertes Schaltverhalten, das beispielsweise die cis- und trans-Zustände eines Moleküls beinhaltet. Wir untersuchen diesen Prozess für Moleküle, die zwei (meta)stabile Konformationen im neutralen Zustand aufweisen, aber nur eine stabile Konformation im ionischen Zustand. Während andere Arbeiten in diesem Gebiet hauptsächlich Schaltprozesse betrachten, die durch thermische Aktivierung oder das direkte Tunneln von einem Potentialminimum der Doppelmulde ins andere stimuliert werden, zeigen wir, dass der Strom das Schalten auch in Form von zwei sequentiellen Tunnelprozessen induzieren kann. Unser Hauptinteresse liegt in der Untersuchung des Regimes stark asymmetrischer Kopplung zwischen Molekül und Zuleitungen, was dem Aufbau eines Rastertunnelmikroskops entspricht. Wir zeigen, dass sich die Transportdynamik durch Fokker-Planck-Gleichungen für die Wigner-Verteilungsfunktion des Moleküls beschreiben lässt. Unser Hauptergebnis besteht darin, dass die mittlere Anzahl von Schaltereignissen pro Zeit extrem klein gegenüber der mittleren elektronischen Tunnelzeit werden kann, welche durch den Strom bestimmt wird. Mit anderen Worten, die Zeit, welche das Molekül in einer der beiden Konformationen verbringt, ist sehr lang gegenüber der Zeit zwischen zwei Tunnelereignissen. Derart auffälliges Schaltverhalten wurde kürzlich in Transportmessungen, z. B. an Azobenzol, beobachtet.